© 2020

JOSEPH R. STRAFACI

ALL RIGHTS RESERVED

COMPARISON OF LOAD RATING METHODS FOR COMPLEX BRIDGES

By:

JOSEPH R. STRAFACI, PE

A dissertation submitted to the

Graduate School-New Brunswick

Rutgers, the State University of New Jersey

In partial fulfillment of the requirements

For the Degree of

Doctor of Philosophy

Graduate Program of Civil and Environmental Engineering

Written under the Direction of

Dr. Hani Nassif, Ph.D.

And approved by

_____

_____

_____

_____

New Brunswick, New Jersey

Spring 2020

Abstract of the dissertation

COMPARISON OF LOAD RATING METHODS FOR COMPLEX BRIDGES

by JOSEPH R. STRAFACI, PE

Dissertation Director:

Dr. Hani H. Nassif, Ph.D.

With the lack of funding to address all infrastructure needs, highway agencies are faced with prioritizing their greatest infrastructure needs. This especially holds true for complex structures, which as defined by the 2018 AASHTO Manual for Bridge Evaluation include movable, suspension, cable stayed, or other unusual characteristic not found in common structures These bridges usually provide access for a great number of users and come with a high cost of replacement.

The purpose of this project was to perform a comparison of load rating methods for Complex Bridges. Focus was placed on the current Load Factor Resistance Rating and Load Factor Rating methodology. This study utilizes a movable bridge as a form of comparative evaluation. The bridge was selected due to its age, complexity, and condition.

To assist in this comparison, analysis by field testing, and a refined method of analysis was utilized in the form of finite element modeling. Additionally, weigh-in-motion sensors were installed at the selected bridge to understand daily truck traffic, identify maximum loading scenarios, and develop a site-specific live load factor.

Based on the analysis performed, it was concluded that the LRFR method is the preferred method when compared to the LFR Method. Given the current code provisions, when compared against each other, the LRFR not only provides the most ideal rating factor, but also provides a clearer picture of how members are being affect by subject loads.

Additionally, based off the comparison performed and results obtained, this project developed a proposed guide for inclusion into the MBE for the evaluation of complex structures. Additionally, based on the analysis performed guidance regarding repaired members, and prediction models was also proposed.

Dedication

This paper is dedicated to my mother Linda who encouraged me to do my best and supported my every endeavor. I also dedicate this effort to my grandmother, Laura Lanzi, who was an inspiration and taught me the importance of education and hard work.

Acknowledgements

I would like to take this opportunity to acknowledge and thank the following people:

My advisor Dr. Hani Nassif for his guidance mentorship, and support, as well as, giving me this opportunity to contribute to our field in such a way.

My mentor and friend, Joseph M. Ettore, County Engineer for the County of Monmouth, who has provided mentorship, guidance and support for the past seven years, as well as, giving me the opportunity to complete this dissertation using one of the County's bridges.

My committee members, Dr. Yook-Kong Yong, Dr. Hao Wang, and Dr. Thomas Tsakalakos for their time and guidance.

To my colleagues at Rutgers, Dr. Adi Abu-Obeidah, Dr. Chaekuk Na, Thales Braguim, Chan Yang, and He Zhang for their help and support with this project.

To my colleagues at HNTB for their technological support, guidance, and mentorship especially Roderick Lewis, Todd Batchelor, Robert Rogoff and Peter Imperiale.

To my colleague and friend Vrata Patel for her help and support in reviewing this dissertation.

TABLE OF CONTENTS

LIST OF FIGURES

LIST OF TABLES

CHAPTER 1

INTRODUCTION

1.1 – Background

As a result of the 1967 US 35 "Silver Bridge" collapse, which killed over 40 people, the Transportation industry has put a precedence on maintaining the safety of our motoring public. To ensure this, the Federal Highway Administration (FHWA) mandated certain inspection protocol be put in place to avoid another disaster. The result was the National Bridge Inspection Standards, a set of guidelines and requirements that engineers can utilize to evaluate the safety of all in-service bridges with a span greater than 20 feet.

In combination with this set of standards, the American Association of State Highway Engineers and Transportation Officials (AASHTO), developed the Manual for Bridge Evaluation (MBE) to aid engineers in their efforts to evaluate these structures. The manual offers guidance on asset management, documentation, testing, and most importantly, evaluation in the form of Load Ratings. These ratings, in conjunction with the above inspection standards, provide owners with a comprehensive document which assists them in making key decisions such as, posting a bridge, replacing a bridge or rehabilitating elements to keep the structure in service.

Per the 2017 ASCE infrastructure report, ASCE has graded the USA with an overall score of D+ for its infrastructure; specifically, a grade of C+ for its bridges. This detailed report indicates that 9.1% of all bridges throughout the United States are Structural Deficient with the average age of 43 years old. (ASCE, 2017)

This especially holds true for complex structures. A complex structure, as defined by the 2018 AASHTO Manual for Bridge Evaluation (MBE 2018), is a "bridge with has either a movable, suspension, cable stayed, or other unusual characteristic not found in common structures," (MBE 2018, Section 1). These bridges, are usually massive pieces of infrastructure, carry vital roadways and are major connectors of infrastructure. There are a variety of examples of these structures today including the Pulaski Skyway, the Golden Gate Bridge, and many of the bridges which connect the city of Chicago over the Chicago River.

Figure 1.1 - Chicago River Movable Bridges (Google Images)

Due to the complex nature of these bridges, they cost a great deal to replace or rehabilitate. For instance, the Pulaski Skyway is amid a multi-billion-dollar rehabilitation program. The Goethals Bridge which connects the New Jersey Turnpike to the Staten Island Expressway which in turn connects to Brooklyn, cost $1.5 billion to replace. Most notably, the Tappan Zee Bridge, which bridges over the Hudson River, cost $3.9 billion to replace.

With inefficient funding to replace everything, owners are now faced with tough

decisions. Per the 2017 ASCE report, the US has 614,387 bridges (with spans greater than 20 feet), with a backlog of $123 billion for bridge rehabilitation (ASCE, 2017). Given the current budgeting issues that the federal government is facing, along with extraneous infrastructure needs such as highway improvements and railway upgrades, the backlog of bridge rehabilitation will only worsen. Therefore, we are finding it more and more common to rehabilitate and repair the existing infrastructure. This effects complex structures particularly as many owners don't have the funds to keep up with maintaining those types of structures.

Based on this information, there is a need for a procedure for complex bridge evaluation on how to best approach these types of repairs and accordingly prioritize them. Additionally, Load Ratings which were initially developed for standard bridge types are not always intended for Complex type structures. The 2018 MBE offers the following regarding this:

> "Ratings of long-span bridges, movable bridges and other complex bridges may involve additional considerations and loadings not specifically addressed in this section and rating procedures should be augmented with additional evaluation criteria where required" (2018 MBE Section 6.1).

Additionally, many of these complex bridges were designed prior to 2000. These were normally designed using the Allowable Stress Design Method (ASD). Allowable Stress bases its design method off the allowable strength of the material used. It was the standard for almost 70 years. Concurrently many of these complex structures are evaluated using the LFD form of load rating analysis which is not in accordance with the current standards for evaluation.

1.2 – Motivation

The Monmouth County Department of Public Works and Engineering has undertaken a study to evaluate their largest bridge asset, Bridge S-31 (the Oceanic Bridge). This bridge, shown

below, has been the County's greatest challenge to maintain and replace. The bridge spans the Navesink River and connects the Township of Middletown to the Borough of Rumson.

Figure 1.2 - Bridge S-31, the Oceanic Bridge (Looking east at Bascule Span)

The bridge is classified as a complex structure due to its movable span. The span is a dual leaf bascule span configuration, which is supported by two massive piers. To further support the movable span, two anchor or flanking spans which are simply supported tie directly into the trunnion system which gives the span enough structural support to operate.

The County is currently amid a ten-year process which will allow them to obtain the required federal funds to replace the bridge. This process involves several stages which requires public support and comment at each level. It also involves federal and state oversight. Meanwhile, the County is still responsible for continued maintenance of the structure. Since the County does not have the funding to replace the bridge, they have been spending a considerable amount of money to keep the bridge in service. Based on this, the County has a desire to better understand how it's bridge responds to different loads, as well as, prioritize repairs going forward until the bridge can be replace.

1.3 – Research Significance

Complex bridges provide agencies the opportunity to provide users with a structure that allows a multitude of benefits. These benefits include spanning long areas, providing multimodal use, and building in tight areas such as the center of a city. However, these bridges come with a high cost. The maintenance and upkeep of these bridges have been a significant issue especially at the lower local level. This has caused owners to let these bridges deteriorate to a point of either disrepair or requiring massive rehabilitation.

The AASHTO MBE does not provide clear guidelines on how owners can go about evaluating these types of structures. Additionally, given the age of many of these bridges, the evaluation code that is used to evaluate them is outdated, and does not provide a clear picture of how the bridge reacts to certain loads. Therefore, it is expected, that this dissertation will provide agencies, especially those in need of funding a better understanding, and a procedure which will allow them to properly evaluate their complex structures and prioritize repairs accordingly.

1.4 – Objectives

The primary objective of this research is to develop a procedure for the evaluation of complex bridges. Additionally, a comparison of the current load rating methodologies, the Load Factor Resistance Rating (LRFR) and the Load Factor Rating (LFR) method which has been mainly utilized on bridges designed under the previous Allowable Stress Design Criteria. It is the goal that at the end of this dissertation, we will have established the benefits of using the LRFR method for complex bridges in particular despite the code the bridge it was designed for. A flowchart for this dissertation is included below:

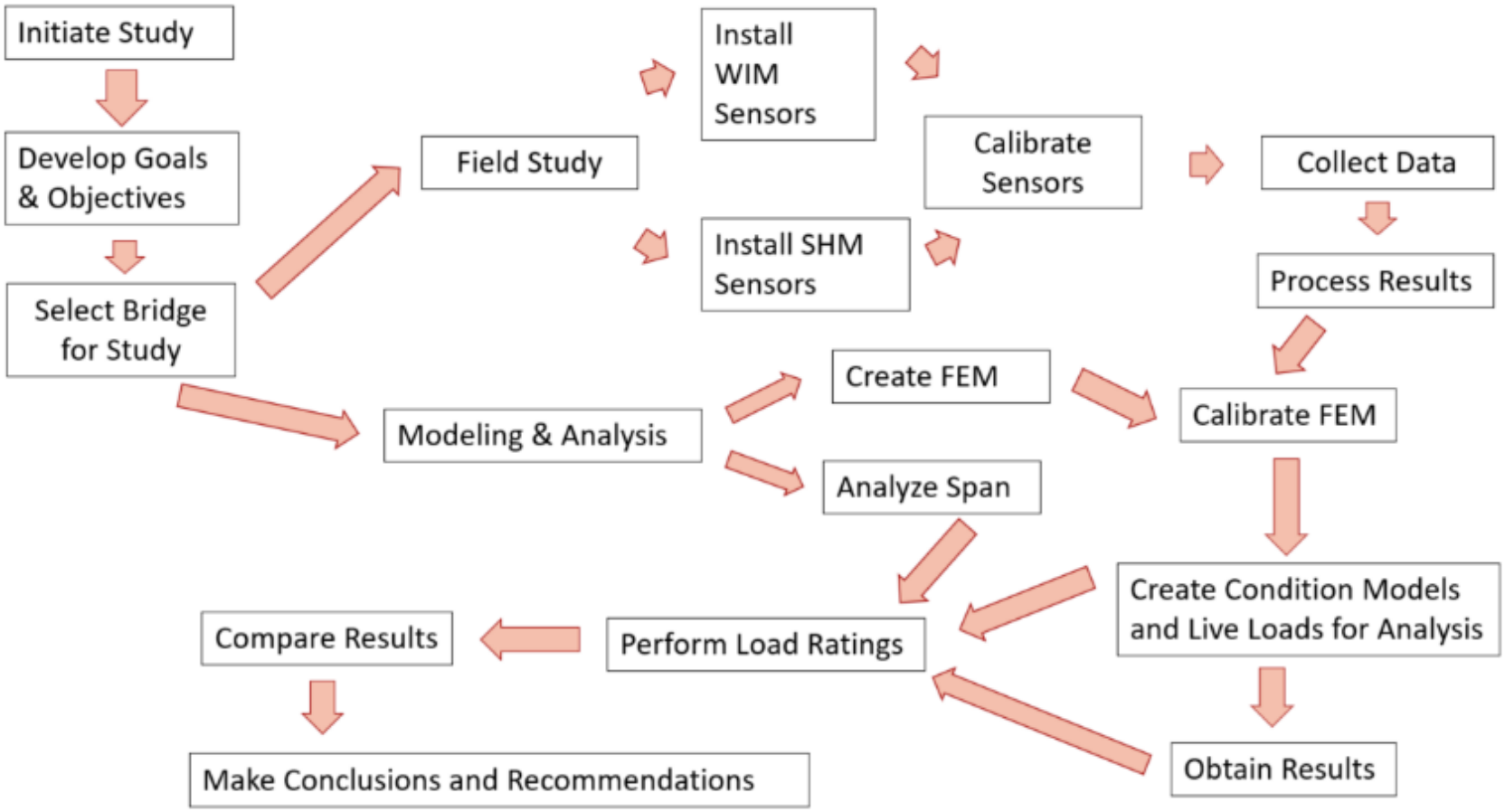

Figure 1.3 - Flow Chart for Proposed Analytical Study

Based off the flowchart in Figure 1.3, the objectives of this dissertation are as follows:

1. Perform a Field Study at a selected bridge which will include the following;
    a. Install Weigh-in-Motion (WIM) Sensors and gather experimental data pertaining to daily truck traffic and their respective weights.
    b. Install Structural Health Monitors at a specific location on a complex bridge and gather experimental data.
2. Perform an Analytical Study which will include Modeling and Analysis. Included under this objective will be the following:
    a. Develop a Finite Element Model
    b. Perform an analysis of the structure and determine its resistance/capacity using traditional design methods.
    c. Calibrate the FEM to the data obtained from the field.
3. Develop a Site Specific Live Load Factor using the WIM Sensors.
4. Develop Load Ratings under LRFR and LFR and Compare results.
5. Develop a Procedure for Evaluation of Complex Bridges

1.5 – Organization of Thesis

This dissertation will include seven chapters. This is done in order to achieve the objectives outlined above. The dissertation is broken out as follows:

Chapter One introduces the problem at hand, provides background, and outlines the objectives of this dissertation. Additionally, this chapter provides a breakdown of each of the chapter provided in this dissertation.

Chapter Two summarizes a literature review. This literature review covers all applicable work related to the research at hand. Since the nature of this work is extensive, the chapter is

broken into sub-topics each related to one of the objectives achieved as a part of this dissertation. Additionally, this chapter also provides background on the bridge in which we will analyze as a part of this dissertation.

Chapter Three offers an overview of each of the existing load rating methodologies, as well as, a comparison of each of the methods.

Chapter Four reviews the entire experimental program undertaken as a part of this dissertation. This chapter will include the installation of both the WIM sensors and the Structural Health Monitors (SHM), as well as, overview of each of their respective data collection and processes.

Chapter Five evaluates the resistance model and analysis. This chapter will cover the development, calibration, and live load models considered in the development of the finite element model. It will also cover the traditional methods performed to develop the resistance model as well. Finally, this chapter will cover how the effects of corrosion were considered into a prediction model.

Chapter Six provides the results from the experimental study for both the WIM and SHM. Secondly, it will discuss the results obtained from the FEM, and provides results calculated using the various load rating methodologies. Within this chapter there will also be a discussion on each of the results obtained.

Chapter Seven summarizes the above results, offers conclusions of the comparison outlined above, and provides a procedure for the evaluation of complex bridges, in which owners can utilize at their structures.

CHAPTER 2

LITERATURE REVIEW

2.1 - Introduction

The purpose of this dissertation, is to evaluate the current methods for load rating a bridge and develop a methodology for the evaluation. This comparison is specific to complex bridges in order to better improve the current AASHTO Manual for Bridge Evaluation. To achieve this, the project focuses on complex deteriorated structures in hopes to understand a member's structural capacity near the end of its service life, as well as, following rehabilitation. This literature review will focus cover all aspects of this dissertation. These topics include evaluation of bridges/structures, Weigh-In-Motion analysis, Structural Health Monitoring, and structural reliability. This review will also provide background on the bridge analyzed as a part of this study, Monmouth County Bridge S-31 (the Oceanic Bridge).

2.2 - Background

The concept of structural rehabilitation is not a novel topic for structural engineers. Engineers, as early as middle ages, have performed investigations to evaluate why a structure has failed, and what one can do to fix it. Today, engineering agencies from the federal to local levels, dispatch teams to investigate structures to provided them with best management reports on how to handle them going forward.

In addition, the concepts of rehabilitation, redundancy, deterioration, resiliency, and understanding the capacity a structural member are not new but are continually being refined. With the development of weigh-in-motion technology; structural health monitors such as strain

transducers and accelerometers; and finite element modeling programs; engineers can have been able to explore how a structure which meets or exceeds its service life continues to stay in service. Furthermore, researchers can now further delve into the concepts of structural redundancy a concept still somewhat theoretical.

Various examples of complex structures include the Pulaski Skyway, Brooklyn Bridge, Manhattan Bridge, George Washington Bridge, Outer Bridge Crossing, and the Newark Bay Bridge. For example, the Pulaski Skyway (See Figure Below) is during several rehabilitation projects with a lack of funding to meet all the needs for rehabilitation. To repair the most critical areas, a series of in-depth hands-on inspections needed to take place to prioritize the most critical repairs.

Figure 2.1 - Pulaski Skyway River Span

Similarly, the Outer Bridge Crossing, Brooklyn Bridge, and Manhattan Bridge are continuously under repair to stay ahead of the curve. The Newark Bay which services some of heaviest traffic in northeast New Jersey, will need to be replaced in the next decade. While the George Washington Bridge, which carries the highest ADT of any bridge in the country, must be

continuously monitored and maintained, as a massive shutdown of any kind tends to cause major traffic implications.

What these bridges have in common is not just the massive ADT, but also a great deal of economic impact as well. Shutting down the Outer Bridge would close off a major route into Staten Island, its ports, and subsequently Brooklyn and New York City. The Newark Bay is in the heart of the port system and directly adjacent to Newark International Airport making it a vital link. While most obviously, the closure of the George Washington, Brooklyn or Manhattan Bridge would close one of several routes into New York City, the economic hub of the United States.

2.3 - Monmouth County Bridge S-31 (The Oceanic Bridge)

The Oceanic Bridge, shown below, is the largest owned and operated by the County of Monmouth, and has been their greatest challenge to maintain and replace. The bridge spans the Navesink River and connects the Township of Middletown to the Borough of Rumson.

Figure 2.2 - Bridge S-31, the Oceanic Bridge (Aerial View Looking East)

A complex structure, the Oceanic Bridge (S-31) was originally constructed between 1939 and 1942. The Oceanic provides a critical link to eastern portion of Monmouth County, as it delivers one of only three routes in and out of the area. A map provided by google maps shows that for this area of Monmouth County there are only two other bridges which provides system linkage, Monmouth County Bridge S-32 and NJDOT's State Route 35.

Figure 2.3 – Map of Rumson/Sea Bright and Middletown (google maps)

The bridge is classified as a complex structure due to its movable span (See Figure 2.4). The span is a dual leaf bascule span configuration, which is supported by two massive piers. To further support the movable span, two anchor or flanking spans which are simply supported tie directly into the trunnion system which gives the span enough structural support to operate. This span was recently rehabilitated in 2011 due to its deteriorated nature.

Per the 2017 NBIS inspection report, Bridge S-31 has an overall span length of 2,712 feet with an overall width of 40.2 feet. The bridge consists of 57 spans total and are a combination of 40 reinforced concrete approach spans, followed by 16 steel deck girder approach spans with a

movable dual leaf bascule span in the center. The bridge is founded on reinforced concrete piers, which are supported on timber piles (2017 NBIS Inspection Report).

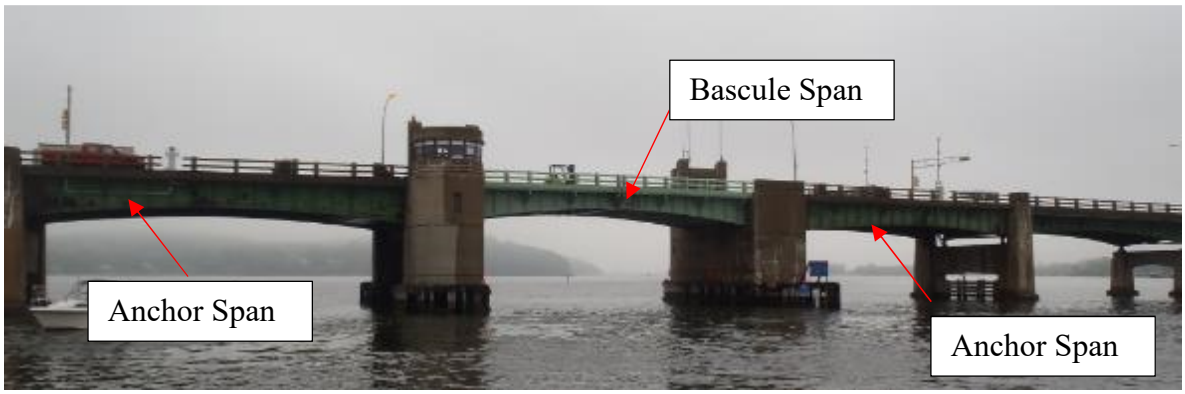

Figure 2.4 - Oceanic Bridge Main Bascule & Anchor Spans

The bridge is a popular route for many of the residents in the area as it connects Navesink River Road to Rumson. When shut down for maintenance, the detour route for the bridge is 12 miles long which creates massive system linkage issues (Figure 2.5 - Green and Red Lines).

Figure 2.5 - Approved Detour Route for Oceanic Bridge

Per the 2017 NBIS inspection report, the overall physical condition of Bridge S-31 is classified as Serious due to the condition of the superstructure, with and overall condition of Critical due to low inventory ratings (2017 NBIS Inspection Report). The bridge is subject to a multitude of priority notices and has a sufficiency rating 23.0 making it a high priority for replacement. The bridge is required to be posted for 15 tons due to the condition of the floor beam at one of the steel spans.

Due to a combination of exceeding its service life, lack of adequate funding, and the environment in which it exists, the Oceanic Bridge has had to undergo a series of rehabilitation projects dating back to the 1970's. Since 2005, the County has had to implement multiple repair contracts for the bridge including the following:

- Repairs to the concrete deck due to spalling in 2008 and again in 2015.
- Rehabilitation of the bascule span and underpinning the pinion Supports in 2011.
- Replacement of the traffic gates and live load anchors in 2013.
- Underpinning and rehabilitation of the southern trunnion support columns in 2015.
- Rehabilitation to the floor beams at Spans 28 and 30 in 2015.
- Structural steel repairs to secondary and main load carrying members in 2015.
- Spall repairs to the concrete pier caps which support the reinforced concrete t-beam approach spans in 2016.
- Rehabilitation of Pier 18 which supports an approach structural steel span in 2016.
- Fiberglass jacketing of over 50 concrete piles which support the reinforced concrete t-beam approach spans in 2016.
- Various mechanical evaluations and miscellaneous repairs to the mechanical system which operates the bascule span.

- Various electrical system evaluations and miscellaneous repairs to the electrical system which powers the bascule span.

The bridge is currently posted for 15 tons, and in relatively repaired condition with no serious defects requiring priority repairs.

However, in 2013 the flanking/anchor spans needed dire repair. This was documented in the NBIS inspection report prepared in 2013 by S&R Engineer's Inc. of Hamilton, NJ. During this inspection, the bridge was classified as Critical due to the low inventory ratings and serious due to the condition of the superstructure. The report also included two emergency priority notifications for immediate action.

These notifications pertained to the floor beams for the two flanking spans (Spans 28 and 30). Notifications were issued because the main floor beams had exhibited section loss up to 100% and these displays were widespread throughout both beams. Shown in the below figure, the floor beams fall directly underneath the finger joint between spans and is directly above Piers 28 and 30.

As we can see from Figure 2.6, the section loss is so severe that it appears the load path had been compromised and was being transferred to the supporting bearings via the steel stiffening angles. Given that the floor beam was directly above the pier, it made the beam susceptible to shear. Furthermore, the anchor span ties directly into the main bascule span, and failure of this span would directly affect the movable span.

Figure 2.6 - Span 28 (Looking Northwest) Floor Beam 2013 Condition

Given this information, S&R also issued the emergency priority notice where they advised the County that this floor beam could not withstand more than 5 tons due to shear; the bridge would need to be posted for this while plans were in development. These notifications led the County to develop emergency replacement plans, which were implemented by George Harms Construction during the winter and summer of 2015.

The repair plans included concrete repairs to the bridge deck, as well as, steel repairs throughout the entire structure, with repairs to Spans 28 and 30 being the most critical area of concern. During construction, the scope increased to include additional steel repairs, as well as, repairs to the southern trunnion steel supports, which were also found to be in critical condition. Figure 2.7 shows an in-progress photo of the floor beam at one of the flanking spans being repaired.

Figure 2.7 - Floor Beam at Anchor Span Mid-Repair

As we can see from the above photo, the method of rehabilitation involved the contractor retrofitting the existing floor beam with new plates and stiffeners. Considering the roadway needed to be open to traffic each morning, the contractor was only allowed to replace rivets one panel at a time and need to secure the area before each morning. Additionally, new angles were installed to add to the rigidity of the member. The figure below shows the completed repaired member. This repair addressed the issues noted in the 2013 emergency notice and as such, the posting was adjusted back to 15 tons.

Figure 2.8 – Span 28 (Looking Northeast) Floor Beam 2016 Condition

While the County over the years has addressed serious concerns as they have developed, due to limited funding, it is important to note that not all the bridge concerns have been addressed. Areas still in need of repair include the following per the 2017 NBIS Inspection Report:

- Structural steel members which exhibit signs of corrosion and section loss.
- Bearings which support the steel superstructure which are completely frozen.
- The concrete bridge deck and sidewalk needs complete replacement/rehabilitation.
- Concrete piles which support the reinforced concrete t-beams to be repaired.
- Pier caps which support the reinforced concrete t-beams in need of spall repairs.
- Complete replacement of the fender system.
- Replacement and upgrade of the submarine cables.
- Upgrades and repairs to the mechanical system.
- Upgrades and repairs to the electrical system.
- Rehabilitation of the southern bascule pier.
- Repair to the bearings which supported the suspended steel approach spans.
- Rehabilitation to concrete piers which support the approach steel superstructure.

It is important to note, that the above defects are not critical and have not been addressed since the County has now engaged in a process to replace the bridge in its entirety. Per the NBIS inspection report, the cost to replace the bridge will approximately be $120 million. Fortunately, due to the condition of the structure and the bridge's SI&A rating, the Oceanic is eligible for federal funding seeing how the County has insufficient funds. In the meantime, the County will continue to monitor and inspect the bridge and make repairs on an as-needed basis while final plans for replacement are developed. Therefore, prioritization of essential repairs to this structure is essential.

2.4 - AASHTO Manual for Bridge Evaluation

A primary reference of this dissertation will be the 2018 AASHTO MBE, specifically Section 6, as this is the standard code currently used to evaluate all types of bridges. Section 6 focuses primarily on how to load rate a structure. This is covered under two parts, Part A which reviews the LRFR method and all its related code provisions, and Part B which reviews the LFR and ASR methods, and its related code provisions.

The 2018 AASHTO MBE, currently outlines a descriptive procedure for load rating a member, or series of members using the Load and Resistance Factor Rating method (LRFR), a focus of this dissertation. This method is utilized, as it is a reliability-based method, and is the current standard used for the design of newer bridges. This is achieved utilizing the main equation below:

$$RF = \frac{C - (\gamma_{DC})(DC) - (\gamma_{DW})(DW) \pm (\gamma_P)(P)}{(\gamma_{LL})(LL + IM)} \qquad (2.1)$$

(6A.4.2.1-1)

Where:

- C is the capacity of the member evaluated and determined based off:

$$C = \varphi_c \varphi_s \varphi R_n \qquad \text{(6A.4.2.1-2)} \qquad (2.2)$$

Additional variables include:

- DC which is the dead load on the member
- DW is the wearing surface (if applicable)
- P are other permanent loads (if applicable)
- LL+IM is the live load in which the member is being evaluated on.

As stated previously the MBE under subsection 1.5 defines complex bridges as the following:

> "Movable, Suspension, cable stayed, and other bridges with unusual characteristics" (2018 MBE subsection 1.5).

Regarding the evaluation of these type of bridges, the MBE specifically under subsection 6.1 describes the following regarding complex bridges:

> "Ratings of long-span bridges, movable bridges, and other complex bridges may involve additional considerations and loadings not specifically addressed in this Section and the rating procedures should be augmented with additional evaluation criteria where desired" (2018 MBE, Subsection 6).

No additional information is offered under the commentary in this section. However, additional information regarding the evaluation of complex bridges is offered under subsection 6.1.6 (Evaluation of Complex Structures).

> "The computation of load-carrying capacity of complex structures, such as suspension bridges, cable-stayed bridges, and curved girder bridges, may require special analysis methods and procedures. General guidance is available in this manual but more complex procedures must be used for the actual determination of load rating" (2018 MBE, Section 6.1.6).

Under the commentary of this section, it specifically states that evaluation should occur on a member-by-member basis, and that the definition is consistent with NBIS Standards. Additionally, the commentary states that if a bridge is not covered under the AASHTO LRFD bridge design manual then a conservative approach must be followed. Following this, the MBE

goes directly into the equations and the different evaluation methods one can utilize when load rating a bridge.

Based on review of the criteria above, the MBE leaves the evaluation of complex bridges open ended. This is generally due to the varying multifaceted nature of these structures. This establishes the need for a procedure for evaluation, especially complex bridges in a deteriorated state. This procedure will aid in prioritizing areas of repair, as well as, give owners a better understanding of their structure.

Included in Part A for the LFR, are additional provisions in which an engineer can utilize when evaluating a member. These include the use of refined analysis or finite element modeling, the use of a site-specific live load factor based of weigh-in-motion data, and the use of field testing as means to determine the rating factor of a member. These provisions are not included under Part B which pertains to the LFR or ASR. These two other procedures in which one can load rate a bridge; the Load Factor Rating and the Allowable Stress Rating can be utilized to load rate an older structure not originally designed using LRFD. A more detailed comparison is provided in Chapter 3 of this dissertation.

2.5 - Condition and System Factors

To better understand the load rating equation, we must investigate the background of each of its variables. To achieve this, we look to Equation 6A.4.2.1-2. This equation provides us with the capacity of the member being rated. The capacity is determined by finding the nominal resistance and applying a system and condition factor to it. Regarding condition, the MBE states the following:

> "The condition and extent of deterioration of structural components of a bridge should be considered in the computation of the dead load and live load effects when stress is chosen as an evaluation approach and for the capacity when the force or moment is chosen for use in the basic rating equation." (AASHTO MBE, Section 6).

Currently, these values per Section 6 of the MBE are capped at 0.85 combined. This has been determined based of reliability studies performed but are not always indicative of what is being seen in the field. When looking at the system factor, one immediately thinks of redundancy. The system factor, is specifically created to take the redundancy of a structure into account. When looking at the Oceanic Bridge, one key reason the structure is still in service is in large part due to its structural redundancy.

NCHRP Report 406 defines bridge redundancy as "the capability of a bridge structure to carry loads after the damage or failure of one of its members" (NCHRP Report 406, 1998), with failure being either brittle or ductile. While the study focuses on failure, the concept of a damaged member and its comparison to a deteriorated member can be argued to be one in the same.

When dealing with the condition factor, one immediately thinks of deterioration in the form of corrosion. As we know, corrosion is one of the leading issues which affects the condition of a structure, especially steel. As defined in Corrosion Engineering by Mars Fontana, corrosion is classified as a "destruction or deterioration of a material because of its reaction with its environment and can be either fast paced or extremely slow" (Fontana, 1986). Fontana also defines eight total forms of corrosion which include: "(1) uniform, or general attack; (2) galvanic, or two metal corrosion, (3) crevice corrosion; (4) pitting; (5) intergranular corrosion;

(6) selective leaching or parting; (7) erosion corrosion; and (8) stress corrosion." (Fontana, 1986).

Additionally, Czarnecki and Nowak (2008) state that there are several forms of corrosion which exist which attack steel, each which attack metal in a different way. Of these types of corrosion, the most common to attack bridges is uniform corrosion, crevice corrosion, stress corrosion and pitting. The results of these types of corrosion are general section loss, pack rust, and isolated holing through of a member. The end results in a reduction in overall capacity and serviceability of a member. Currently, the effects of corrosion are accounted for in the condition factor which has a minimum limit of 0.85. This correlates directly to the FHWA coding guideline which means that the member has a condition factor of 4 (minimal acceptable limit) or less. It should be noted the MBE does have provisions for cases which section loss is severe in which the engineer is to use judgment in calculating the resistance of a member.

Despite this, the way in which corrosion and section loss is accounted for is a subjective way of applying this factor as you are relying on the accuracy of the inspection team and the opinion of the evaluator. Czarnecki and Nowak discuss the effects of corrosion and agree that a time versus penetration curve is the best way to predict and analyze it (Czarnecki and Nowak, 2008).

Under a reliability-based study performed by Kayser and Nowak, they were able to conclude that the resistance of a steel bridge could be evaluated, predicted and measured using models based on the rate and location of corrosion. This was achieved analyzing a typical steel structure and was concluded that safety could be measured based on the slenderness of the member (Kayser and Nowak, 1989). It defines clearly that as corrosion increases an I-Beam which supports the superstructure is more susceptible to buckling.

Darmawan's 2013 Time Dependent Reliability Analysis of Steel is another study which is related to the subject of corrosion is. In the study, he proposed that steel bridges close to the sea cannot escape corrosion, and that steel bridges are more vulnerable to corrosion as they are susceptible to chloride attacks. Corrosion would be classified as a form of damage which would in turn affect its redundancy and overall capacity (Darmawan, 2013).

While these two studies do not play a direct role in this dissertation, it is important to understand the existing research about corrosion as it relates directly to the condition of a bridge. Darmawan, as well as, Czarnecki and Nowak, both cite a prediction model developed by Komp in 1987. This is shown below as referenced in Darmawan's study.

$$C = At^B \quad (2.3) \text{ (Darmawan, 2013))}$$

Where:

C = average corrosion penetration in μm

t = number of years

A and B are taken from a table shown below which compares various corrosion model parameters based on type of steel and environment.

Table 2.1 - Corrosion Model Parameters (Darmawan, 2013)

Environment	Unprotected carbon steel		Weathering steel	
	A	B	A	B
Rural	34.0	0.65	33.3	0.50
Urban	80.2	0.59	50.7	0.57
Marine	70.6	0.79	40.2	0.56

NCHRP Report 406, proposes that to ensure the safety of a structure for public use, structures need to be designed to accommodate and sustain these damages, and still operate at a

reduced capacity. It also proposes that a bridge can be deemed safe it if provides one or all of the following:

- Provides a reasonable safety level against first member failure
- Provides an adequate level of safety before it reaches its ultimate system capacity under extreme loading condition
- Does not produce large deformation under expected heavy traffic loads
- Can carry some traffic loads to or loss of a component (NCHRP Report 406)

Further Report 406 also defines several limit states in which a structure may see these include the following:

- Member Failure
- Ultimate Limit State
- Functionality Limit State
- Damaged Condition Limit State (NCHRP Report 406, 1998)

Member failure is defined by the report as "a check of the individual member safety using an elastic analysis and member capacity as defined by current specifications" (NCHRP Report 406, 1998). While damaged condition limit state is defined as "the ultimate capacity of the bridge system after the removal of one main load-carrying component from the structural model" (NCHRP Report 406, 1998). Like load ratings, Report 406 performs a reliability-based approach to analyze the equations presented in the report. (NCHRP Report 406, 1998)

Much of what is included in Report 406 is taken from NCHRP Report 301 (Load Capacity Evaluation of Existing Bridges, 1987). This report presents the basis for the current load rating methodology, and a detailed look into how to properly evaluate an existing bridge. It also performs a review of the 1980's Manual for Bridge Evaluation and proposes the use of weigh-in-

motion data, mixed with field performance data to provide a detailed evaluation of a structure in its existing condition. While most of the report presents information that has now become the basis of our design codes, one of the more important contributions the report makes in relation to this report is the inclusion of a flowchart which gives us the evaluation process.

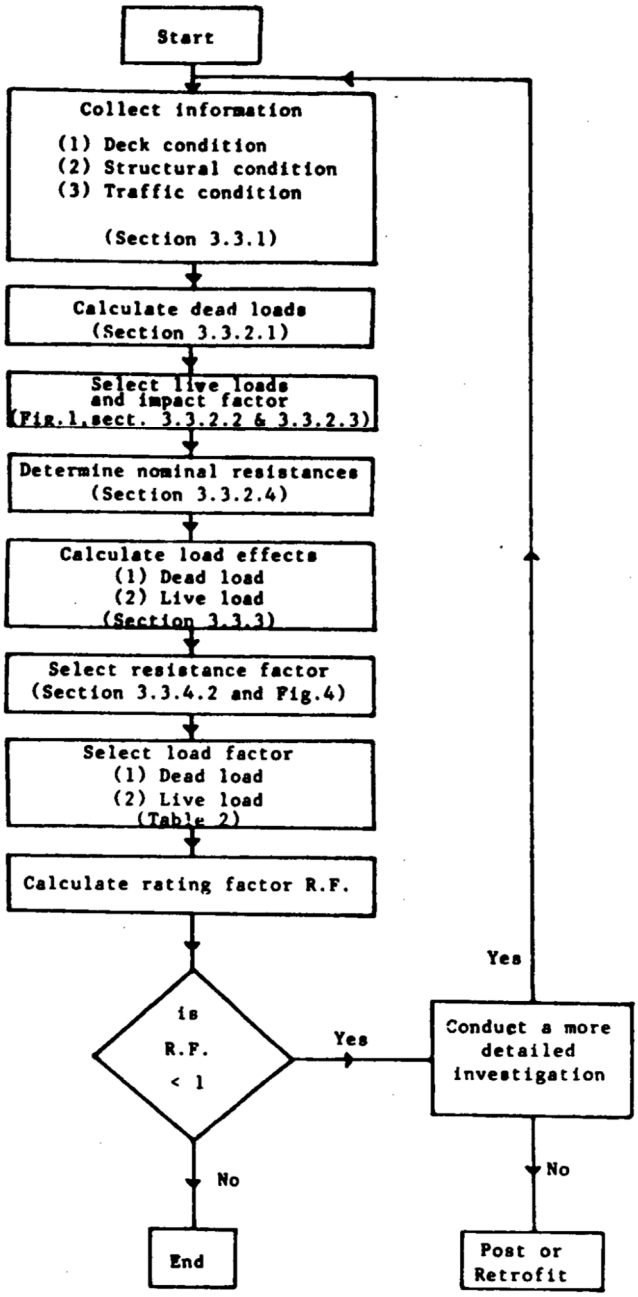

Figure 2.9 - Flowchart to evaluate an existing structure (NCHRP Report 301, 1987)

Given the information provided by these reports, many engineers have utilized strain gauges and WIM sensors to evaluate bridges for various means. What this dissertation proposes in contrast to the others is it will take all available methods to evaluate a member or a span and combine them. In addition, it evaluates members previously rehabilitated giving us more insight on how a structure will react to various loads once repaired utilizing standard industry methods such as re-establishing loss section with plate members. This method relies on some of the most basic concepts learnt in statics, as well as, mechanics of materials.

2.6 - Load Rating Methodology

One of the main topics this dissertation will explore is the effectiveness and accuracy of current load rating methods. This will be done comparing the LRFR method to the LFR method. As we are aware, a load rating is the common practice used by the industry to evaluate a structure. These ratings dictate the priority of replacement, identify areas for repair, and determine whether a bridge needs to be posted or not.

Gao's "State of Practice for Load Rating Highway Bridges" in the United States presents a detailed review of the current Load Rating procedure for bridges. In this paper Gao provides valuable insight into the current practice, its issues, as well as, other key statistics to consider. One key portion of the paper is an explanation of the LRFR method, which FHWA is trying to promote. Gao states that:

> "Load Ratings are not only essential to ensure public safety but also important for bridge maintenance, management, and operation. Lack of a correct load rating or lack of a weight limit posting could allow heavier vehicle that exceed the bridge's load capacity to cross a bridge and might cause severe structural damage or collapse of a bridge." (Gao, 2013)

In the paper, Gao explains the methodology for both inspecting and rating a bridge. It is explained how various members are rated on a scale from 0 to 9 to prioritize areas of repair or replacement, and how the NBI database managed by FHWA generates lists of bridges eligible for replacement. A key figure is provided below:

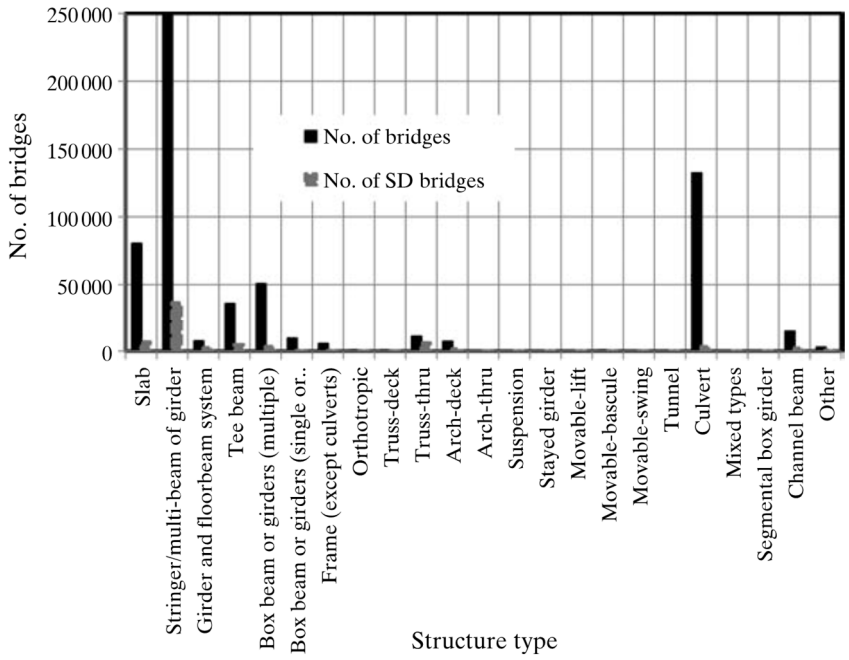

Figure 2.10 - NBI Statistics (Gao, 2013)

As we can see from Figure 2.10, both Stringers/multi-beam of girder are not only the most common type of bridge, but also contain the highest number of Structural Deficient Bridges. This figure provides us with key insight of a global view of the United States, bridge inventory. Based on this data, FHWA is looking to maintain the condition of its infrastructure by maintaining a “state of good repair”. The report also reviews the fact that all load ratings must be performed in accordance with the AASHTO MBE, something this project will utilize substantially. This report also indicates that bridges must be re-rated whenever a change in structure or traffic condition happens.

Additionally, Gao indicates that per an evaluation performed by FHWA from 2007 to 2010, not all bridges which require load postings are posted in accordance with NBIS procedures. Again, this is a serious issue as it could cause severe damage or collapse.

The report also includes valuable information on the various load rating methods. Per Gao, the ASD and LFD load rating methods are un-calibrated and based off pure engineering judgment. Something to consider when analyzing the Oceanic. It promotes the use of LRFD/LRFR which is a reliability-based design code with factors developed off probabilistic models and based off a limit state function.

To further understand the LRFR methodology, it is important to understand that the LRFD was calibrated for a reliability safety index of 3.5. Additionally, because we have an inventory and operating rating, the operating reliability safety index is reduced to 2.5, to "balance safety and economy" (Gao, 2013).

The paper also discusses key factors used in the rating equation, such as the condition and system factor; the system factor is defined to account for the level of redundancy. While the condition factor is defined as a factor to account for increased uncertainty in the capacity of the deteriorated member and ranges from 0.85 to 1.0.

2.7 - LRFR versus LFR

Due to the existence of multiple evaluation methods, main objective of this dissertation will be dedicated to comparing the LRFR Code to the LFR Code for Load Rating. NCHRP Report 700 written by Mlynarski, Wassef, and Nowak, provides a comparison of the LRFR methodology to the LFR methodology for a sample of 1,500 bridges.

This multi-level comparison was performed on a variety of bridges in which each member was load rated in accordance with the two methods. However, this was not done via

experimental field study only an analytical study was performed. Additionally, this study was only performed on standard type bridges (i.e. simply supported, continuous, etc.) not complex type structures. The goal of the study was to accomplish the following:

- Determine key differences between the two codes
- Develop refinements to the load rating process.
- Explain changes in truck weight restrictions to the public.
- Refine the LRFR code and modify the MBE as required. (NCHRP Report 700, 2011)

For the study, bridges were load rated using BRIDGEware^{tm} for both LFR and LRFR in shear and moment. 12 different vehicles were ultimately used for the study including HS-20, HL-93 and the three AASHTO legal loads (Type 3, 3S2, and 3-3) the remaining vehicles were taken from the various states used for the study. A total sample of bridges were taken from various states throughout the United States via a survey, a complete list is shown in Table 2.2.

Table 2.2 - AASHTO Database used for (NCHRP Report 700, 2011)

State/Agency	# of AASHTO Data Sets
Alabama	3,139
Illinois	3,232
Michigan	378
Missouri	4,644
New York	5,412
Oklahoma	44
South Dakota	1,135
Tennessee	53
Total	18,037

From this list of over 18,000 bridges, 1,500 were extracted trough a selective process which resembled the cross section of the NBI data base and had specific type bridges, the researchers were interested in. Bridges were also broken down into a histogram by year built shown in the below figure. As we can see from the graph the largest groups of bridges were built between 1960 and 1980 meaning many of these bridges have already hit their intended design service life. This is important as most of bridges study will have most likely seen some form of deterioration in one form or another. Furthermore, these bridges were built under a different code from LRFD, giving us a good idea on how they compare when measured against those standards. This histogram is helpful in this project, as the Oceanic was built around 1940 which is represented by 6.37% of the data above.

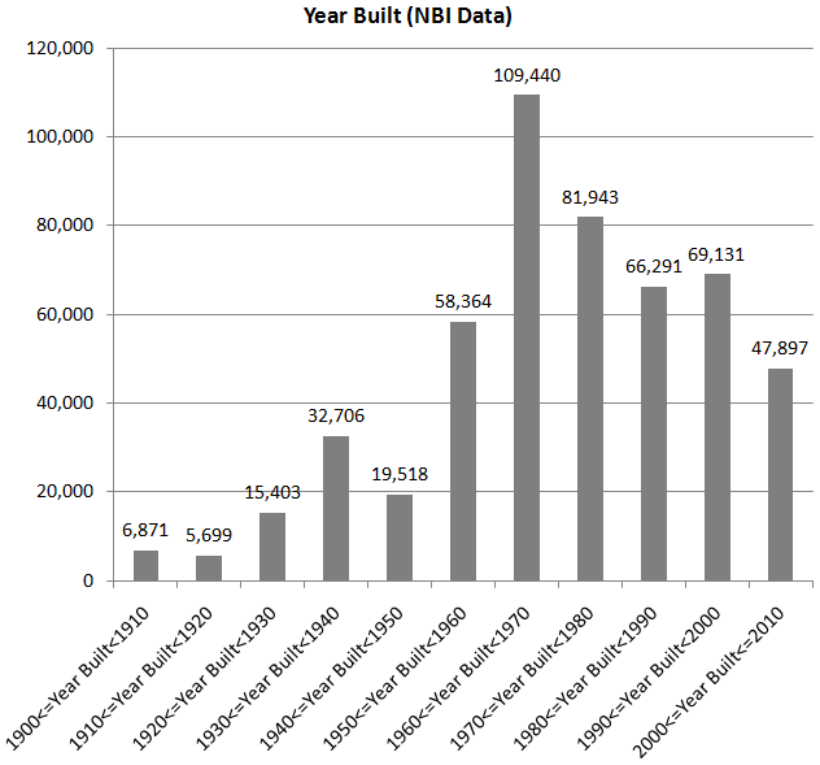

Figure 2.11 - Bridge Age Histogram (NCHRP Report 700, 2011)

To further assess the different configurations and materials Table 2.3 was developed to classify each girder type. As we can see the largest number of members tested for this were simple span steel girders.

Table 2.3 - Girder type tested and number of girders (NCHRP Report 700, 2011)

Girder Type	*Number of Girders*
Simple Span Steel	1037
Simple Span Prestressed Concrete I	467
Simple Span Prestressed Concrete Box	377
Simple Span Reinforced Concrete T-Beam	295
Simple Span Reinforced Concrete Slab	99
Continuous Span Steel	418
Continuous Span Reinforced Concrete Slabs	105
Continuous Span Prestressed I	238

In total 73,000 test runs were made for this study using the BRASS engine software. Assumed target reliability indices were inputted in accordance with current MBE standards, and members were load rated for each of the following modes of failure:

- Moment-Inventory/Operating
- Shear-Inventory/Operating

Once the data had been computed and the testing was run, main sources of differences between the LFR and LRFR were determined. However, based on the comparison it was expected that the LRFR loads were expected to be 20% to 40% higher than LFR. Other key differences included the following:

- Differences in the factored live load for the LRFR which were greater than the LFR for both moment and shear. This is important as this means that inherently the LRFR rating factors would be lower than LFR factors.
- Atypical bridge characteristics such as girder spacing, different abutment skew angles, or sidewalks gave significant differences between the two methods.

- When stiffeners were not included for steel girders the shear values appeared to control. Once included it appeared that ratings were generally lower since the LFR did not include this criterion. (NCHRP Report 700, 2011)

Upon further analysis across the board it was determined that LFR yielded higher values than the LRFR values. The table below illustrate these comparisons for simple span steel structures

Table 2.4 - Simple Supported Steel LRFR vs. LFR Comparison (NCHRP Report 700, 2011)

LRFR/LFR Range	Moment				Shear			
	LRFR		LFR		LRFR		LFR	
	No. of Girders	% of Total Inventory (1037)	No. of Girders < 1.0	No. of Girders > 1.0	No. of Girders	% of Total Inventory (1037)	No. of Girders < 1.0	No. of Girders > 1.0
0.0-0.09	0	0.0%	0	0	9	0.9%	0	9
0.1-0.19	2	0.2%	2	0	42	4.1%	0	42
0.2-0.29	15	1.4%	1	14	25	2.4%	0	25
0.3-0.39	10	1.0%	2	8	17	1.6%	0	17
0.4-0.49	35	3.4%	9	26	7	0.7%	0	7
0.5-0.59	12	1.2%	6	6	8	0.8%	0	8
0.6-0.69	17	1.6%	10	7	5	0.5%	0	5
0.7-0.79	49	4.7%	38	11	4	0.4%	0	4
0.8-0.89	96	9.3%	77	19	0	0.0%	0	0
0.9-0.99	50	4.8%	48	2	0	0.0%	0	0
> 1.00	59	5.7%	59	0	0	0.0%	0	0
Total	346		252	93	117		0	117
Average LRFR/LFR	0.98				0.65			

As we can see from the table above when comparing the two side by side shear yields more conservative values than moment, but both are more conservative in comparison to the LFR method. This is mainly due to the introduction of various factors, such as the system and condition factor, and increase live load factors in relation to a higher safety index.

2.8 - Development of the Live Load Factors

The LRFD design code was initially developed mainly off a study performed by Nowak in 1993. In this study, Nowak used weigh-in-motion data to perform a statistical analysis and develop a live load and dynamic load model for a 75-year service life for various bridges. Nowak

proposes many of the factors used in the LRFD including multi-presence factors, lane loads, and the girder distribution factor. This was further developed in 1995 when the LRFD code was calibrated (Nowak, 1995). Per this review, Nowak proposed the following LRFD code calibration procedure:

1. First, a selection of representative bridges commenced. For this, 200 bridges of various spans, widths, materials, and from various geographic regions around the United States were selected to present a well diverse group. Emphasis was placed on newer type structures, so a proper 75-year service life model could be developed.
2. Using surveys and the establishment of weigh-in-motion sensors in various locations, data was gathered to model the live load on various structures.
3. Using the data gathered above, cumulative distribution functions were derived for both the load and resistance models. This was done for various options and configurations.
4. Using the models from part 3, develop an iterative reliability analysis procedure to determine a reliability index measured in β.
5. Selection of a Reliability Index Target based off the above to provide a value to provide "consistent and uniform safety margin for all structures"
6. Calculation of Load and Resistance factors so that the target value of β is met. (Nowak, 1995).

This study was essential as it laid the groundwork for many of the calibration studies performed today. Additionally, the LRFR load rating method, as well as, continued modifications to the LRFD code are made using this procedure.

2.9 - Structural Health Monitoring

One key piece of this dissertation will focus on the use of strain gauges and accelerometers, as they are essential in understanding the true capacity of a member. For this dissertation, a field study will be performed on Bridge S-31 in which SHMs will be attached to the anchor span to gather field data and determine the capacity of the structure. Further information on this is provided in Chapter 4.

For Structural Health Monitoring, Seo et. al provided an up to date summary review of SHM applications for highway bridges. This paper was helpful as it reviewed specific literature on the use of strain transducers and accelerometers. Per their review, it was concluded that a large number of studies considered damage detection, but only a small number devoted their study to structural capacity or projected remaining service life (Seo, 2014).

The review concluded that when SHM was used to compare load rating methods to field studies; load ratings were found to always be more conservative than field measurement tests. In the various studies reviewed, FEM modeling was intertwined with field testing, and in some instances, WIM data was used to further calibrate the model (Seo, 2014).

Seo concludes that for structural capacity studies, load ratings are the traditional method of comparison. Additionally, field tests are validated using finite element models. Key conclusion made is that a "significant gap found from the review is combining the features to automated finite element updating methods for estimating current structural capacity of existing bridges following the bridge design codes." (Seo, 2014).

Sanayei et. al in 2015 presented a report which performed a load rating of a fully instrumented bridge by comparing various LRFR reports. In this study, they take a typical three-

span continuous bridge shown below with steel girders and use strain gauge measurements and compare them to traditional methods, and a finite element model.

Figure 2.12 - Powered Mill Bridge, Massachusetts (Sanayei, 2015)

The study presents a detailed understanding of how one currently evaluates a structure using NBIS procedures. The bridge tested was the Powder Mill bridge. The Powdered Mill Bridge is a multi-lane structure and was constructed in 2004 for HS-25 Loading. The bridge is a redundant multi-span structure and in relatively good condition. The report presents facts that "diagnostic load test can be performed to monitor a bridge's response to known load conditions" (Sanayei, 2015). It also presents the understanding that the NDT response of a strain transducer gives us an analytical response for comparison to traditional methods.

Strain transducers were attached to each of the girders, shown below, to find the maximum load induced on the structure. This non-destructive test method was compared to traditional methods, as well as, a finite element model. The testing was done in accordance with standard industry practices.

The report uses the load rating equation for LRFR. Rating factors obtained through the NDT were developed using equations provided for by the NCHRP through Non-Destructive

testing means in their 1998 Manual for bridge rating through load testing. In conjunction with the field testing performed, a finite element model (Figure 2.13) was developed for the bridge using given data from the original plans with various assumptions and modifications. These modifications included additional parapet stiffness addition, reduction in concrete stiffness for negative moment regions and updating of concrete strength off testing data.

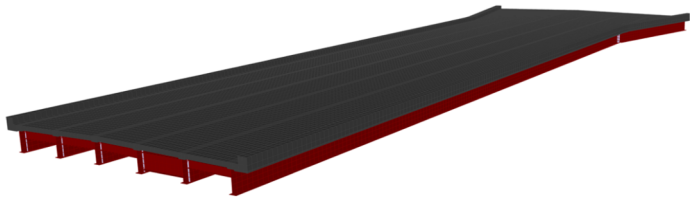

Figure 2.13 - Powered Mill Bridge Finite Element Model, Massachusetts (Sanayei, 2013)

Following the development of the FEM, a comparison of the three methods was performed. Based off this, the following comparison graph was developed.

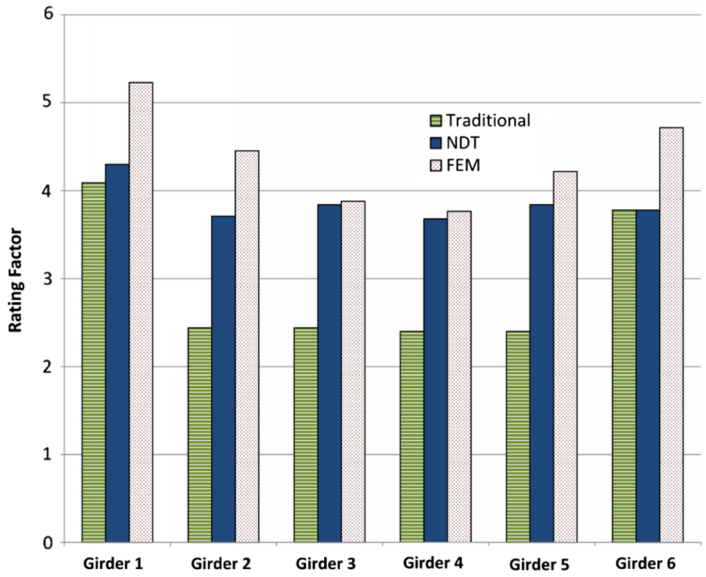

Figure 2.14 - Powered Mill Bridge Comparison (Sanayei, 2013)

As a result of this comparison, Sanayei could make the conclusion that the FEM model presented the most conservative method of obtaining the capacity of a member, and that it

provides a more realistic evaluation of the structural system and its redundancy. It proves that the traditional method provides a more conservative approach, leading to a smaller rating factor.

This study serves as a basis for structural health evaluation to be performed as a part of this project. The assumptions and conclusions made, assist in understanding how to embark on the testing to be performed, and assists in developing preliminary assumptions and hypothesis. However, this study concentrates only on a "new" bridge, it does not account for issues such as corrosion, or non-redundant systems. This study also does not include the use of WIM sensors nor does it compare various evaluation methods against each other. Finally, this study focuses on a normal type bridge and does not include a complex bridge evaluation.

While utilizing the Canadian code for design, Feldman et. al, prepared a similar study for the Red Deer River Bridge in Saskatchewan. For this study, strain gauges were attached to three span continuous reinforced concrete bridge for a two-day period. This test was conducted by using 45 concrete strain gauges to instrument the central span. What is integral about this study is that strengthening was done to the structure in 1989 when external steel was added in areas of high positive movement (Feldman, 2011).

For the study, a total of 135 traffic events were recorded including 31 controlled tests. The girders were evaluated using the CAN/CSA-S6-06 code. Analysis were performed for flexure and shear in accordance with Canadian standards. It was determined by this study that for most gauges yielded capacity results which exceeded the traditional design methods. While this study does include similar elements, it does not include WIM data, as well as finite element model validation and calibration.

Phares and Wipf also performed a study which delves into the use of structural health monitors as a use of load rating a structure for Iowa DOT in 2003. For this investigation, they

used strain sensors provided by BDI and attached them to Iowa Boone County bridge #11. The bridge, was 38 ft - 10in long and was 19ft - 9in wide. The bridge consisted of a timber deck supported by steel stringers (Phares, 2003).

Strain gauges were attached to each of the beams and a loaded tandem-axle dump truck weighing approximately 42 kips (21 Tons) was used as control test to determine the max strain on the girders. Individual members were evaluated using the LFD method for load rating a structure and compared accordingly. Per the investigation, it was determined that the load rating calculations provided a more conservative figure than the field gauges. Meaning, that the bridge had greater capacity than calculated, with ratings on average 42% higher.

This study validated the use of strain gauge sensors as a means of determining the capacity of a structure over traditional load rating calculations. This study however, does not utilize the use of WIM sensors or a finite element model, nor does the study include any information on the condition of the structure and how it was accounted for in this evaluation.

2.10 - Weigh-in-Motion Sensors

The 2018 MBE classifies WIM sensor work under Section 6A.4.4.2.2. The purpose of a WIM sensor experimental study is to determine the appropriate live load factor to be utilized for a structure. Currently, the 2018 MBE contains generalized live load factors which were developed to provide owners with “an acceptable level of reliability” (2018 MBE Section 6A.4.4.2.2).

Under this section it states that if the ADTT can be estimated then modifications can be made. Furthermore, under the commentary, guidelines are given to develop a site-specific live load factor. This is done using a series of equations which in turn determine a site-specific live

load factor. A commonly used practice throughout the United States site specific live load factors are developed off the use of weigh-in-motion sensors at specific locations.

Some examples of development of modified live load factors include Pelphrey et. al's study in 2008. As a part of an agreement with Oregon DOT that team developed and proposed state specific live load factors in 2006. These values are shown in the below table:

Table 2.5 - State Specific Load Factors for Oregon

Traffic Volume	Load Factor	
	LRFR	Oregon-Specific
Unknown	1.80	1.40
ADT$\geq$ 5,000	1.80	1.40
ADT$=$ 1,500	1.67	1.34
ADT$\leq$ 500	1.51	1.30

In their paper, Pelphrey et. al took data four times for a period of two weeks to obtain seasonal variations. Additionally, data was sorted and classified. Once the data had been obtained, using NCHRP Report 454 factors were developed. In 2012 a similar procedure was also implemented in Alabama (Uddin, 2011). In this report WIM data was collected from six locations throughout Alabama to develop state specific live load data. These sites ranged from state to interstate routes with no local roadway data. Despite standard practice, data was gathered over the course of a year in both directions to account for any variations (Uddin, 2011).

This study was conducted in response to the high live load factors used in accordance with the LRFR. The procedure in which the WIM was recorded and sorted from each location was identical to that performed by Pelphrey and in accordance with NCHRP Report 454. As a result, it was concluded that a two-week period is sufficient time to gather data to determine the live load factors, although it must be continuous. In addition, when compared to the LRFR

factors, the factors were found to be 20% lower for legal vehicles and 35% less for permit vehicles.

As the basis for these studies NCHRP Report 454 was published to establish proper protocols for collecting and using traffic data in bridge design. This study pertains mainly to the AASHTO LRFD code and specify guidelines of collecting WIM data to understand truck traffic at a bridge. Sivakumar, et. al propose a procedure for using traffic data in bridge design as follows:

1. Select WIM sites for collecting traffic data for bridge design
2. Quantities of WIM data required for load modeling
3. WIM calibration and verification tests
4. Protocols for data scrubbing, data quality checks and statistical adequacy.
5. Generalized multiple-presence statistics for trucks
6. Protocols for WIM data analysis for one-lane load effects for design
7. Protocols for WIM data analysis for two-lane load effects for design
8. Assemble axle load histograms for deck design
9. Filter of WIM sensor errors/WIM scatter from measured WIM histograms.
10. Accumulated fatigue damage and effect gross weight from WIM Data
11. Lifetime maximum load effect Lmax for superstructure design
12. Develop and calibrate vehicular models (NCHRP Report 454, 2001).

While these steps do not particularly pertain to analyzing an in-service bridge, several do play a role. For instance, protocols on data scrubbing is an important step to develop a realistic load model and determine a site-specific factor.

This was further modified under NCHRP 12-83. During this study, the procedure for gathering weigh-in-motion data was modified to reflect the flowchart shown below. As we can

see, this flow chart provides a simpler form of analysis for scrubbing WIM data. It also shows two forms of filtering. This flowchart which can be implemented at any bridge location will be utilized as the basis for our WIM experimental study (NCHRP 12-83, 2014).

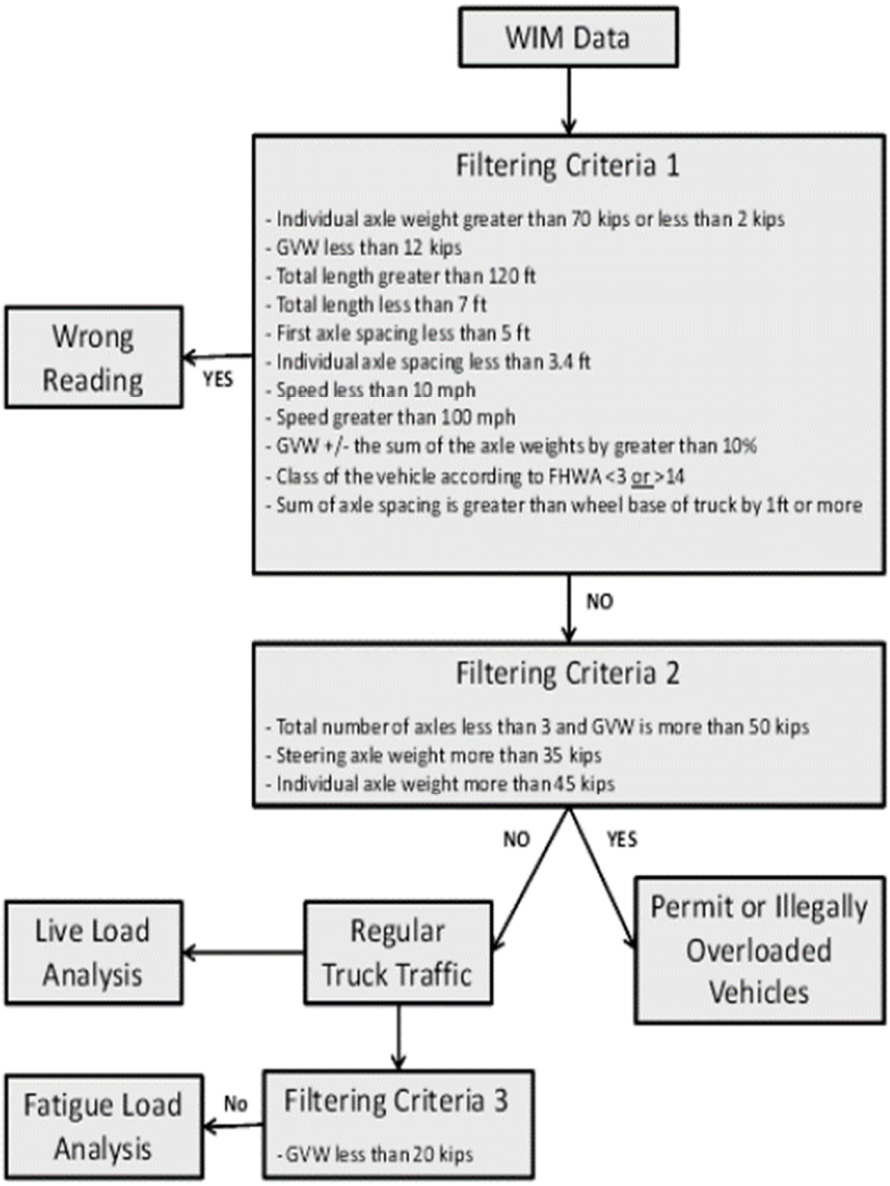

Figure 2.15 - WIM Flowchart (NCHRP 12-83, 2014)

Based off this information, one can infer that many of the studies performed were for general areas and not for a specific site. Additionally, WIM studies are rarely if never done in conjunction with SHM to assist in understanding a bridge's behavior.

CHAPTER 3

COMPARISON OF LOAD RATING METHODS

3.1 - Introduction

As discussed, one of the main objectives of this research is to compare available Load Rating Methods primarily the LRFR and LFR Method. This will be done in conjunction with developing a refined procedure for the evaluation of complex bridges. This chapter provides a detailed overview of these two methods, draw comparisons, as well as, provide information on the other two existing methods which can be utilized, ASR (allowable stress rating) and engineering judgement.

As per chapter two, the 2018 MBE will serve as a primary reference for this chapter. Currently, three specific analytical load rating methodologies exist: Load and Resistance Factor Rating (LRFR), Load Factor Rating (LFR), and Allowable Stress Rating (ASR). These three methods serve as the primary means in which one can analyze the member of the bridge.

A fourth method, engineering judgement also exists as a methodology that can be utilized. However, this method is reserved as a last resort, as it is more ambiguous and relies on the professional expertise of the Engineer evaluating the structure. As stated above, the purpose of this chapter is to provide an in-depth review of each of the methodologies described above so that a detailed comparison can be made regarding these methodologies.

Currently, the 2018 MBE, it specifies that load ratings “provides a basis for determining the safe load capacity of a bridge.” (AASHTO MBE, Section 6). Further it states that “Load

Rating require engineering judgement in determining a rating value that is applicable to maintaining the safe use of the bridge" (AASHTO MBE, Section 6).

These statements leave a sense of ambiguity, as it leaves it to the Engineer in Charge to determine whether the load rating calculated is appropriate for a bridge. When dealing with complex bridges, the 2018 MBE is vague regarding their evaluation. Under Section 6.1 which falls under Section 6 for load ratings. Under this subsection it states the following regarding the evaluation of complex type structures:

> "Ratings of long-span bridges, movable bridges and other complex bridges may involve additional considerations and loadings not specifically addressed in this section and rating procedures should be augmented with additional evaluation criteria where required." (AASHTO MBE 6.1)"

Additionally, under the Section 6.1.6, Evaluation of Complex Structures it states the following:

> "The computation of load-carrying capacity of complex structures, such as suspension bridges, cable stay bridge, and curved girder bridges may require special analysis methods and procedures. ***General guidance is available in this manual but more complex procedures must be used for the actual determination of the Load Rating."*** (AASHTO MBE, 6.1.6).

Under Section C6.1.6, the commentary of this section it goes on to say:

> "The definition of complex bridges in **Section 1** is intended to be consisted with NBIS requirements for inspection. There are many types of complex structures that require special analysis methods and procedures to determine the load carrying capacity." (AASHTO MBE, C6.1.6).

Based on this information, we establish a need for a procedure which allows for bridge owners to evaluate their complex bridges in a way which allows them to prioritize members for repair, as well as, get a true understanding of how their structure reacts establishing a need for research.

The current standard for reporting load ratings is that Bridge Inspection Reports provide "As-Built" and "As-Inspected" load ratings for different loading types. This is done in accordance with NBIS Standards. "As-Built" ratings measure the bridge's performance in accordance with the standard it was designed to.

"As-Inspected" considers criteria such as section loss, wearing surfaces and other factors. It is important that both these values be provided so that the engineer may assess what the effect deterioration has on a member. For example, if the As-Built Rating is 1.00 and the As-Inspected rating is 0.95 then the engineer can determine that based on the level of deterioration there is only a 5% reduction in the rating factor.

The result of this evaluation is normally shown as a "rating factor". A rating factor falls on a 0 to 1 scale. A rating factor greater than or equal to one means that the bridge either meets or exceeds the current design standards it is being evaluated for. While, a rating factor of lower than one means that the bridge does not meet the current design criteria. This depending on the situation may result in either a load posting or a strengthening of the structure. Under the LFR and ASR methods, this rating factor is converted to tons based off the weight of the truck used in the rating.

A flow chart which describes the various checks of a load rating is shown below. Note that this chart which is taken from the 2018 MBE was refined for the current LRFR method. However, this flow chart may also be applied to the LFR and ASR methods as well.

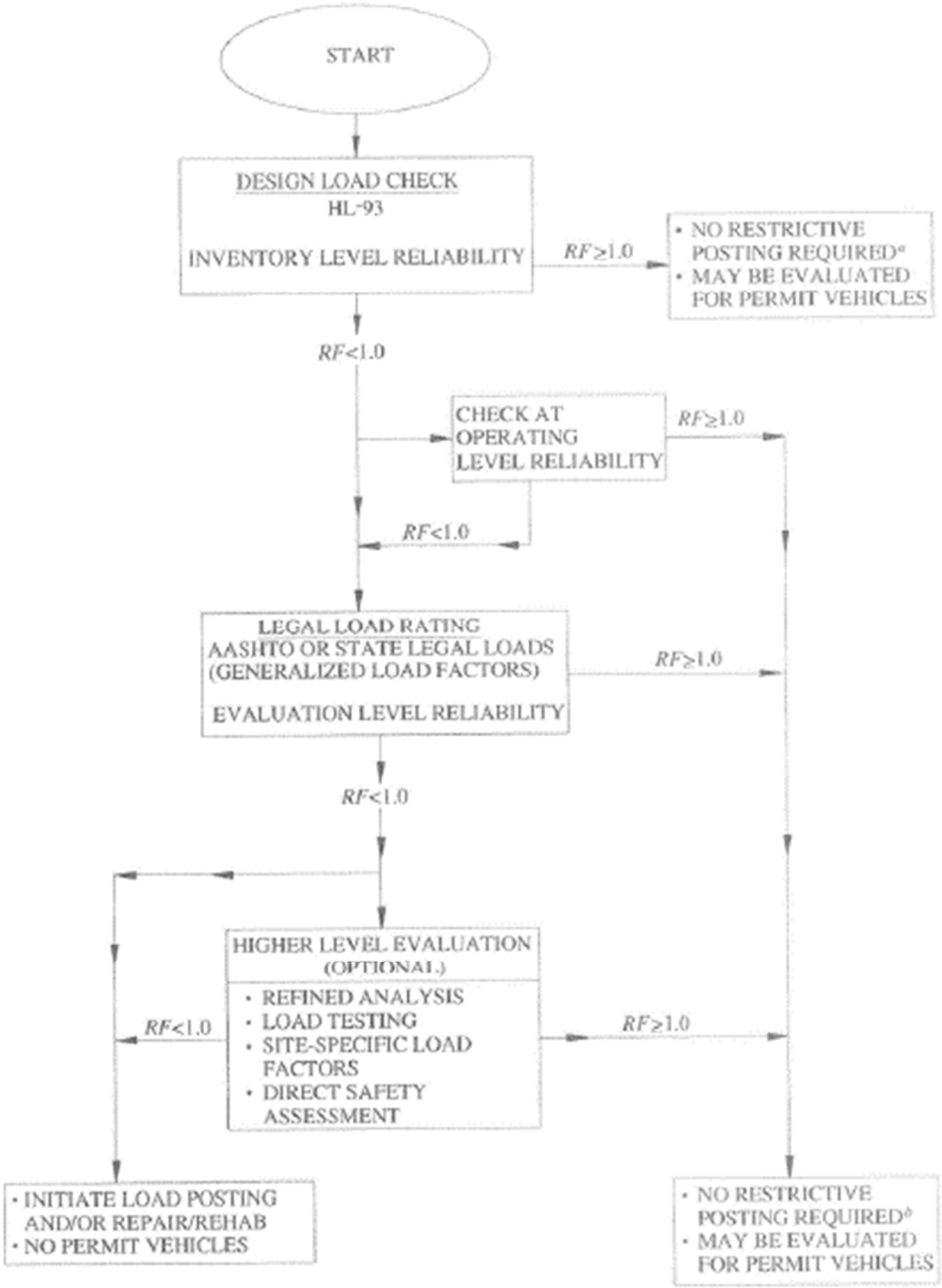

Figure 3.1 - LRFR Rating Flow Chart (2018 MBE, Section 6)

It is important to note that older bridges designed under working stress or load factor design, do not always meet the LRFR design conditions. In this event, bridge owners have the option to evaluate the bridge using either the LFR or the ASR method. The Oceanic Bridge is an

example in which this procedure is utilized. That is why a comparison of these methods is important as an objective of this dissertation is to establish the use of the LRFR method for complex structures regardless of the design code they were originally designed for.

In accordance with the current standards, two ratings are developed based off the live load factor applied to live load crossing the bridge. These ratings are defined as inventory and operating rating. Per 6B.2.1, and inventory ratings corresponds to the design level of stresses but pertains mainly to the existing bridge and the material conditions with regards to its current condition (i.e. section loss). This type of evaluation provides a rating or ton limit which can safely utilize a bridge for an indefinite period.

The operating rating on the other hand, determines the maximum permissible live load in which a bridge can take, per 6B.2.2. Allowing vehicles of this nature to cross a bridge a daily basis would in turn reduce its overall service life capability. The following subsections provide a description of each of the three load rating methodologies. Included are key equations, factors and considerations as described by the MBE.

3.2 - LRFR Methodology

Under the current MBE, the LRFR method governs as the standard in which bridges are evaluated. As discussed, the LRFR method is derived from the Load Resistance Factored Design Method or LRFD method utilized in the current AASHTO Design Manual.

The LRFR method was originally developed to provide a reliability index of 3.5. Based on recent studies as described previously in the Literature Review section of this dissertation, the LRFR procedure reduced this index to 2.5 which was based on a calibration of the live load model. The methodology for this method revolves around three types of procedures including:

1. Design Load Rating
2. Legal Load Rating
3. Permit Load Rating

The result of these ratings is to evaluate the serviceability and safety of the structure. The Design Load Rating as described in section 6A.1.5.1, is done in accordance with the HL-93 Live Loading as specified in the AASHTO LRFD code. This standard is used as a "first-level" assessment to determine if the bridge meets the LRFD design standards. The intent of this Design Load Rating is to determine how well the bridge performs in accordance with the LRFD code.

Per the MBE, the purpose of the HL-93 check is to assess what bridges may need to be posted for state legal loads. Meaning that any bridges which rates above one for this check, would be screened out.

The second type of load rating which is performed is the Legal Load Rating, in accordance with section 6A.1.5.2. This type of rating is specific to the state legal loading and is considered a second level evaluation. The procedure of this evaluation is to determine the adequacy of the bridge according to specific legal design loads. Currently in the state of New Jersey the following loads are used as shown in the below table.

Table 3.1 - New Jersey Legal Loads (NJDOT)

Truck Type	Type	Weight
3	Type 3 Unit	25 Tons
3S2	Type 3S2 Unit	40 Tons
3-3	Type 3-3 Unit	40 Tons
SU-4	Four Axle, Single Trailer	27 Tons
SU-5	Five Axle, Semi-Trailer	31 Tons
SU-6	Six Axle, Multi Trailer	35 Tons
SU-7	Seven Axle, Multi Trailer	39 Tons

Per NBIS reporting standards ratings for the above legal loadings, as well as, the HS-20 and HL-93 loadings are published as a part of the biennial inspection report.

The final type of load rating is a Permit Load Rating. This type of rating is different from the first two, as it checks the bridge for a specific type of load. The MBE warns that this type of rating should only be reserved for bridges which have rating factors greater than one for both design and legal loading.

As referenced in Chapter 2, and per section 6A.4.2.1 of the 2018 MBE, the below equation serves as a general expression in which a load rating is determined. It should be noted that this equation evaluates on a member-by-member basis. Therefore, all loads should be analyzed accordingly.

$$RF = \frac{C - (\gamma_{DC})(DC) - (\gamma_{DW})(DW) \pm (\gamma_P)(P)}{(\gamma_{LL})(LL + IM)} \qquad (3.1)$$

(6A.4.2.1-1)

Where:

C is capacity of a member and is determined based on the following equation:

$$C = \varphi_c \varphi_s \varphi R_n \qquad \text{(6A.4.2.1-2)} \qquad (3.2)$$

The capacity is comprised of three variables including:

- Rn which is the nominal member resistance or design capacity of the member.
- φ_c which is the condition factor as defined below.
- φ_s which is the system factor as defined below.

Additional variables include the following:

- DC which is the dead load acting on a member
- DW which is the dead load due to wearing surface acting on a member
- P which is permanent loads other than dead loads.
- LL which is the live load
- IM which is the Dynamic Load Allowance
- γ_{LL} which is the live load factor applied to (IM+LL)
- γ_{DC} which is the dead load factor applied to DC
- γ_{dw} which is the dead load factor applied to DW
- γ_{p} which is the factor applied to P (AASHTO MBE Section 6)

The above factors vary based limit state in which the member is being evaluated for. This table taken from the MBE is shown below for the varying limit states of evaluation. However, for this dissertation our focus is the Strength I design limit state was evaluated as it generally the controlling limit for most bridges. Additionally, it is easily comparable and is what is generally utilized in NBIS reports.

Table 3.2 - Load Factors for different Limit States (AASHTO MBE Section 6.4)

Table 6A.4.2.2-1—Limit States and Load Factors for Load Rating

Bridge Type	Limit State*	Dead Load γ_{DC}	Dead Load γ_{DW}	Design Load Inventory γ_{LL}	Design Load Operating γ_{LL}	Legal Load γ_{LL}	Permit Load γ_{LL}
Steel	Strength I	1.25	1.50	1.75	1.35	Tables 6A.4.4.2.3a-1 and 6A.4.4.2.3b-1	—
	Strength II	1.25	1.50	—	—	—	Table 6A.4.5.4.2a-1
	Service II	1.00	1.00	1.30	1.00	1.30	1.00
	Fatigue	0.00	0.00	0.75	—	—	—
Reinforced Concrete	Strength I	1.25	1.50	1.75	1.35	Tables 6A.4.4.2.3a-1 and 6A.4.4.2.3b-1	—
	Strength II	1.25	1.50	—	—	—	Table 6A.4.5.4.2a-1
	Service I	1.00	1.00	—	—	—	1.00
Prestressed Concrete	Strength I	1.25	1.50	1.75	1.35	Tables 6A.4.4.2.3a-1 and 6A.4.4.2.3b-1	—
	Strength II	1.25	1.50				Table 6A.4.5.4.2a-1
	Service III	1.00	1.00	0.80	—	1.00	—
	Service I	1.00	1.00	—	—	—	1.00
Wood	Strength I	1.25	1.50	1.75	1.35	Tables 6A.4.4.2.3a-1 and 6A.4.4.2.3b-1	—
	Strength II	1.25	1.50	—	—	—	Table 6A.4.5.4.2a-1

* Defined in the *AASHTO LRFD Bridge Design Specifications*

Other applied factors include the system and condition factors which is applied directly to the design capacity to determine the overall evaluation capacity. The condition factor or φ_c directly correlates to the coding given to a structural member per NBIS Inspection guidelines. Table 3.3 is pulled from the 2018 MBE and provides the different condition factors which can be applied to a member based off this information.

Table 3.3 - Condition Factor (2018 MBE Section 6.4)

Structural Condition of Member	φ_c
Good or Satisfactory	1.00
Fair	0.95
Poor	0.85

Table 3.4 - Condition Factor Conversion to NBIS Coding (2018 MBE Section 6.4)

Superstructure Condition Rating (SI & A Item 59)	Equivalent Member Structural Condition
6 or higher	Good or Satisfactory
5	Fair
4 or lower	Poor

The other factor applied to the Capacity of the member is φ_s or the system factor. This factor directly relates to how the bridge was constructed/designed. This value can be found using Table 6A.4.2.4-1 in the MBE as shown below. For example, in the case of the Oceanic Bridge, because we are evaluating a floor beam with spacing greater than 12 feet and has non-continuous stringers φ_s equals 0.85.

Table 3.5 - System Factors for different Structural Configurations (2018 MBE, Section 6.4)

Superstructure Type	φ_s
Welded Members in Two-Girder/Truss/Arch Bridges	0.85
Riveted Members in Two-Girder/Truss/Arch Bridges	0.90
Multiple Eyebar Members in Truss Bridges	0.90
Three-Girder Bridges with Girder Spacing 6 ft	0.85
Four-Girder Bridges with Girder Spacing ≤4 ft	0.95
All Other Girder Bridges and Slab Bridges	1.00
Floorbeams with Spacing >12 ft and Noncontinuous Stringers	0.85
Redundant Stringer Subsystems between Floorbeams	1.00

It should be important to note that a limitation in the MBE clearly indicates that $\varphi_c\varphi_s$ cannot be less than 0.85, (2018 MBE, 6A.4.2.1-3). Therefore, even in the worst condition the most one could limit the capacity of the member is by 15%. Therefore, when dealing with significantly deteriorated members such as the Oceanic Bridge floor beam, the engineer must take special precautions.

Under Section 6.1.2 of the MBE it clearly states that the "condition and extent of deterioration of structural components of the bridge should be considered" in the computation of the Load Rating Factor (2018 MBE, Section 6.1.2). Additionally, the section goes on to state that the analysis should be one based on a thorough field inspection. Under C6.1.2, the MBE states that the effective cross-section properties should be used to determine the capacity of a member. This must be done in conjunction with the above two factors.

Overall, as we can see from the above equation, the rating factor is determined taking the capacity of the structure subtracting the known dead loads and taking the difference over the live loads. By doing this we can determine how the structure is designed for the various live loads. The MBE currently provides for several criteria on how to determine the appropriate live load factor to be applied to the Rating Factor Equation. For general design loads one can use the live load factors shown above in the load factor table.

These factors are generalized and have been developed to provide a certain level of safety for bridge owners throughout the country. The MBE however, does offer reductions to these factors based on known commercial traffic on the bridge. This is covered under Section 6A.4.4.2.3, and Table 6A.4.4.4.2.3a-1.

The commentary also covers the use of developing a Site-Specific Live Load factor for situations when the truck weight and truck volume are known. This data should be taken via weigh-in-motion sensors and follow a distinct procedure. Specifics to this procedure is covered under the weigh-in-motion experimental chapter of this dissertation. However, it is important to note that this accommodation for a site-specific factor cannot be extended to the LFR or ASR method. It should be noted in accordance with Commentary, 6A.8.3 (pg. 6-58) in when a RF is

between 0.3 and 1.0, one must use the following equation to establish a safe posting load for that vehicle type. If the factor is below 0.3 then the bridge must be closed to traffic.

$$\text{Safe Posting Load} = \frac{W}{0.7}\ [\ (RF) - \ 0.3\ ]\ (6A.8.3\text{-}1) \qquad (3.3)$$

3.3 - LFR/ASR Methods

Under Part B of Section 6, the MBE covers the Allowable Stress Rating (ASR) and Load Factor Rating (LFR) methods. The reason this section is included, is to allow for bridge owners to utilize these provisions for older structures which do not meet the current LRFR requirements.

One of the reasons that a bridge does not meet the current standard, was that it was designed for a previous live load type. For example, if a bridge was designed using HS-20 or HS-25 design loading, it is possible that even in pristine condition, the LRFR rating would yield a result lower than 1.00. In this scenario an owner could use the LFR or ASR method to provide a better result.

Like the LRFR method, the LFR and ASR methods provide for two rating levels, Inventory and Operating. These evaluations are also done in accordance with the underlying design code of each method. For example, the LFR method is based off the Load Factor Design Method, while the ASR method is based off the Working Stress Design Method or ASD Method.

The Allowable Stress Rating Method, per article 6B.3.1 “constitutes a traditional specification to provide structural safety.” (2018 MBE Section 6B.3.1). The main point here is that the actual loading is combined to determine the max stress of the member which is compared to the design stress (allowable working stress) of that member. This is in line with the principle of ASD which relied on the stresses of the material rather than the loads acting on the bridge.

The Load Factor Rating Method, per article 6B.3.2 "is based on analyzing a structure subject to multiples of actual factored loads." (2018 MBE 6B.3.2). Unlike the ASD method the LFR method is based on different factors being applied to each type of load. The result being that the rating determined does not exceed the design strength of the member.

One key difference is that the factors regardless of the methodology used are locked in. Meaning they cannot be modified like the LRFR method. For example, the live load factors under the LFR and ASR cannot be modified using Site-Specific Data. Additionally, the resistance values do not account for structural redundancy nor condition. Leaving method of analysis even more subjective.

Under Section 6B.4, a general expression is given. This expression can be utilized for both the ASR and LFR Methods. This equation is as follows:

$$\mathrm{RF} = \frac{\mathrm{C} - \mathrm{A_1 D}}{\mathrm{A_2 L(1+I)}} \quad \text{(6B.4.1-1)} \qquad (3.4)$$

Where:

- RF is the rating factor calculated.
- C which is the capacity of the member.
- D which is the dead load effect on the member. Because these methods deal with older structures, provisions regarding the treatment of composite and non-composite members are included.
- L which is the live load effect on a member. This value depends on the type of truck being analyzed and span length.
- I which is the impact factor applied with the live load. This factor is usually 0.75.
- A1 which a factor for Dead Load
- A2 which is a factor for Live Load.

As stated above, it should be noted that unlike the LRFR method, the capacity does not have a system or condition factor applied to it, but generally follows the governing design code used to analyze the member. To account for deterioration, the engineer must consider this when developing the section properties of the member.

Additionally, the LRFR the rating factor is multiplied by the live load applied to the structure and is given in tons, as opposed to a factor ranging from zero to over one. This rating is determined using the following equation:

$$RT = (RF)W \text{ (6B.4.1-2)} \qquad (3.5)$$

Where:

- RT is the rating in Tons.
- W is the weight of the truck used to determine the Live Load Effect or L.

A key difference in the ASR and LFR Methods is the use of the live and dead load factors applied to each equation. For ASR the values of A1 and A2 are both equal to 1.0. While for the LFR Method A1 is equal to 1.3 and A2 varies. The value of A2 is equal to 2.17 for inventory level while the A2 equals 1.3 for operating.

A secondary difference is how C is calculated. Under LFR the value of C is the same regardless of the live load factor applied, while under ASR the value of C changes due to what type of level the engineer is trying to obtain. This is because of the main design criteria for ASR is the design capacity of the member not the loading conditions.

3.5 - Other Differences Noted

While the above sections, explain how each load rating method is performed, there are some key differences noted within the 2018 MBE that apply only to the LRFR and do not apply to the LFR ASR methods. The first is the use of analysis by field testing. Under 6A.3.4, the 2018

MBE allows for a bridge to be evaluated by field testing. It directs those wishing to use this as a form of evaluation to refer to Section 8 for further information. This provision is not included under Section 6B of the MBE which applies to the LFR and ASR methods.

The second provision which applies to only the LRFR method is the use of a site-specific live load factor. The LRFR allows for this specifically under 6A.4.4.2.2 and provides guidelines on how to obtain this under the commentary. However, this is not included at all under the LFR method. Therefore, engineers are limited to only the factors specified within the evaluation code.

Finally, per the 2018 MBE, finite element modeling is allowed under the LRFR method under part A, but not under the LFR method in part B. Under Section 6A.3.3, it allows for a refined method of analysis which refers one back to the AASHTO design code and guidelines regarding finite element modeling. However, under Section 6B, the refined method of analysis is also not included. Therefore, it can be surmised that the LFR code is limited to a traditional type of analysis.

3.6 - Summary Discussion

As we can see from the previous sections, on a conceptual level each of the three load rating methodologies are similar in nature. The basis of which the equations are set up are generally the same. Meaning that the general rating expression is based on taking a member's capacity, subtracting the dead load and dividing the difference by the live load implemented on the structure.

However, as we can see they are many key differences between the three methods. One key difference is the flexibility the 2018 MBE gives engineers. This is through allowing them to use finite element modeling, a Site-Specific Live Load Factor from WIM Data, and the use of experimental field testing. This flexibility allows for the engineer to re-evaluate members with a

refined form of analysis where others cannot. Additionally, the LRFR method focuses on the resistance of the member and how it responds to the live load induced. While the other two methods are more arbitrary in nature.

Other differences to note pertains to the Dead Load. In which in each scenario a different dead load factor is applied. This based on the principal in which resistance is calculated. However, a notable difference is that the LRFR separates out permanent and wearing surface loads while the LFR and ASR do not account for this. Finally, capacity considers evaluations from NBIS report where the LRF and ASR do not.

CHAPTER 4

FIELD INSTRUMENTATION AND MONITORING

4.1 - Introduction

This chapter provides for an overview of the experimental program which took place as a part of this dissertation. Included in this experimental program was the installation and testing of a weigh-in-motion system. Additionally, the installation and testing of structural health monitors was also included.

The focus of the study for this dissertation is Monmouth County Bridge S-31, the Oceanic Bridge. This bridge served as the area of study for both the experimental and analytical portions of the project. The first part of this chapter will cover the structural health monitoring and testing, while the second part will cover the weigh in motion sensors.

4.2 - Structural Health Monitoring

4.2.1 - Structural Health Monitoring Overview

The purpose of the SHM experimental field study is to provide us with vital information which not only gives us an understanding of how the bridge reacts to certain loads, but also give us information to calibrate and adjust the finite element model as a part of the analytical study. Based off the results gathered from this study, we hoped to achieve the following objectives:

- Obtain the maximum strain for each tested member.
- Use experimental results to calibrate the finite element model developed.
- Compare the 2016 results to the 2018 maximum strain results.
- Identify the experimental load capacity of the tested members.

- Compare experimental data to analytical data and draw conclusions.

For the experimental portion of this dissertation, installation and testing of the structural health monitoring system played a critical role in understanding the capacity and internal reactions of the analyzed span. The experimental study focused primarily on the main anchor span which is adjacent and ties directly into the main bascule span. This shown in the below:

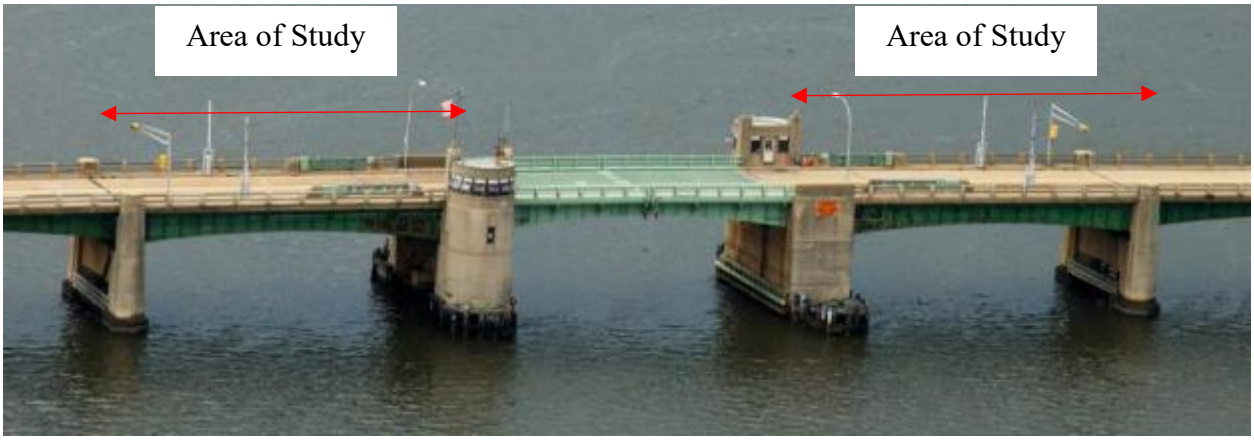

Figure 4.1 - Area of Study for Structural Health Monitoring

These anchor spans are located Spans 28 and 30. These spans tie directly into the trunnion which supports the main bascule span. A trunnion provides the necessary support to allow the bascule span to rotate up and down. Therefore, the serviceability of this member is critical, as it ties directly into the complex system of the structure.

The floor beam system within these spans, are designed to provide stability of the anchor span. Additionally, the floor beams on the bascule side is designed to specifically to accommodate the counterweight system, allowing it to fit between the main bascule pier and the first span. Based on this understanding, the flanking spans are not only critical from a structural point of a view, but also provide an additional form of balance for the bascule span due to its moveable nature.

Despite tying directly into the bascule span support, the configuration of the flanking span is simply supported. As described above this span consists of a stringer floor beam system which ties directly into a fascia girder on each end. This configuration is similar to adjacent steel spans, except for the fact that those approach spans are continuous cantilevered spans, as opposed to simply supported.

Due to this configuration, all structural steel spans for this bridge are classified as both non-redundant and fracture critical in accordance with NBIS guidelines. To better understand the configuration of the flanking span, a cross section as provided in the original 1939 construction plans is provided below.

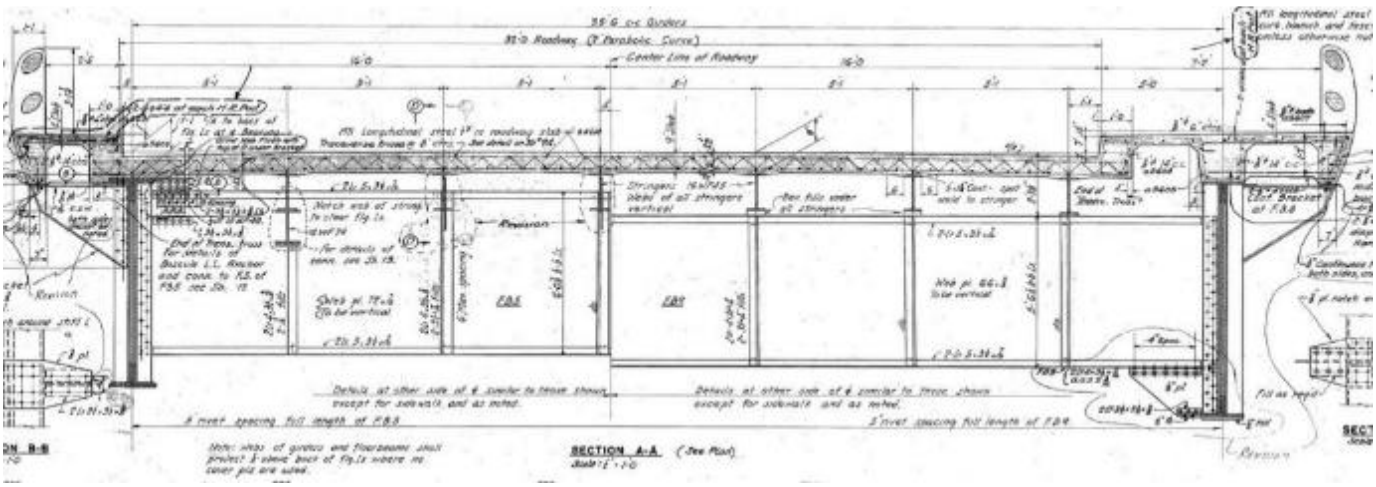

Figure 4.2 - Original 1939 Cross Sectional Plan for Flanking Spans 28 and 30

Figure 4.2 represents the cross section at the pier and adjacent to the counterweight system. As per the figure, the floor beam is approximately six feet deep. The deck is supported by six stringers, while the fascia girder varies in depth. In between these two main floor beams are smaller 36WF194 beams spaced approximately 17.75 feet apart. A partial cross section of the intermediate floor beam is provided below. Additionally, an elevation view of the main fascia girder is also provided below.

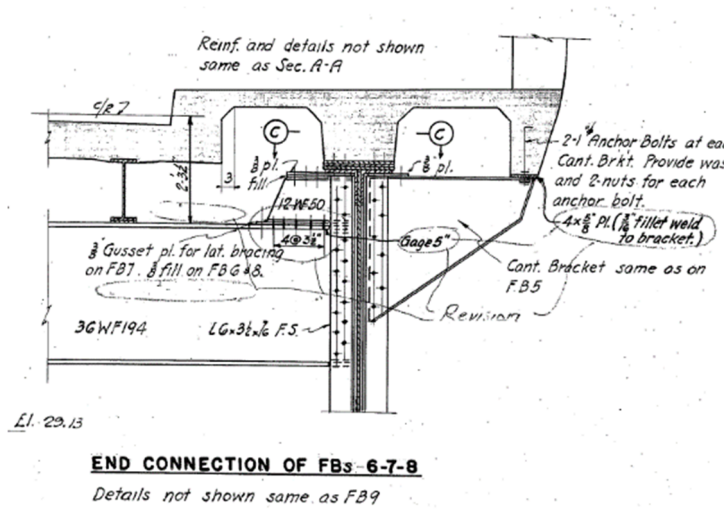

Figure 4.3 - Detail of Intermediate Floor beam underneath Sidewalk

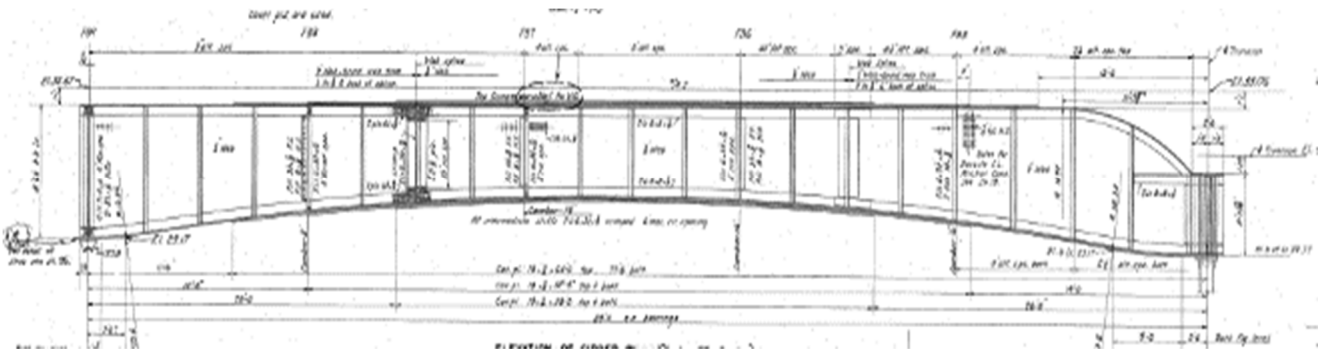

Figure 4.4 -Fascia Girder Elevation View at Spans 28 & 30

For the fascia girder, it consists of a built-up member supported by multiple cover plates. On the outer end, the girder is supported by a simple rocker bearing, while on the other end, the beam is completely fixed and ties directly into the bascule pier trunnion system. Due to the deterioration of the main floor beam located at Piers 28 and 30, a rehabilitation contract was implemented in 2015. This project, completely rehabbed these members accounting for the lost section due to corrosion. A photo of the repaired member is provided below.

Figure 4.5 - Floor Beam following 2015 Rehabilitation

As you can see from Figure 4.5, the floor beam was repaired utilizing a series of new plates. Rivets were removed and replaced with high strength bolts. Additionally, fill plates and angles were also installed to stiffen and, increase the moment of inertia of the member.

4.2.2 - SHM Experimental Study and Procedure

For the SHM experimental study, two rounds of testing were performed. Both were done with the purpose of determining the maximum strain on the tested members and gather additional data for the finite element model calibration. These tests were performed in April 2016 and August 2018 respectively.

The procedures and location of sensors were identical for both rounds of testing with the only difference being that the loaded trucks used for the testing were slightly different. In 2016, a three-axle vehicle was utilized, while in 2018 only a two-axle truck was utilized. For both tests the max loading of the truck was around 30 kips which was equal to the posted load on the bridge. This difference in loading scenarios was a benefit as it allowed for the team to see any differences in reactions from one loaded truck to another.

For each test, the team was led by Rutgers team assisted by Monmouth County forces. Access was provided to the spans utilizing a snooper provided by the County. The snooper utilized was a tag-along model shown in figure 4.6.

Figure 4.6 - Snooper used for Installation of the Strain Gauges and Accelerometers

The next step, utilizing this information, was develop a sensor plan for monitoring. For this effort, optimal locations were identified based on access, and proximity to maximum moment shear areas within the span. Since the snooper only had so much reach, the floor beams at Piers 28 and 30 were chosen, as well as, the main fascia girder. The interior floor beams, and the floor beam directly adjacent to the counterweight was inaccessible due to these limitations.

Based on these restrictions, a sensor plan diagram shown below was developed. This figure illustrates a plan view of the framing plan of Spans 28 and 30. It is important to note these spans are identical. The plan calls out each strain transducers and accelerometers installed. Note that to further identify the member being tested, a dark blue line was utilized. As shown in the figure below, a total of four (4) strain transducer and three (3) accelerometers were installed for each span with a total of 8 strain transducers and 6 accelerometers at both spans.

The monitoring system utilized was provided by Bridge Diagnostics Inc. (BDI). These strain gauges utilized for the study were the ST350 Strain Transducers (Figure 4.7). These transducers were chosen as they can be easily attached to structural steel and can be reused at other locations.

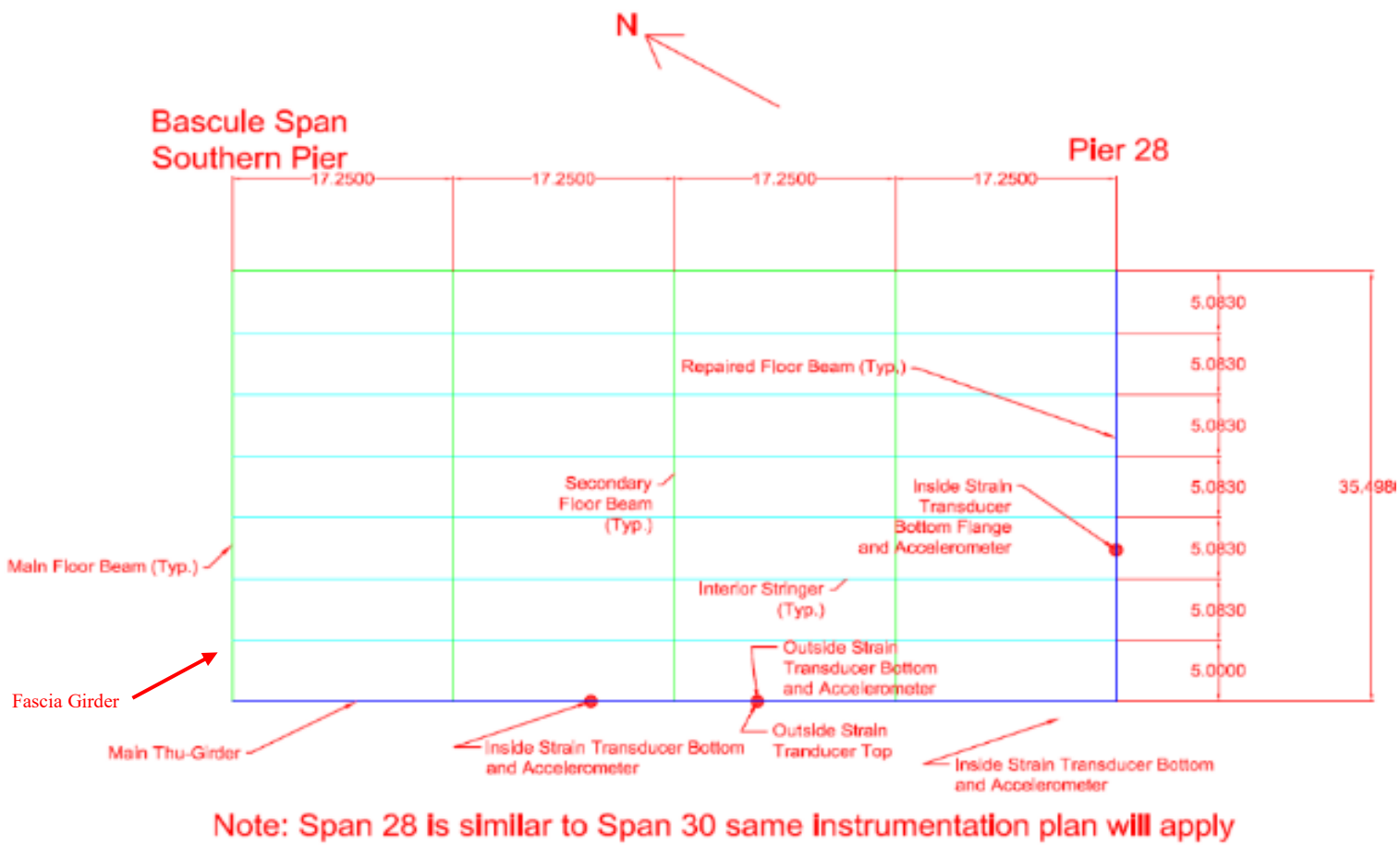

Figure 4.7 - Layout of Sensors

(Blue Line Indicates Tested Member)

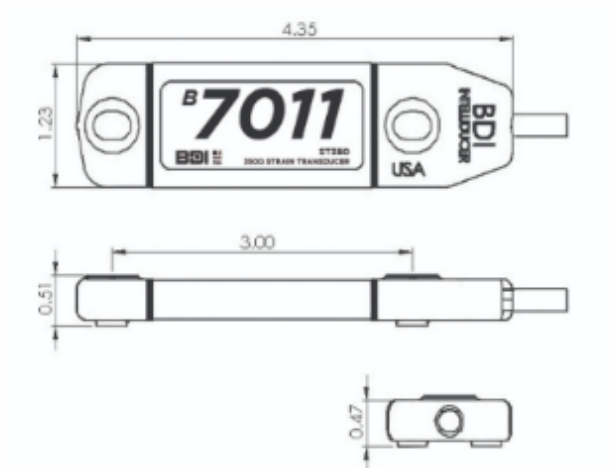

Figure 4.8 - BDI Strain Transducer (BDI, 2019)

Accelerometers chosen for the study were the A1512 model (figure below). These monitors which provide dynamic results were selected as the provide high stability and can be mounted in various locations.

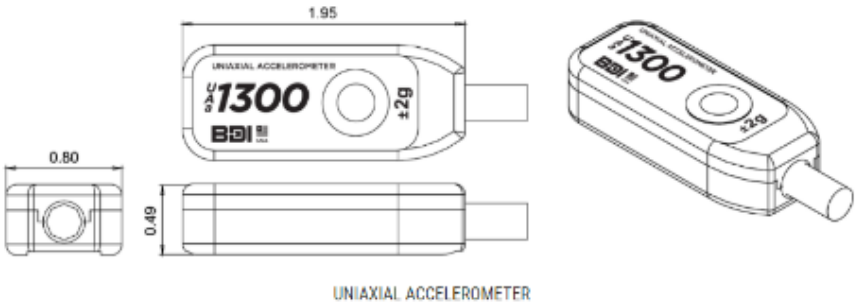

Figure 4.9 - BDI Accelerometer (BDI, 2019)

To gather the data, a STS4-4 node data acquisition device was utilized. These 4-channel devices provide direct access to the accelerometer and strain gauges. For this project several devices were utilized to account for the multiple strain gauges and accelerometers. A figure of the device is provided below.

Figure 4.10 - BDI Node Data Acquisition Device (BDI, 2019)

The strain transducers and accelerometers were attached to the structural steel using an epoxy glue. Cables were held using a series of clamps and were connected to the data acquisition device located near the parapet. A photo of an attached strain transducer used for this work is shown in Figure 4.11 below.

Figure 4.11 - Strain Transducer attached to the top flange of the Fascia Girder

For each member (3) strain transducers were installed on the exterior fascia girder (1 on top flange and two on bottom flange) on the west facia between the interior floor beams (approximately 6-ft from the center interior floor beam of each span). Additionally, one (1) strain transducer and accelerometer was installed on the repaired main exterior floor beam between 3rd and 4th stringers. The below figures provide an examples of sensor location on the exterior fascia girder and on the repaired floor beam. Note that both members have similar configurations and sizes.

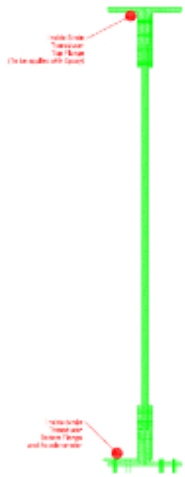

Figure 4.12 - Sensor Location for Fascia Girder

Figure 4.13 - Sensor Location for Repaired Main Floor Beam

As discussed, both floor beams at Spans 28 and 30 were repaired as a part of the 2015 Repair Project. To better understand the placement of the above sensors, Figures have been provided below.

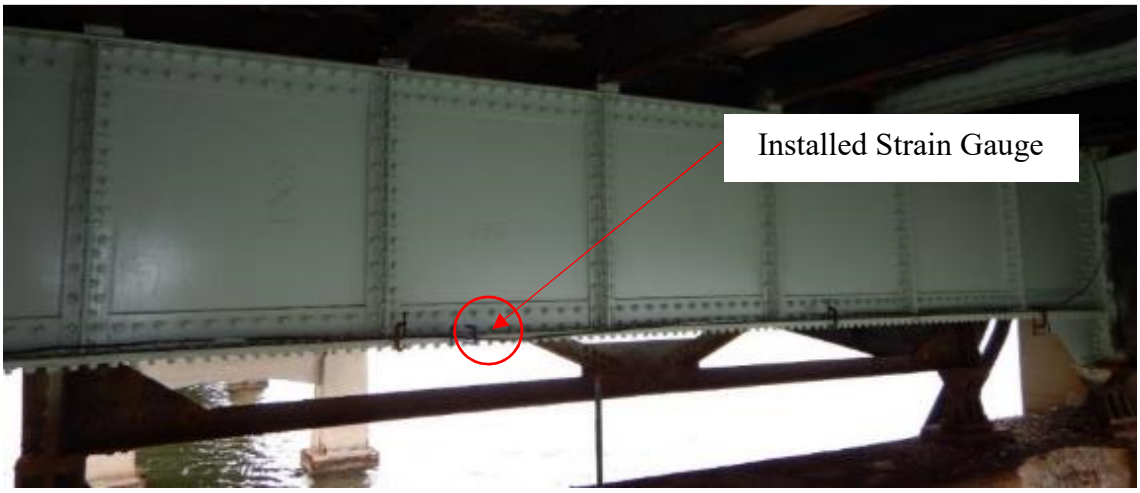

Figure 4.14 - Strain Gauge Placement on Repaired Floor Beam at Span 30

Figure 4.15 - Strain Gauge Placement on top and bottom flange of Fascia Girder

These photos were taken in during the 2018 testing. The figures show areas specifically where the strain transducers were installed. For the testing of the spans, Table 4.1 and was developed to shows the Strain Gauge/Accelerometer number and its corresponded number in the BDI inventory.

Table 4.1 - Strain Transducers/Accelerometer for Span 28 (Sample)

Span 28							
	West Thru Girder					**Repaired Floor beam**	
No.	B1S1	B1S2	B1S3	A1	A2	B2S1	A3
Sensor ID							

For the diagnostic testing performed, two types of truck were utilized for the testing performed. As discussed, there is a 15-ton limit on the bridge. Therefore, great care was taken to ensure the weight restriction was not exceeded. This was done by weighing the truck (each axel) and loading it to approximately the posting. These weigh tickets were also important as it provided us with additional information for the finite element model calibration. The figure below shows the truck utilized for the 2018 testing.

Figure 4.16 - Truck used for 2018 Testing (Side View)

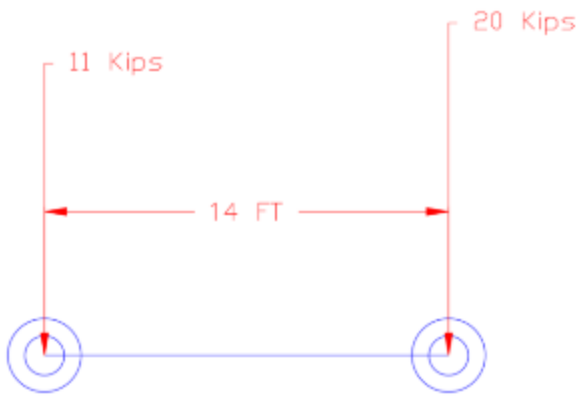

Figure 4.17 - 2018 Axle Configuration

The figure above illustrates this vehicle it's the axle configuration and each axle weight. The wheels are spaced approximately 14 feet apart and weights were taken from the loading ticket provided by the County.

A different truck was utilized during the 2016 testing. This is acceptable, as the ABAQUS model can be run for different load criteria. This is also beneficial as it allows us to compare the tested member in the field for various loads to see how the member reacts. For the 2016 testing, an empty dump truck as shown below was weighed at a nearby county facility. An example of the truck utilized is shown in the below figure.

Figure 4.18 - Triaxle Truck used for 2016 Testing

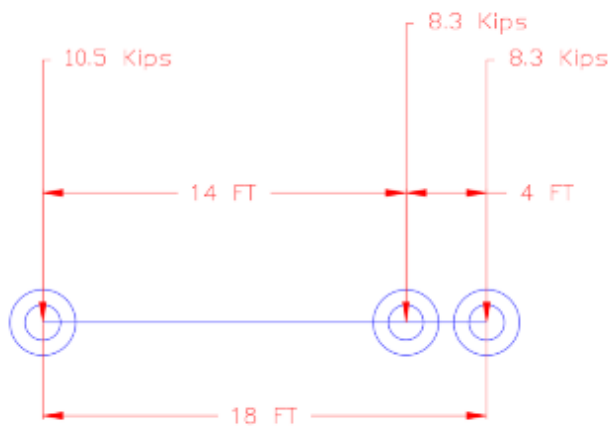

Figure 4.19 - 2016 Axle Configuration

Figure 4.19 illustrates this vehicle it's the axle configuration and each axle weight. The wheels are spaced initially 14 feet apart and the rear two wheels were 4 feet apart. Additionally, like the 2018 truck weights were taken from the loading ticket provided by the County.

For all tests the truck was run from southbound lane, directly above the members being tested. For both sets of testing, Figure 4.20 illustrates this testing in relation to the western curb.

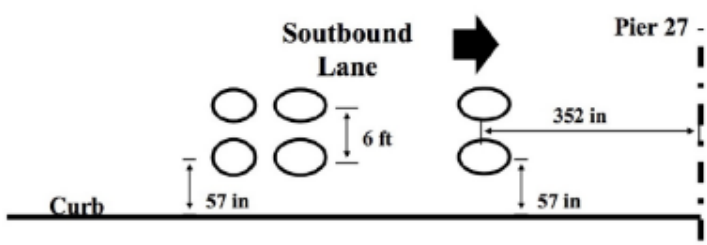

Figure 4.20 - Test Location in relation to Southern Fascia Girder

To see the distribution from the responses of the truck, it is better to run the truck as close to the thru girder as possible. Since there is only one lane in the southern direction this is achievable. From plan view, the truck will be approximately 48 inches off the western curb and three feet away from the thru girder. All instrumentation will be below the southbound lane. A cross sectional illustration is shown in the below figure.

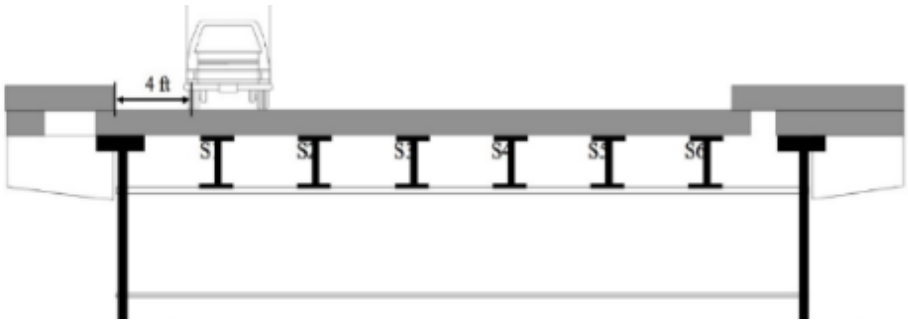

Figure 4.21 - Dynamic Load Test Configuration (2016 & 2018 Tests)

For this test, the calibration truck was run in the southbound lane while the bridge is temporarily closed to traffic. For this testing, multiple runs were required as the responses need to be consistent for acceptability. To perform a diagnostic test, the truck first started at a crawling speed. To minimize the impact that may affect the testing results, the speed was controlled to 10, 20, and 30 mph. All testing was done under a full lane closure. Table 4.2 provides a sample table for field notes.

Table 4.2 - Field Notes for Testing

Path No.	Speed	STS file	Start Time	Time truck at mid-span	Notes
1	10				
1	20				
1	30				

For the work to commence, certain traffic control measures needed to be put in place so that the team could get access to the span below, as well as, run the required diagnostic tests. For the work the northbound lane was completely closed on the bridge to allow the snooper access to the western side of the structure. Since the cross section of the roadway is narrow, alternating lanes of traffic needed to be implemented.

As stated previously, during the static and dynamic testing, the County forces shut down the entire structure to vehicular traffic for a period of 5 minutes at a time. For the static testing, the truck provided for by the County performed the required testing runs in the southbound lane. During the dynamic testing, the bridge was closed, and the truck was run at various speeds to perform the required testing.

4.2.3 - SHM Data Analysis

Once the data had been collected, it was subsequently analyzed to determine the maximum strain, as well as, the incremental strain on the member as the truck was run over the span. These results were then compared to the ABAQUS model. Specifics regarding the calibration of the FEM model is included in Chapter 6 of this dissertation.

Additionally, the overall maximum strain observed at the floor beam and the fascia girder were obtained to perform an experimental load rating for comparison to the FEM model, and classical method. To achieve this, the maximum strain needed to be converted to a live load for input into the Load Rating Equation. The first step was to convert strain over to stress. This was done using the following equation:

$$\sigma = E\epsilon \qquad (4.1)$$

Where:

- σ is equal to the stress on the member in PSI
- E is equal to the Modulus of Elasticity of Steel in PSI (29 x 10^6 PSI)
- ϵ is equal to the maximum strain observed during the field experimentation

Once stress had been determined the following step was to determine the live load induced on the member. To find the maximum moment, the following equation was used:

$$\sigma = \frac{Mc}{I} \qquad (4.2)$$

Where:

- c is the centroid of the Member which stress is being induce in inches
- I is the measured moment of inertia of the member in in^4
- M is the Moment acting on a member

As discussed, for the floor beam to properly analyze the data, the maximum shear force needed to be determined. To achieve this, the following equations were utilized.

$$\tau = G\gamma \qquad (4.3)$$

Where:

- τ is equal to the stress on the member in PSI
- G is equal to the Shear Modulus of Elasticity of Steel in PSI (11.5 x 10^6 PSI)
- γ is equal to the maximum strain observed during the field experimentation

Once the strain stress had been determined on the floor beam, the following step was to find the maximum shear. To determine this the following equation was utilized.

$$\tau = \frac{VQ}{It} \qquad (4.4)$$

Where:

- V is the shear force acting on the member
- Q is the first moment of Area of the member being analyzed
- I is the Moment of Inertia for the member
- t is the thickness of the material

4.3 Weigh-in-Motion Sensors

4.3.1 - Weigh-in-Motion Overview

In conjunction with the SHM, and to determine, the loading Bridge S-31 sees daily, the installation the installation of weigh-in-motion (WIM) sensors were essential. These sensors not only give us firsthand knowledge of the load seen daily but give us key insight which will assist with this project.

Objectives of this experimental study include the following:

- Understand the daily truck traffic at the Oceanic Bridge.
- Determine if, when, and how often the weight limit posting is exceeded.
- Determine the maximum load observed on the structure.
- Develop a site-specific live load factor.

4.3.2 - Weigh-in-Motion Sensor Installation

The weigh in motion sensors were installed on June 18 and 19, 2018. They were installed by the Rutgers RIME group, assisted by J. Ford Electric and Monmouth County. WIMS were only installed on the Rumson (south side) of the bridge. Sensors were not installed on the Middletown side as they would have just provided redundant information. A configuration of the WIM sensors is shown in figure 4.21. This configuration was utilized for both lanes.

For the work to commence, certain traffic control measures needed to be put in place so that the team could install the sensors correctly. For the work both lanes were interchangeably closed on the approaches to allow saw cutting and installation. This was done using a combination of flagmen and crash trucks.

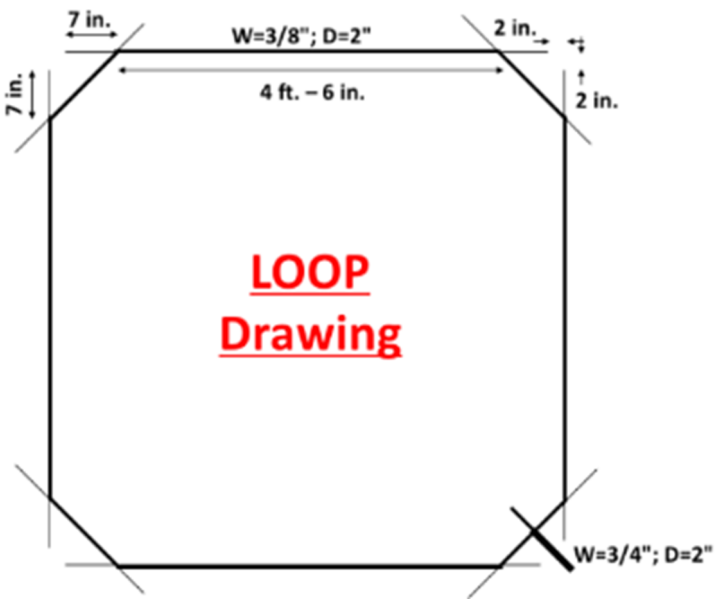

Figure 4.22 - Loop and Cable Slot Configuration

When saw cutting impeded on the adjacent lane, traffic was halted completely so the work could be completed. Since the cross section of the roadway is narrow, alternating lanes of traffic needed to be implemented. To accomplish the installation of the WIM sensors the following equipment for the pavement cutting operation was used:

- 36HP wet-cutting pavement saw (self-propelled)
- Diamond blade, 20 mm (3/4 in.) wide or equivalent
- Diamond blade, 10 mm (3/8 in.) wide or equivalent
- Concrete drill bit, diameter 13+ mm (1/2+ in.)
- Power washer with > 500-gal water
- Large Capacity Air Compressor (min 150 CFM)
- Electrical Power or Generator
- Other appropriate equipment for pavement cutting and cleaning

For the sensor installation and grouting the following equipment was used:

- Low speed mixing drill
- Mixing paddle compatible with the mixing drill
- Putty knifes or masonry trowels 80~100 mm (3~4 in.)
- Wire brushes
- 25~50 mm wide (1~2 in.) Duct Tape x 450 m (1500 ft) or more
- 20 m (60 ft.) or longer tape measure
- Pavement spray (any color is OK, but white or silver is preferred)
- Lope, diameter 1/2 in., length 20+ ft.
- Disposal plastic gloves x 100
- PVC Pipe, diameter = 37 mm (1.5 in.), length as needed

Additionally, the following equipment for sensor installation was used:

- 11-ft. BL WIM Sensors and brackets x 8
- 6 x 6-ft Saw Cut Loop x 8
- AS475, 10 kg x 35
- WIM System
- Aluminum shielding tape, Diameter 25 mm (1 in.) x 500 ft.

Utilizing the above equipment, the Rutgers team followed an intricate procedure to install the WIM sensors. The procedure for installation is as follows:

1. Clean the asphalt surface, no water could be used to clean the surface.
2. Measure and mark the location of the WIM sensors, loops, and cables on the lane using pavement crayons or paint according to the WIM sensor plan.

Figure 4.23 - WIM Installation Step 2

3. Cut the pavement for the WIM sensor slots using saw-cutting machine as shown below

Weigh-In-Motion Dimensions and Figure showing Cut-outs

a. Width = 20 mm (3/4 in.)
b. Depth = 25 mm (1 in.) ~ 37 mm (1.5 in.) * see below
c. Length = 3500 mm (11 ft. 8 in.)

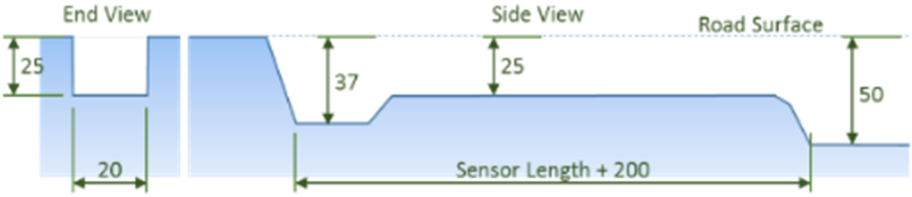

Figure 4.24 -WIM Installation Step 3 WIM Sensor Slot

Weigh-In-Motion Loop Dimensions and Slot Size

a. Width = 10 mm (3/8 in.)
b. Depth = 50 mm (2 in.)
c. Area = 1800 x 1800 mm (6 x 6 ft.)

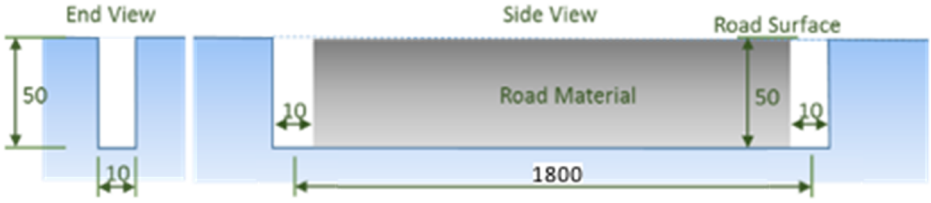

Figure 4.25 - WIM Installation Step 3 WIM Loop Slot

Figure 4.26 - WIM Installation Step 3 WIM saw cutting

4. Once the saw cutting was completed clean all slots with appropriate manner to remove dust (i.e. pressurized water and air was used for this step).

5. Following Step Four, use a propane torch or air blower to dry the slots completely.

6. Once dry, Duct tape along the sides of the slot for sensor and cables.

7. Wipe the WIM sensors using cloths soaked with alcohol.

8. Place the installation brackets on the sensor.

9. Place the sensors loop and cable with brackets into the slot.

Figure 4.27 - WIM Installation of Sensors

10. Once the sensors have been installed, mix the grout.

11. Pour the grout mixture over the sensors, loops, and cables. Spread Grout smooth.

12. For loop and cable, spread the grout smooth to make the grout not to be higher than the duct tape. It should be noted that for the grout generally is gravitated in 5~10 minutes. For WIM sensor, it is very important to add small amount of grout and re-spread it to make the grout to be slightly higher than the pavement by 1.5 mm (1/16 in). This task is not needed for loop and cable.
13. As soon as the grout sets (15~20 minutes), remove duct tape prior to final setting of the grout. Cure the grout for at least additional 30~40 minutes until the grout is hardened.
14. The same procedure is repeated for the next lane.
15. Install Power Source and laptop hookup.

Figure 4.28 -WIM Conduit Hookup

4.3.3 - Calibration Testing

Following the installation of the WIM sensors, the next step was to perform calibration to obtain the most accurate data for loadings seen on the structure. It was agreed to calibrate the WIM sensors simultaneously with the installation and testing of the strain gauges and accelerometers because forced were limited. Calibration of the WIMs were performed on August 30, 2018.

For this work, a truck provided by the County shown in the figure below was run over the bridge and WIM locations. This was the same truck utilized for the structural health monitors. For some cases, the calibration truck stayed in designated locations on the bridge. For the testing a member of the calibration team coordinated continuously with the calibration truck to ensure the proper protocol testing was followed.

For the testing it was essential that the weights were known to do this the County provided a loaded truck with a Gross Vehicle Weight (GVW) at around 30,000 lb. To verify, the loaded truck was sent to the scale to measure the GVW. For the testing it was determined that the GVW was 15.52 tons. The figure on the following page shows the route the truck ran to perform the required calibration test.

Figure 4.29 - WIM Calibration Truck Route

4.3.4 WIM Data Gathering & Analysis

Following the installation and calibration of weigh-in-motion sensors, the data gathering phase began. Every two weeks data would be gathered in the field from the WIM sensor. This data once collected would be processed and analyzed. Following the flowchart provided in NCHRP 12-83, the data was processed, and outliers were eliminated.

Due to the 15-ton posting of the bridge, the following two filters were not utilized to initially to ensure a proper sample size for statistical analysis was gathered. These filters included:

- Total number of Axles are less than three
- Gross Vehicle Weight (GVW) is less than 12 Kips

Data was gathered for a 120-day period during the summer. The summer season was chosen as this area, due to proximity of Sea Bright and Monmouth Beach, two frequently visited beach towns. Therefore, the feeling was that the data obtained would provide an accurate peak representation of the daily truck traffic at the bridge.

Following the data acquisition and processing phased, the sample data was analyzed in accordance with the 2018 MBE to determine the Site-Specific Live Load Factor. To determine this the following equations from C6A.4.4.2.3 of the 2018 MBE were utilized:

$$\gamma_L = 1.8\left[\frac{2W^* + t_{(ADTT)}1.41\sigma^*}{240}\right] > 1.30 \quad \text{(C6A.4.4.2.3a-1)} \qquad (4.5)$$

$$\gamma_L = 1.8\left[\frac{W^* + t_{(ADTT)}\sigma^*}{120}\right] > 1.80 \qquad \text{(C6A.4.4.2.3a-2)} \qquad (4.6)$$

Where:

- W* is the mean truck weight for the top 20% if the weight sample of trucks (Kips)
- σ* is the standard deviation of truck weight for the top 20% (Kips)
- T(adtt) is the fractile value appropriate for the maximum expected loading event. This is determined using Table C6A.4.4.2.3a-1 shown below.

Table 4.3 - Maximum Expected Loading Event (2018 MBE)

ADTT	Two or More Lanes	One Lane
5000	4.3	4.9
1000	3.3	4.5
100	1.5	3.9

Both equations were utilized, and the lower factor is ultimately chosen as the site-specific factor. For this study, although filters regarding two axle trucks and loads less than 12 kips were not applied due to the weight restriction; a separate analysis was conducted using these filters and compared accordingly.

Additionally, in accordance with the 2018 MBE, the maximum load effects (Lmax) was calculated in order to estimate the maximum load effect on the bridge expected over a 5-year period based on data gathered during this period. To achieve this, data was assembled following the data scrubbing had taken place. Once a normal distribution of data had established the data the top 5% of data points were extracted and complied into a sperate analysis. From here the

sample mean, deviation, variance and coefficient of variation were all calculated. Following this a cumulative distribution function was developed using the following equation.

$$Z = \frac{GVW - \mu}{\sigma} \qquad (4.7)$$

Where Z is equal to the cumulative distribution function (CDF), μ is the sample mean, σ is the sample and standard deviation of the extracted data points. Once the CDF has been developed, the next step was to determine the slope and intercept m and n respectively and determine the following:

$$\mu_{event} = \frac{-n}{m} \qquad (4.8)$$

$$\sigma_{event} = \frac{1}{m} \qquad (4.9)$$

Following this, we needed to determine the total number of trucks for 5 years this was determined by taking the ADTT and multiplying it by 1,825 days. As this follows a Gumbel distribution we need to solve for μn and σn. These are obtained using the following equations in the MBE.

$$u_N = \mu_{event} + \sigma_{event} \times \left[\sqrt{2\ln(N)} - \frac{\ln(\ln(N)) + \ln(4\pi)}{2\sqrt{2\ln(N)}} \right] \qquad (4.10)$$

(C6A.4.4.2.3a-3)

$$\alpha_n = \frac{\sqrt{2\ln(N)}}{\sigma_{event}} \qquad (4.11)$$

Finally, we solve for Lmax using the below equation:

$$Lmax = \mu_{max} = \mu_n + \frac{0.577216}{\alpha_N} \qquad (4.12)$$

Once Lmax has been determined, we can determine the live load factor for this case. This done using the following equation:

$$\gamma_L = \left[\frac{L_{\max 2}}{\mathrm{LE}_2}\right] 1.8 > 1.3 \qquad (4.13)$$

Where LE2 pertains to the maximum load effect from one 3S2 Truck which weighs 120Kips. Following this, the Live Load Factor developed can be used in our load rating analysis.

CHAPTER 5

RESISTANCE MODEL

5.1 Introduction

The purpose of this chapter is to review the analytical study performed as a part of this project specifically the resistance model development. The resistance model development consisted of three parts, the traditional approach, finite element modeling and corrosion prediction modeling. Each are critically important to the analytical study, and the analysis performed as a part of this dissertation.

The traditional approach involves determining the resistance of the tested members utilizing traditional design methods. While the modeling section focuses on the development of an FEM of the flanking span that was tested. Finally, as corrosion does play a role in all bridges, a corrosion prediction model was developed. All work in this section pertained Spans 28 and 30 as per the experimental chapter of this dissertation.

5.2 Traditional Resistance Model

For the traditional resistance model, the AASHTO Design Standards, AISC design manual and 2018 AASHTO MBE were utilized as primary references. As field testing was only performed on the main fascia girder and floorbeam at spans 28 and 30, the traditional study was limited to these members as well.

The first member analyzed was the fascia girder. Since the fascia girder for Span 28 is identical to the fascia girder for Span 30, calculations were performed once. It should be noted that conditions of both beams were similar based off a field inspection performed as well.

In total, three overall conditions were analyzed for the fascia girder. These included the following:

- As-Inspected Condition - 2016/2018 Inspections
- Original As-built Condition - 1939 Condition
- Predicted Corroded Condition - 2029 Condition

For the 2018 As-Inspected condition, losses were calculated using a combination of field data obtained from a site visit, in combination with data obtained from the NBIS Inspection Report. For the 2029 condition, a corrosion prediction equation was utilized which is expanded on later in this chapter.

For each of these three conditions, flexure capacities were calculated using the AASHTO and AISC design codes. For corroded conditions, calculations took this into account when calculating the respective moment of inertia and section modulus. The capacity of the fascia girder under the above three conditions are shown in the below table. These capacity values were subsequently inputted into each of the Load Rating Equations for further evaluation and comparison.

Table 5.1 - Fascia Girder Capacity for each Condition Case

Member Capacity		
Type	Rn	Unit
1939 As-Built Condition	11,998.00	K-FT
2018 As-Inspected Condition	11,564.00	K-FT
2029 Predicted Condition	10,478.00	K-FT

5.3 Corrosion and Prediction Modeling

The Oceanic Bridge is subjected to varying degrees of section loss throughout the entire bridge. Section loss/spalling ranges from corrosion of the concrete piers due to tidal fluctuations, to complete section loss to the supporting pile bents at the concrete T-Beam Approaches, to even spalling of the concrete deck. While these losses have a direct effect on the performance of the oceanic bridge, none quite affect the loading capacity like the condition of the structural steel.

Figure 5.1 - Spalling of Pile Bents (Approach Spans)

Figure 5.2 - Spalling of Concrete Deck and T-Beams (Approach Spans)

The structural steel superstructure supports some of the most critical spans of the Oceanic Bridge. Additionally, it makes up the majority of all the long spans. These spans as discussed vary from continuous to the simply supported flanking span, which tie indirectly to the dual leaf steel bascule span. All spans are comprised of the same configuration, a stringer floor beam system. The original paint on the bridge was lead. No re-painting of the steel has ever been performed due to the level of containment it would take to remove the paint. As a direct result, we see some extreme cases of section loss throughout each of the steel spans. Examples of this section loss can be found in some of the below figures.

Figure 5.3 - Span 22 Floor beam 1 - 5 LF of Section Loss along Bottom Flange

Figure 5.4 - Span 34 Floor beam 7 Section Loss along the Top Flange

Figure 5.5 - Section Loss and Corrosion at Rocker Bearing Connection

To compound the issue, Bridge S-31 is over the Navesink River which flows directly into the Atlantic Ocean. As a result, the Navesink is subjected to tidal flows and therefore contains brackish properties. This high saline environment increases the rate of corrosion. Additionally, the bridge scuppers located above the bridge fall directly on the outer girders, this poses as problematic during the winter season when de-icing salts are laid down on the bridge. Finally, as the joints at each span are the same as the ones installed in 1939, salt infiltration, as well as water infiltration from above is particularly higher in these areas.

There are 16 total spans at Bridge S-31 with steel superstructures including the main bascule span located at Span 29. Per the recent NBIS Inspection report published, using the NBIS Coding system the structural steel superstructure is rated as follows:

Table 5.2 - NBIS Inspection Results for Steel Superstructure

Span	NBIS Rating	Section Loss (Range)
21	3	20 - 30%
22	4	10 - 20%
23	3	20 - 30%
24	5	5 - 10%
25	4	10 - 20%
26	4	10 - 20%
27	4	10 - 20%
28	3	20 - 30%
29	Main Bascule Span	
30	4	10 - 20%
31	5	5 - 10%
32	5	5 - 10%
33	4	10 - 20%
34	4	10 - 20%
35	5	5 - 10%
36	4	10 - 20%
37	4	10 - 20%

As we can see from the above table, the structural steel ranges from serious (Span 28) to fair (Spans 24, 31, 32, 35), with the remaining spans found in poor condition. The worst span being the main flanking span, Span 28. Even after the 2014/2015 repairs, it is still rated in serious condition.

Since the Oceanic Bridge has an expected remaining service life of 10 years. The County, needs to keep the bridge in service until a new bridge is constructed. Therefore, as a part of this dissertation, a prediction model was developed to determine and gauge the level of section loss and associated strain on the main-thru girder located at Spans 28 and 30.

To determine the level of section loss, the below prediction equation developed by Komp in 1987 as described by Darmawan in 2013 was utilized for this exercise. This equation is as follows:

$$C = A/t^B \quad (5.1)$$

Where:

C = average corrosion penetration in μm

t = number of years

A and B are taken from a table shown below which compares various corrosion model parameters based on type of steel and environment.

Table 5.3 - Corrosion Model Parameter (Darmawan, 2013)

Environment	Unprotected carbon steel		Weathering steel	
	A	B	A	B
Rural	34.0	0.65	33.3	0.50
Urban	80.2	0.59	50.7	0.57
Marine	70.6	0.79	40.2	0.56

For this project, unprotected carbon steel was selected, as well as, the marine environment. This gave us values of 70.6 and 0.79 for variables A and B respectively. Additionally, the number of years inserted into t was 90 years which represents the bridge at the time of its demolition in 2029. Utilizing this equation, we obtained a value of 2470 μm or 0.097 inches.

This level of section loss was applied to all planes of the structural steel fascia girder for a new revised section. Accordingly, this data was inputted into the original capacity equations calculated for the fascia girder as referenced in the previous section. Additionally, this level of section loss was applied to the 2029 ABAQUS sub-model. From this the goal was to obtain

future load rating results based off the level of section loss noted. These results can be compared directly to the as-inspected model, as well as, actual results obtained in 2029.

5.4 Finite Element Modeling

The second part of this chapter involves the development of a finite element model. For this dissertation an FEM was developed for the entire anchor span. Again, as the conditions and configurations were nearly identical for Spans 28 and 30 only one model was created and analyzed.

Finite element modeling provides a series of benefits, including enhanced analysis; better insight into the redundancy of the flanking span system; and ease of analyzing the flanking span under different loading conditions. The model also allowed for the analysis of the flanking span under different physical conditions. The model developed can be seen in the figure below:

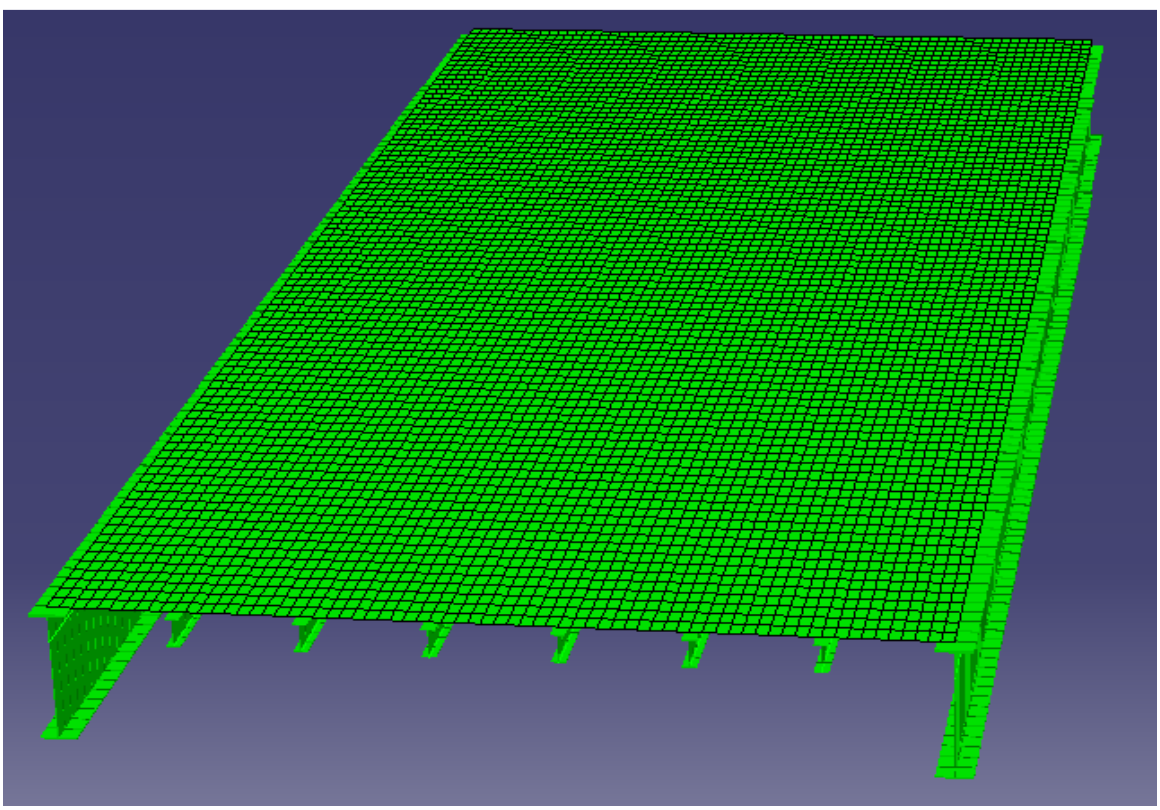

Figure 5.6 - Finite Element Model of Spans 28 and 30

This model served as a basis not only for comparison of different load case scenarios, but also assisted in comparing traditional load rating methods to experimental outputs. Additionally, due to the deteriorated nature of Bridge S-31, and it's given load posting, the FEM model provided insight into how the span would react to loads well above the 15-ton posting.

5.4.1 Model Development

All modeling was done utilizing ABAQUS CAE ("Complete Abaqus Environment"). ABAQUS CAE was chosen, because it provides users with some advanced tools including meshing. It also provides advanced visualization, can incorporate AutoCAD type models to develop the FEM, and is considered the complete analysis product of the ABAQUS line. ABAQUS CAE also allows for input files, which was utilized as a part of this project.

ABAQUS was also chosen for this project, as material properties can be specified, this was important due to the varying condition of Bridge S-31. It also, allows for the use of input coding as stated above, finally the level of analysis performed by this software in contrast to others provided us with results which closely mimicked the field experimentation results obtained.

For this project, several separate sub-models were developed. The first model developed matched the As-Inspected condition of S-31 during the 2016 and 2018 Load Testing of the flanking span. The purpose of this model was to serve as a baseline to match the current existing conditions of the Bridge S-31. It also served as a method of comparison to previously performed load ratings, and for other FEM models being considered as a part of this project.

This 2018 model included the rehabilitated floor beam 9 following the 2015/2016 repairs. It also considers the semi-deteriorated condition of the remaining steel members which included the main fascia girder being analyzed, as well as, the severely spalled concrete deck. This model

was the one calibrated to the experimental data gathered as a part of the Structural Health Monitoring Experimental Study.

Per review of the inspection reports, as-built plans, and analysis of other spans, the flanking span is subjected to the highest loads of the steel superstructure aside from the main bascule span. The main bascule span was not considered as a part of this study, as it had been previously rehabilitated and is not the subject of the controlling 15 ton posting. The floor beam at Spans 28 and 30 were prior to the 2015/2016 Rehabilitation Project. Additionally, the fascia girders at this span provide the greatest depth of any of the steel girders located on the bridge.

The approach steel girders adjacent to the flanking span, which make up the continuous system were also not considered. This is due to the fact that they are not subjected to the magnitude of the loads experienced by the flanking span. Additionally, these spans do not provide the stability, the flanking span serves in stabilizing the main bascule span during the opening and closing process.

The next model developed matched the original 1939 as-built drawings. This model was used as a basis of comparison for the 2018 inspected model to determine what changes have occurred over the past 80 years to the fascia girder primarily.

It also served as a mid-point comparison for the floor beam to see what changes exist between the rehabilitated member and the original floor beam member. This model considers all elements to be in good working condition.

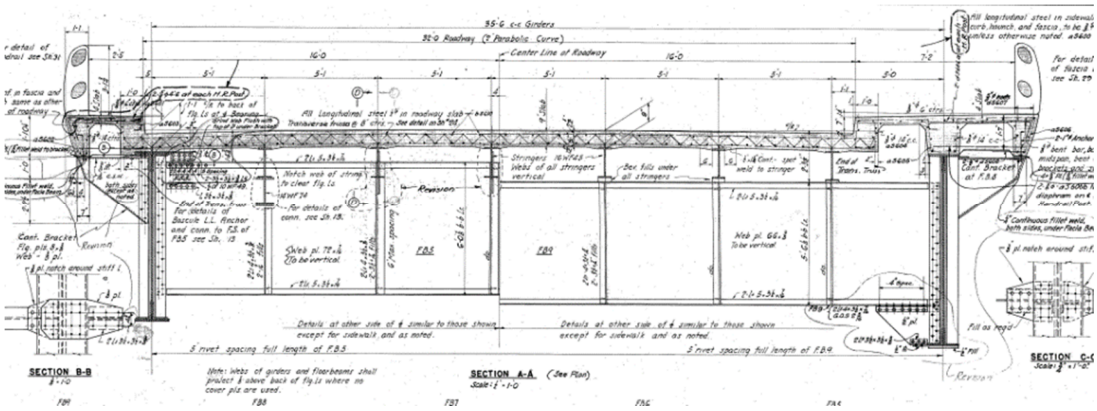

Figure 5.7 - As-Built Plan Utilized to develop 1939 Model

The final model developed was the 2013 pre-repair condition of the bridge. This model accounts for 30 to 100% section loss to floor beam 5. Due to the limitations of ABAQUS, to account for this section loss, an average section loss to the web and flanges of the floor beam was applied. This accounted to an approximate 50% overall reduction in section. A similar method was applied when performing traditional calculations to determine the capacity of the deteriorated member (See Figure 5.8).

Per review of the inspection reports, it was determined that the condition of the deck, fascia girder and other elements at Spans 28 and 30 were relatively similar to the condition found in 2016 and 2018. Therefore, the remaining portion of the 2018 as-inspected model was left as is.

The purpose of this model was to determine whether the 5-ton priority posting was valid, and if a relationship could be determined for pre and post repairs. It also allowed for us to understand the internal redundancy of the span further and determine the effects section loss of the floor beam had on the remaining members of the span.

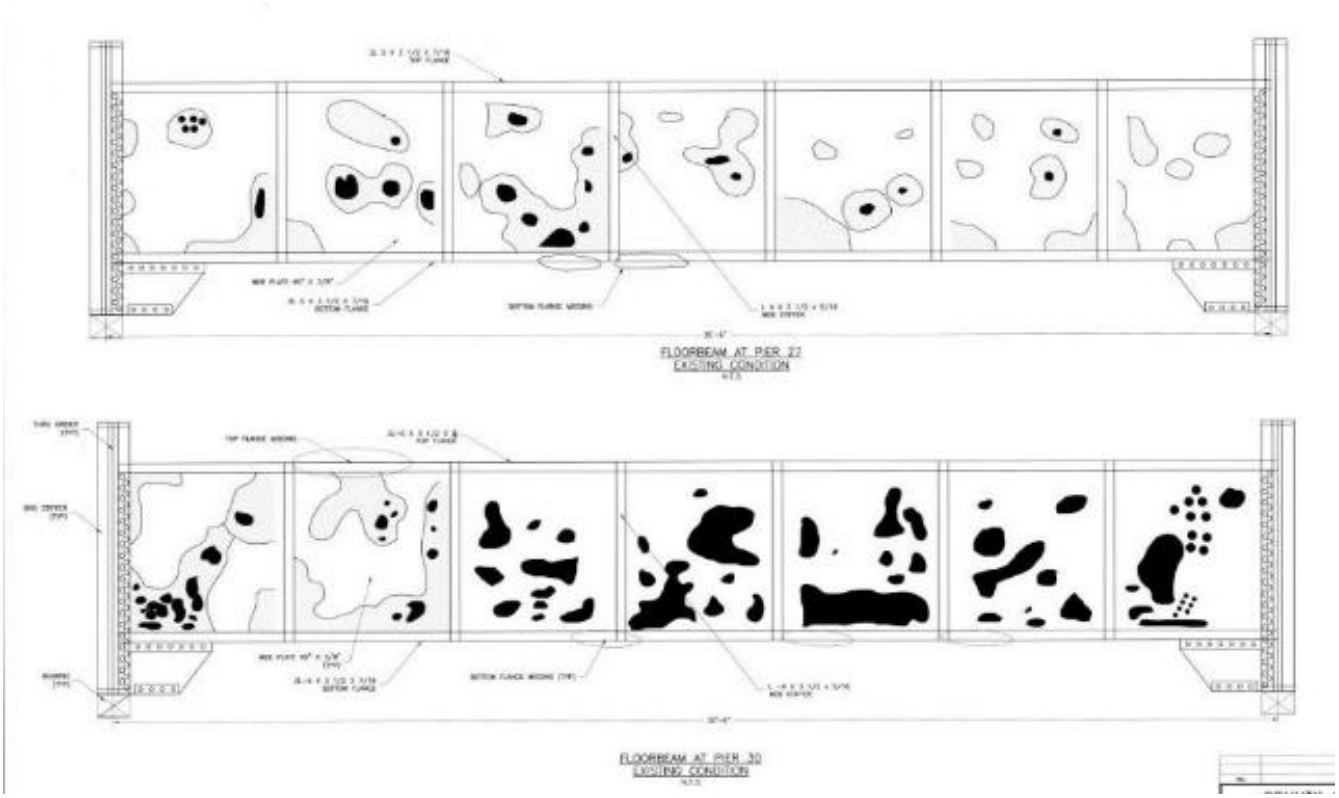

Figure 5.8 - Plans from 2014 Rehabilitation Repair to determine Section Loss to Floor Beam 9

5.4.2 - Model Development & Assumptions

Due to the limitations of ABAQUS, some parameters were required to be modified or assumed. As discussed, for the modeling portion of this project only one flanking/anchor span was modeled. As noted previously, this was because Spans 28 and 30 are practically identical. The model was developed utilizing the input file method, opposed to the CADD drawing method.

For the model, the node and element layout can be seen in the figure below. The model contains 712 beam elements, 35 floor beam elements, and over 6230 deck elements. Each longitudinal beam element is 12” in length the numbering of which increases by 1 in the longitudinal direction. Each deck element is 1/10th of the girder spacing in length, the numbering

of which increases by 100 in the transverse direction. The length of the span is 89ft and the overhangs, as well as, parapets were not considered in the model.

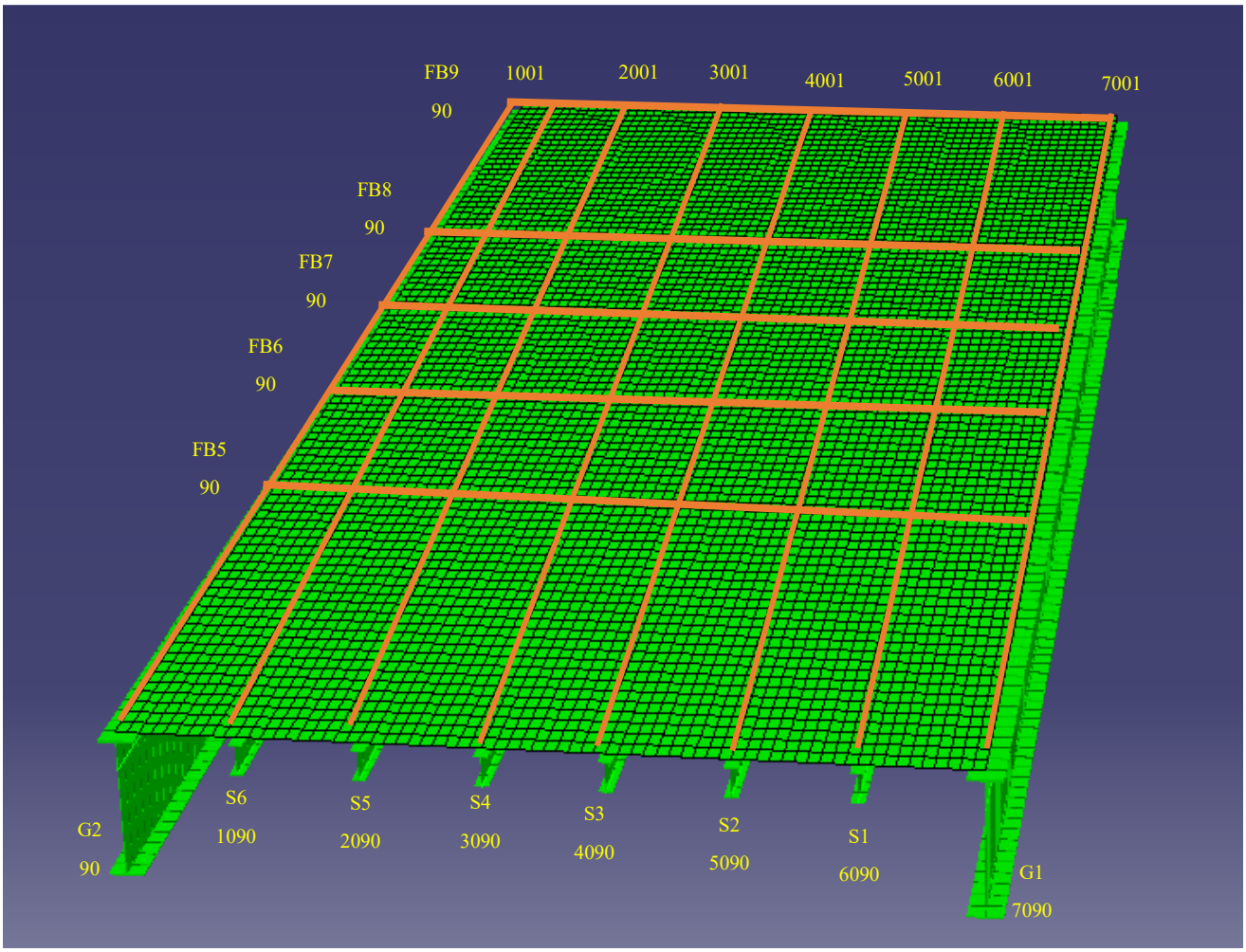

Figure 5.9 - Finite Element Method Node and Element Layout

An outlier of the model is the fact that no floor beam exists at the terminus where the main thru girder and stringers meet the main trunnion system. This is because the area between floor beam 5 and the terminus accounts for the main counterweight of the movable span. Additionally, the load of the deck and more importantly the live load is not transferred to the main flanking span, but to the main bascule girder. Figures taken from the field and extracted from the as-built drawings illustrating this can be found below:

Figure 5.10 - Area between Floor Beam 5 and Main Bascule Pier

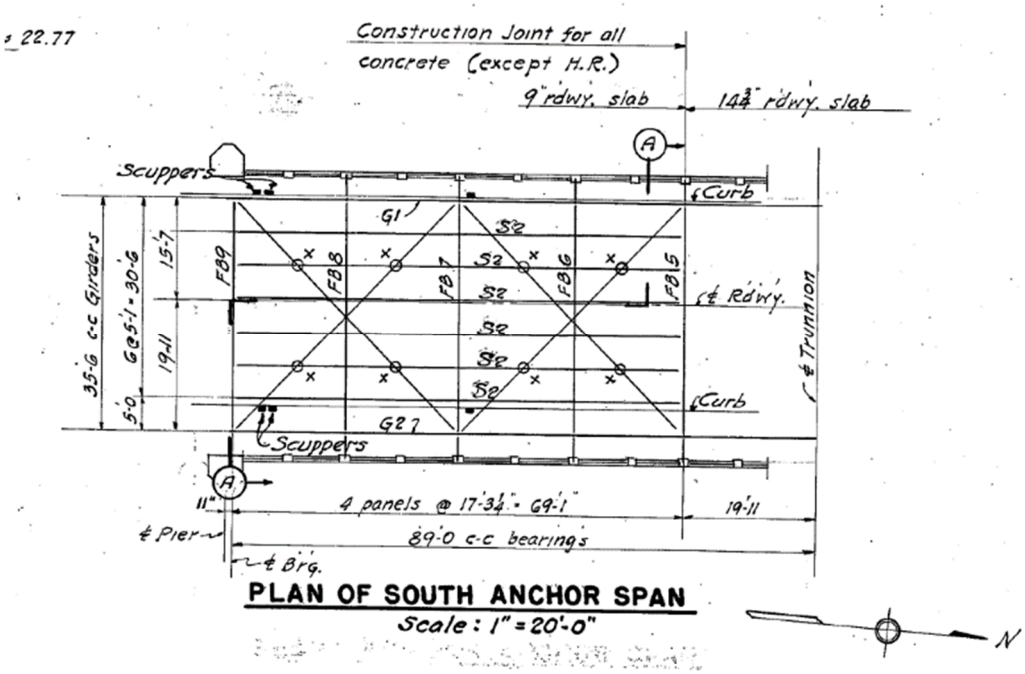

Figure 5.11 - Framing Plan of Southern Flanking Span

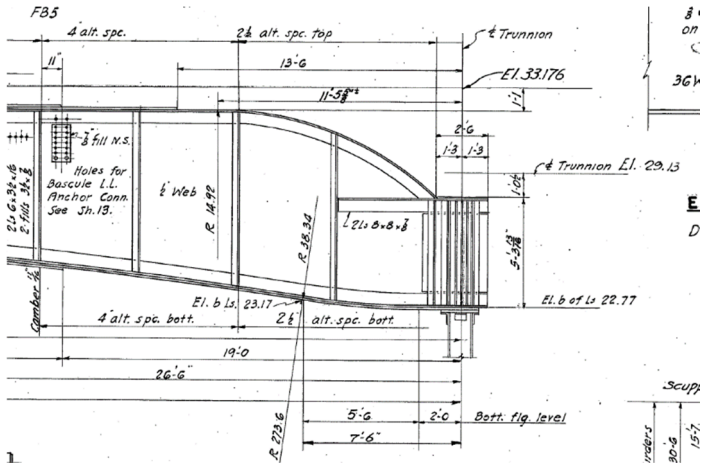

Figure 5.12 - Elevation of Main Fascia Girder between Floor beam 5 and Trunnion Support

Note that in Figure 5.12, there is a distinct gap between the top of deck and the trunnion support. This is reflected in the field and shows that there is no transfer between the deck and the main fascia girder proving that the beam in this location does not take any load from the deck above or the live load traveling over the span in that location.

Other modifications/assumptions were made in developing the model. Since ABAQUS contains a number of limitations, some parameters of the structure needed to be modified or assumed. These assumptions/modifications were considered and applied to all models developed. However, additional considerations such as section loss to members was applied as applicable. The assumptions made for these models were as follows:

- Although the barrier parapet and sidewalk found on both sides of the bridge will increase the stiffness of the thru girders, they were not included as a part of this model. The model only contains the deck from curb to curb width. This is appropriate as the sidewalks and parapets are mainly supported on floor beam brackets and do not have direct effect on either the main fascia girder or the floor beam.

- Although the overhangs (both steel and concrete) will increase the stiffness of the thru girders slightly, they were not included in the model.
- F'c of 4000 PSI was an assumed design parameter. This was based of review of the as-built drawings, and consultation of the 2018 MBE. However, due to the numerous patches in the deck, and because no cores were taken it is unknown what the true strength of the deck is. This value could be significantly greater or lower than 4000 PSI.
- The Modulus of Elasticity of concrete was determined to be 3.6x10^6 PSI, although given the above information this could be greater or lower.
- The design truck was placed within in the center of the southbound lane, taken to be 4ft from G2, this was similar to the actual load tests performed in the field during the 2016 and 2018 testing.
- As we can see from the above as-builts, for the fascia girders, the girder depths vary throughout the length of the span. This was typical of the era which included architectural considerations into the design. Therefore, to model this in ABAQUS, an average depth was used for the entire length of the span for these fascia girders. The cover plates were included in the model.
- For the stringers and floor beams 5 through 8, it was assumed that they were in satisfactory condition with minimal section loss. This was due to their relative containment within the stringer floor beam system and based off the visual inspection of the span performed.
- The curve in the top flange as noted above in Figure 5.12 was not modeled in ABAQUS with the curve. Instead it was modeled with connection to the deck.

- Due to the above constraint, live loads were only run for the first 71 feet of the span in accordance with the framing plan shown above in Figure 5.10.
- It was assumed that span had composite action between the deck and the steel girders, which was proven during the field inspection.
- The model was created using longitudinal nodes at every foot. As the floor beams did not always fall evenly at each node, the floor beam locations were rounded to the nearest foot.
- No haunch was modeled when developing this model.
- Due to the nodal layout, the spacing of the wheels was approximated to get as close to six feet as possible.
- The stress from the model was reduced by the proportion of the modeled moment of inertia compared to the moment of inertia of the section including the concrete sidewalk, barrier, and steel bracket.
- To account for the section loss in the span (2018 Model only), the stress was increased by the condition factor of 1/0.95.
- For the deteriorated floor beam and the corroded condition fascia girders (2029 Model) an average section loss was applied over the course of the girder.
- For the 2013 deteriorated floor beam a different material DETSTEEL was specified to predict the effects of holes in the web. For this material the Modulus of Elasticity and thickness of the web were both reduced to simulate the effects of holes in the web.

5.4.3 - Live Load Models Considered for Model

For each of the models noted above, several live load models were utilized to analyze the max strain experienced in the fascia girder, as well as, the floor beam. These models included the following:

- 2016 Experimental Truck
- 2018 Experimental Truck
- HS-20 Truck
- Maximum Wim Load

Initially, a maximum WIM load -Type 2 truck was considered as a part of this study. However, after performing traditional calculations, and obtaining observed strains in the fascia girder/floor beam, it was determined the Type 1 truck provided more extreme results and was therefore, chosen as the vehicle for analysis. Diagrams of each of the trucks load tested can be found in the figures below:

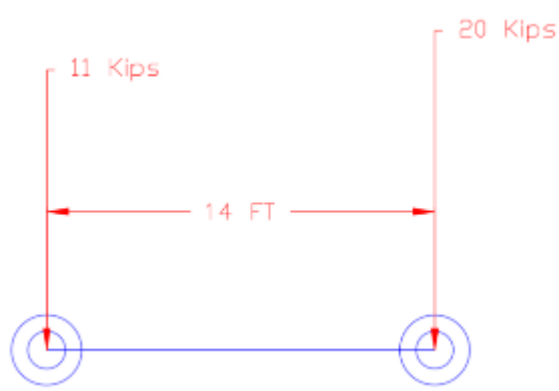

Figure 5.13 -2016 Experimental Truck

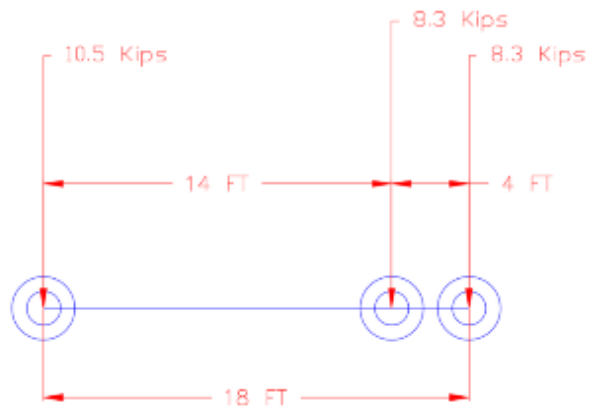

Figure 5.14 - 2018 Experimental Truck

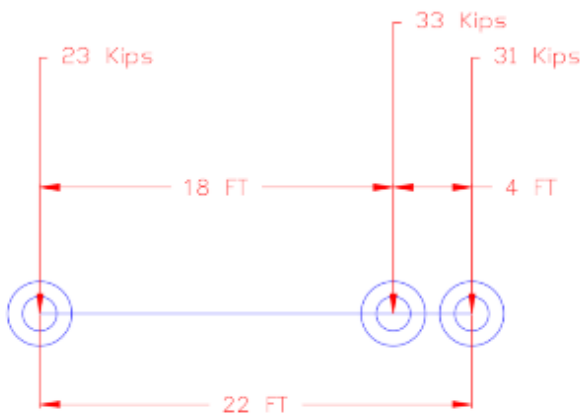

Figure 5.15 - Maximum WIM Load Trucks Type 1

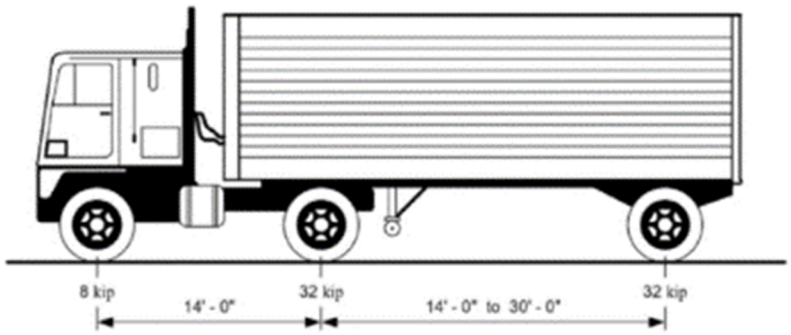

Figure 5.16 - HS-20 Load (Google Images)

5.4.4 - Model Calibration

Following the creation of the models the next step was to calibrate the model. To do this, we needed data obtained in the field from the static and dynamic testing, as well as, a model which utilized the experimental truck. This was done for both the 2016 and 2018 trucks. For each calibration performed, maximum strains were obtained from the field experiment, as well as, a curve showing the dynamic forces for that test. Meanwhile, the 2016 and 2018 trucks were inputted into the 2018 ABAQUS Model. In ABAQUS, maximum strains were extracted in the location in which strain gauges were applied. Additionally, since loads were plotted every foot to display truck movement along the span, a curve was created accordingly to represent the truck crossing over the span. Following this, the curves were transposed over each other, and the maximum strains were obtained. For the model to be calibrated, maximum strains should be similar (normally FEM data providing more conservative results, and the graph should display some similarity to the field data. It should be noted that FEM data is normally displayed in linear fashion and points in between analysis are not generally similar. Once the model has been successfully calibrated, results can be obtained and processed accordingly.

5.4.5 - Data Collection and Processing

Subsequently after the creation and calibration of the models and accordingly the input of each of the live load models noted above, the following step was to obtain data for each load case under each condition. Similar to the calibration step, maximum strains were obtained from both the floor beam and the fascia girder for each of the condition cases, under each load case. Like the calibration step, graphs were developed to show the change in strain compared to where the truck was on the flanking span. These graphs should be consistent with the calibration stage but are different based on number of axles and overall vehicle weight. Once the maximum strains

were obtained under each load case they needed to be converted over to live load moment. To achieve the process utilized under the experimental study was followed. This involved the following:

For the fascia girder, the first step was to convert strain over to stress. Once stress had been determined the following step was to determine the live load induced on the member. To determine this, the moment-stress equation was utilized. Since the fascia girder moment of inertia was relatively consistent for the three load cases, the centroidal axis remained the same. Moment of Inertias were modified slightly for each of the load cases used. As discussed, for the floor beam to properly analyze the data, the maximum shear force needed to be determined. To achieve this, the shear stress equation was utilized. Following this, the next step like the experimental tests was to find the maximum shear. Once these values had been determined, the results were inserted into the live load variable of the Load Rating Equation for finite element modeling. These results were compared to the Load Rating Results obtained in the field, as well as, traditional methods.

CHAPTER 6

DISCUSSION OF RESULTS

6.1 – Overview

The purpose of this chapter is to provide a summary of the results from the analytical and experimental portions of this dissertation. This chapter is divided into several parts. The first part will go through the experimental field data obtained and the results based off data processing. The second part will review results obtained from the FEM calibration and analysis. The third part will provide the load rating results for each of the cases described previously. As load ratings were performed for both the LRFR and LFR, they will be subsequently compared as a part of this third part. Finally, a brief discussion on an overall comparison of these results will be provided for in the final part of this chapter.

6.2 – Experimental Results

The purpose of this subsection is to provide discussion of results pertaining to the experimental portion of this dissertation. Included in this subsection will be a review of the results obtained through the WIM sensors and the SHMs.

6.2.1 – Weigh-in-Motion Results

The Oceanic Bridge is subject to peak traffic specifically during the summer season. Therefore, the data gathering period for this study was 120 days or four-months beginning on April 24, 2019 and ending on August 22, 2019. This period gives an ample sample size to determine a site-specific factor for Bridge S-31.

Per the relative frequency histogram provided below, a total of 5,069 trucks passed over Bridge S-31 during the 120 days. This gives the bridge an ADTT of approximately 43 trucks per day. Per the 2015 NBIS Report, S-31 has an ADT of approximately 14,000 vehicles per day, making the ADTT approximately 0.3% of the daily traffic. As discussed previously, Bridge S-31 is posted for only 15 tons which would account for this very low percentage.

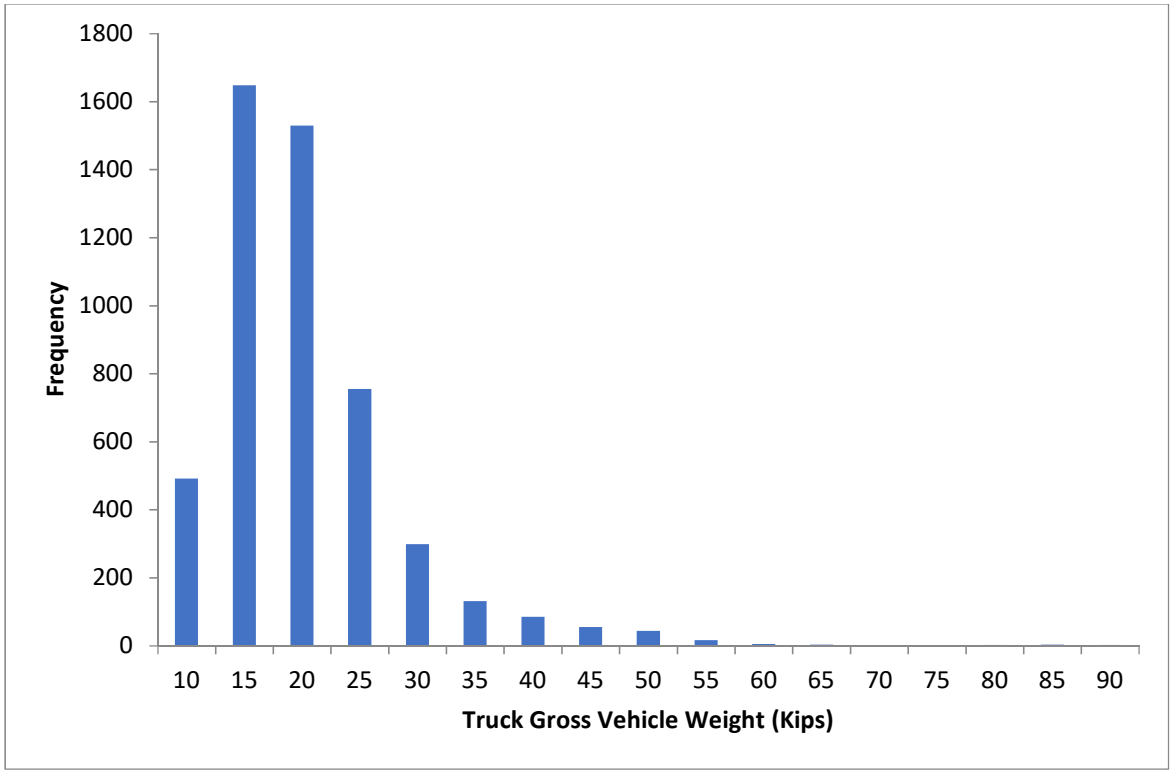

Figure 6.1 - Bridge S-31 WIM Data Relative Frequency Histogram

Per the weigh-in-motion (WIM) sensor results, the average speed crossing the bridge was 31 miles per hour, just under the current speed limit. The average truck had two axles and had a Gross Vehicle Weight of 18.26 Kips or 9.13 Tons. The minimum observed loading was 8 kips or 4 tons. It should be noted that the average GVW measured under these conditions is approximately 6 tons under the weight limit posting.

The maximum load observed over the course of the four-month period was 88 kips or 44 tons which was 29 tons over the 15-ton posting. Additionally, of the 5,069 trucks which crossed the bridge during the study period, 6.85% or 347 trucks exceeded the 15-ton posting. A full breakdown of the trucks observed as a part of this investigation is provided for in the appendix of this dissertation.

Two methods of analysis were utilized. The first excluded the use of two-axle trucks, while the other method included all vehicles as shown above. To determine the site-specific factor, the commentary under Section 6A.4.4.2.2 of the AASHTO MBE was closely followed for both methods.

Following subsection 6A.4.4.2.2 of the 2018 MBE, in which all trucks were considered, it was determined that the 20% cutoff of the vehicles observed was 22 Kips. Based off this information the average GVW was 26.39 Kips with a standard deviation of 5.19 Kips. Using the MBE, the following live load factors were determined:

Table 6.1 - Live Load Factor Calculation (With Two-Axle Trucks)

Factor	Live Load Factor Value	# of Lanes
γL	0.462	One Lane
γL	0.512	Two Lanes or More

Per C6A.4.4.2.3a-1, the minimum site-specific live load factor a bridge can have is 1.30. Therefore, based on this analysis and in accordance with the MBE, the recommended live load factor based on the site-specific data is increased to **1.30**. Not using this limitation, the live load factor utilizing this method would be **0.512**.

For the method in which two axle trucks were eliminated from the data set, a relative frequency histogram was developed. Based off this new information the number of trucks is

decreased to 645, an 87% reduction. However, most of trucks filtered out fall within the lower Gross Vehicle Weight categories.

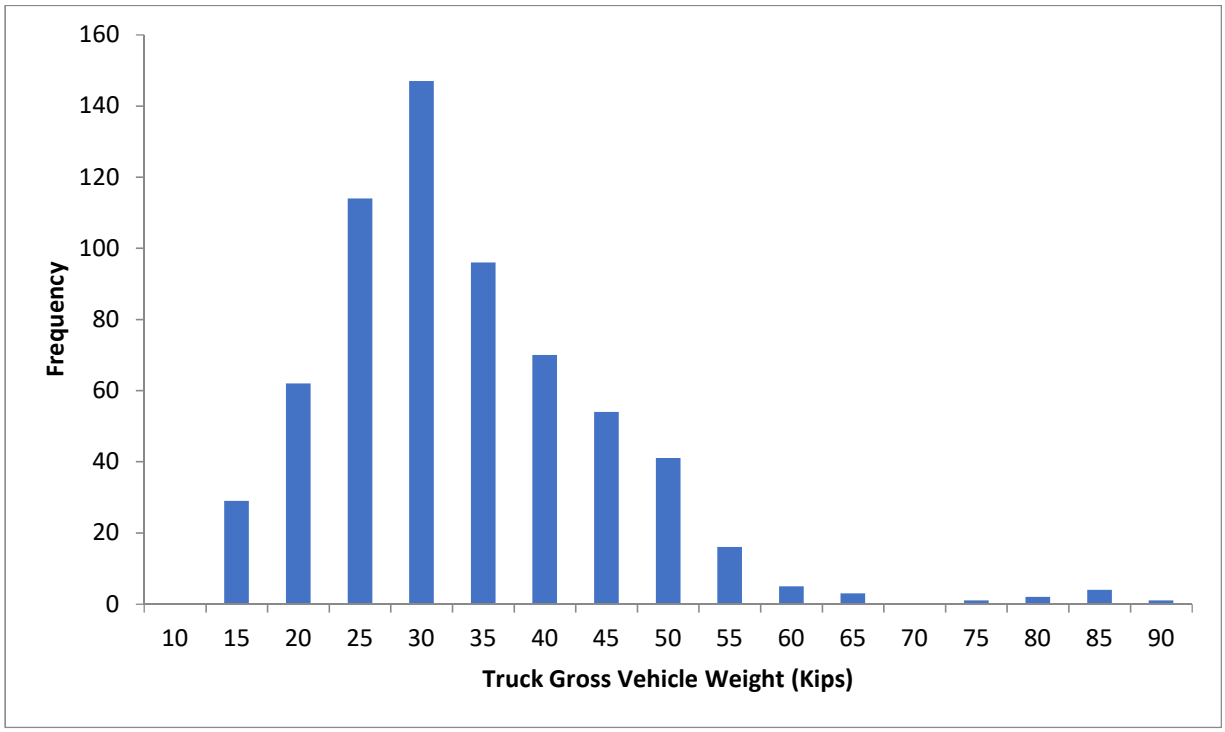

Figure 6.2 - Weigh-in-Motion Relative Frequency Histogram (Without 2-Axle Trucks)

Using the same analysis following Section 6A.4.4.2.2, it was determined that the 20% cutoff of the vehicles observed was 40 Kips. Based off this information the average GVW was 41.36 Kips with a standard deviation of 1.30 Kips which was utilized to determine the site specific live load factor. Note the average GVW in this case is 5 tons heavier than the load posting for the bridge.

Per this information, the following was determined:

Table 6.2 - Live Load Factor Calculation (With Two-Axle Trucks)

Factor	Live Load Factor Value	# of Lanes
γL	0.637	One Lane
γL	0.650	Two Lanes or More

Similarly, the first method, due to the minimum Live Load Factor limit, per C6A.4.4.2.3a-1, the recommended Live Load Factor based on the site-specific data is increased to **1.30**. Not using this limitation, the Live Load Factor utilizing this method would be **0.650**. It should be noted that eliminating the two axle vehicles result in an increase in the live load factor by 27%.

Furthermore, utilizing the two-axle filter per NCHRP 12-83 Flowchart, the number of vehicles in this data set with the filter applied was reduced to 645 trucks. Of these trucks 293 or 45.43% exceeded the 15-ton posting. The overall average vehicle weight was 31.39 Kips with a standard deviation of 11.49 kips.

It can be inferred from above, that the elimination of two-axle type trucks from the data group is beneficial in the development of a site-specific factor. This is due to the fact that by eliminating the two-axle trucks we are creating a more normal distribution when compared to the histogram that includes all trucks. Additionally, focus is placed on the heavier trucks which normally require more than two axles to operate, relating in a more realistic site-specific factor.

Therefore, it was ultimately determined that the method in which the two axle trucks are eliminated per the NCHRP 12-83 flowchart was followed. As such, a live load factor of **1.3** per the MBE be utilized.

Following this, Lmax was determined. Lmax as discussed in the previous chapter pertains to the maximum live load the bridge will see over a five-year period. For this analysis, the first step was to develop a cumulative frequency diagram as shown in the below figure.

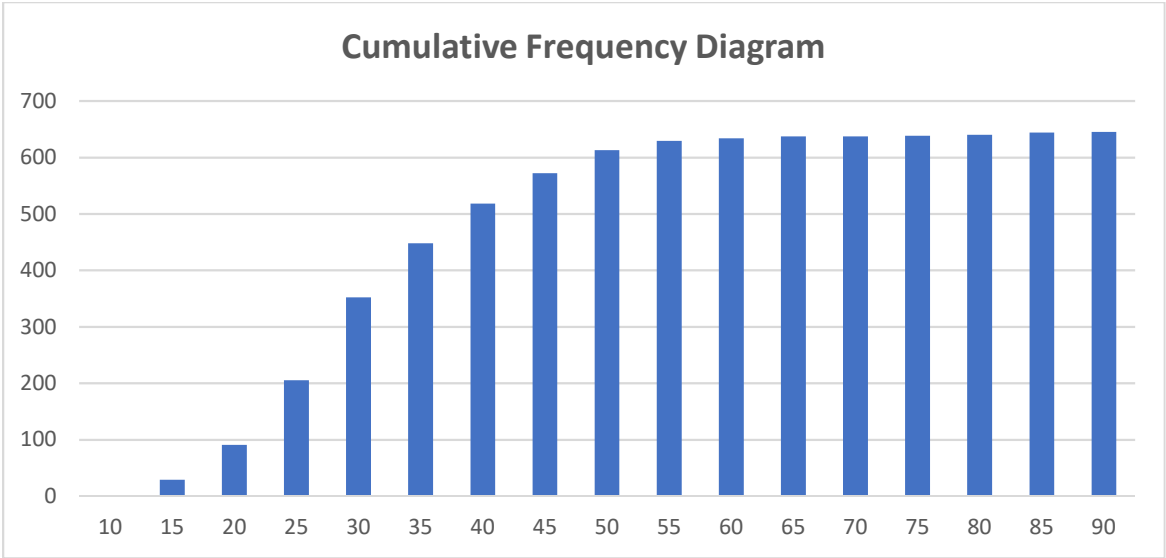

Figure 6.3 - Cumulative Frequency Histogram

Once the histogram was developed the next step was to determine what the top 5 percentiles of trucks were for this data set. Based off the analysis performed the study was limited to 40 trucks all with a weight over 50 kips. From here the sample mean, standard deviation variance and coefficient of variation was all calculated. These sample results are shown in the below table:

Table 6.3 - Sample Truck Data Statistical Results

Sample Mean	59.03
Sample Standard Deviation	11.98
Variance	143.56
Coefficient of Variation	20.30%

Using this information, we were able to develop the cumulative distribution function as shown in the below equation:

$$F(z) = 0.087(GVW) - 2.73$$

Where 0.087 is equal to the slope of the line and -2.73 is the intercept. Using this information, we were able to calculate the mean and standard deviation for the event which were 59.025 and 11.98 respectively. Based off this we obtained a Lmax equal to 105.693 using equation C6A.4.4.2.3a-5 from the 2018 AASHTO MBE. The final step was to develop the site-specific factor based off this information. This is shown in the below table for one and two lanes respectively:

Table 6.4 - Live Load Factor Calculation

# of Lanes	γl	2018 AASHTO Minimum
One Lane	1.59	1.80
Two Lanes	0.79	1.30

As S-31 is two-lanes we use a live load factor of 0.79. However, since the 2018 MBE sets the minimum Live Load Factor to 1.30, our factor used for the equation is therefore, increased to meet this minimum. As we can see this 1.30 factor is the same as what was calculated previously. Therefore, our Site-Specific Factor as calculated in accordance with the 2018 MBE is 1.30. Again, it should be noted that for S-31 the live load factor is likely lower due to the 15-ton posting. This proves to us that the posting is effective as it relates in site-specific factor in both the short term and using the 5-year max analysis of less than the minimum required factor by 2018 MBE. Since both the site-specific short term and Lmax live load factors are below the minimum required by the 2018 MBE, a separate analysis under the LRFR method was undertaken in which the actual Live Load Factor calculated was utilized. For this exercise a Live Load Factor of 0.79 was selected as it relates to the long-term load prediction of S-31.

The last part of the WIM Study was to identify the maximum live load observed at the project site during the study period for utilization in the live load finite element model. Per our

study it was recommended the vehicle shown in the figure below be utilized. As we can see from the figure, the vehicle is a 3-axle truck with a GVW of 87 Kips or 43.5 tons which exceeds the posting by 28.5 tons.

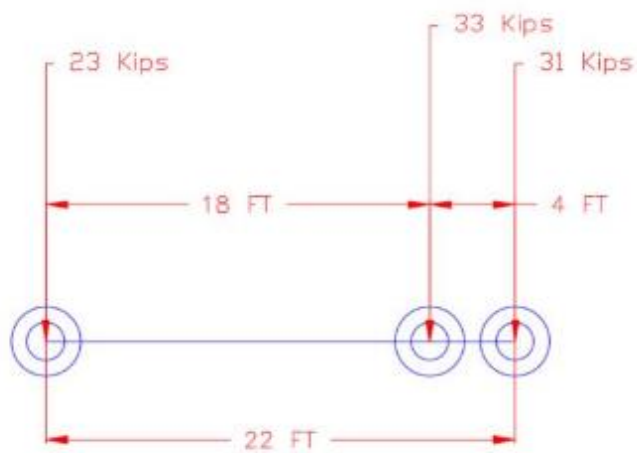

Figure 6.4 - Maximum Observed Load Case per WIM Sensors

6.2.2 – Structural Health Monitoring Results

As discussed previously, two load tests were performed at Bridge S-31. One during April 2016, and the other during August 2018. Both tests were done at identical locations utilizing similar trucks. Vehicles chosen were loaded up to the 15-ton load posting.

While there are several small differences, overall the two testing events were practically identical. The results obtained therefore could be compared to determine if any significant changes were noticed in the members over the course of the two-year period. Additionally, the testing provides us with additional field information to further calibrate the finite element model.

6.2.2.1 - 2016 Testing and Results

The maximum strains were obtained from the field for the different sensors and the shown in the below table. This information was taken following the plotting of the dynamic

results in Microsoft Excel. For each test the graph plotted, and maximum strain observed was obtained for FEM calibration. Additionally, the maximum strain observed was utilized for the Load Rating analysis. A graph for one of the fascia girder results is provided below as an example. This was taken at the bottom fascia girder. Per the results, sensor B3227 observed the highest strain with a value of 17.96. It should be noted that the observed strain at the floor beam (B2054) was 11.15. A full breakdown of all the results can be found in the appendix of this dissertation.

Table 6.5 - Maximum Observed Strains (2016 Field Testing)

	B3225	B3227	B3216	B2054
Field - Dynamic	15.64	17.96	12.93	11.15
Field - Static	13.86	16.05	12.03	0.34

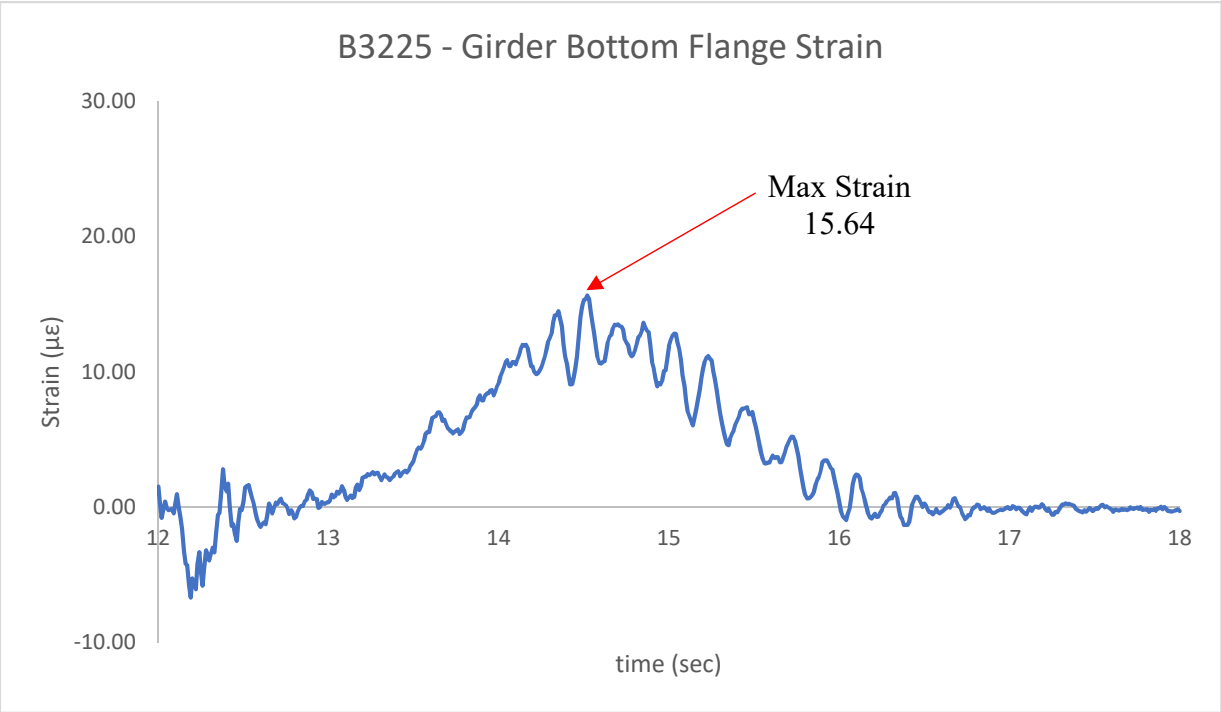

Figure 6.5 - Strain at B3225, Dynamic

6.2.2.2 - 2018 Testing and Results

During the 2018 testing, both Spans 28 and 30 were tested unlike 2016 where only one span was tested. However, test gauges were all placed in identical locations and directly below the southbound lane. Static test and dynamic testing was performed, and a typical dynamic strain data is shown in the below figures. Additionally, the tables provided below include the maximum strain observed for each of the gauges installed per the respective span. Similar to the 2016 results a full breakdown of the results can be found in the appendix of this dissertation.

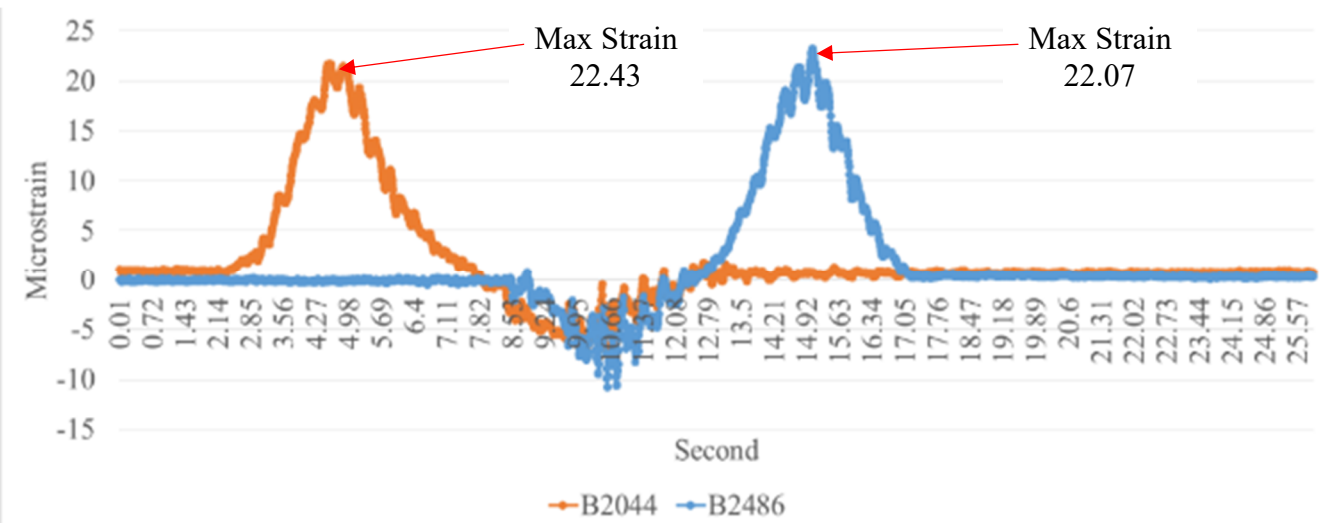

Figure 6.6 - Typical strain data collected from dynamic testing at Fascia Girder

Table 6.6 - Maximum Strains of South Span from Dynamic Testing

Run	B3684 (Bot)	B3227 (Bot)	B2486 (Bot)	B3691 (Top)
30 mph	9.82	15.47	22.07	1.84

Table 6.7 - Maximum Strains of North Span from Dynamic Testing

Runs	B2048 (Bot)	B2044 (Bot)	B2054 (Bot)	B2059 (Top)
30 mph	11.61	22.43	13.11	-2.02

As we can see from the above tables, the maximum strain was observed during the 30mph test. The maximum strain was observed on the north span with a max strain of 22.43 at the fascia girder. The results of this Strain Gauge (2044) is shown in the below figure.

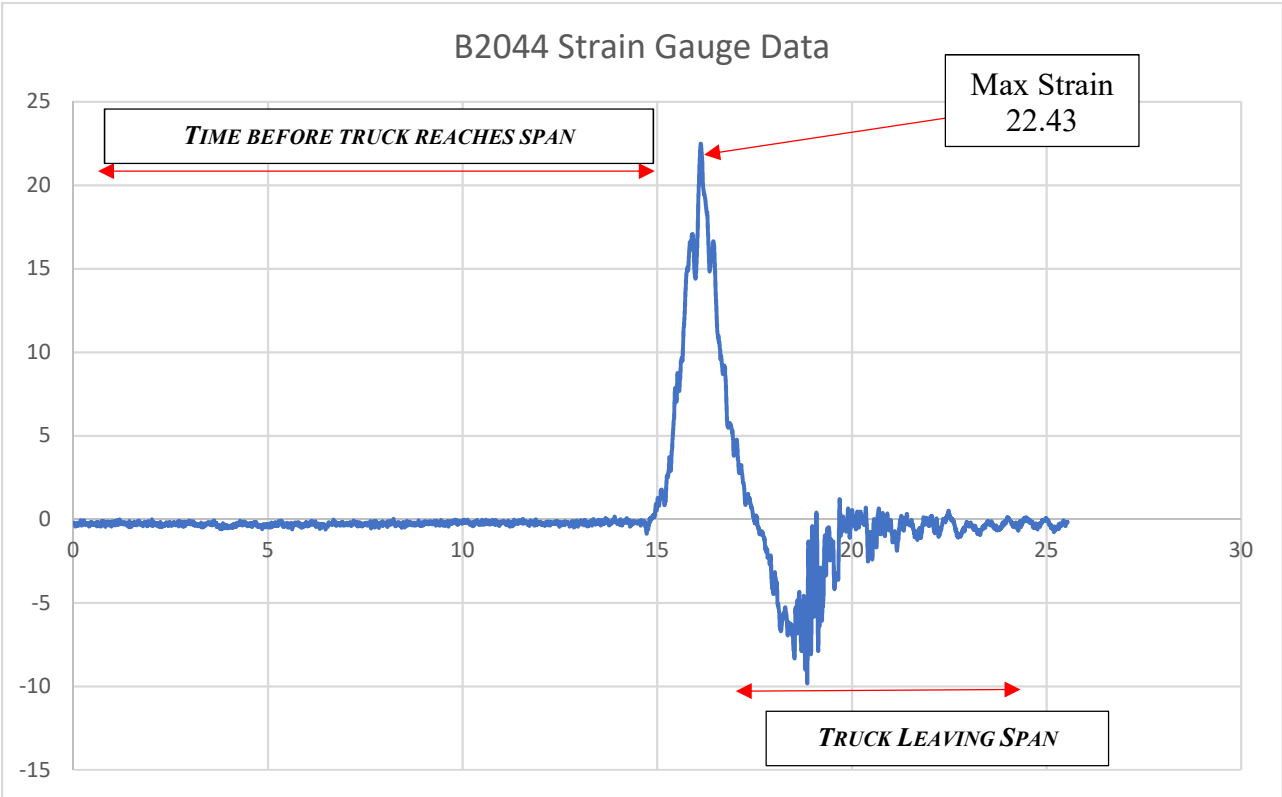

Figure 6.7 - B2044 Strain Gauge Data

For the floor beam, the maximum strain observed was at sensor B2048 with a maximum strain of 11.61. Again, this was located on the north span. The graph of this gauge is shown in the figure below. As one can observe the strain stays the same, around zero, for the majority of the test. This is because the gauge is located on the outer floor beam near the pier. Additionally, the variation in output following the maximum strain can be attributed to the load (axle) transferring from one span to the next adjacent span. While the bridge is simply supported, the decks are connected to a degree which causes this response.

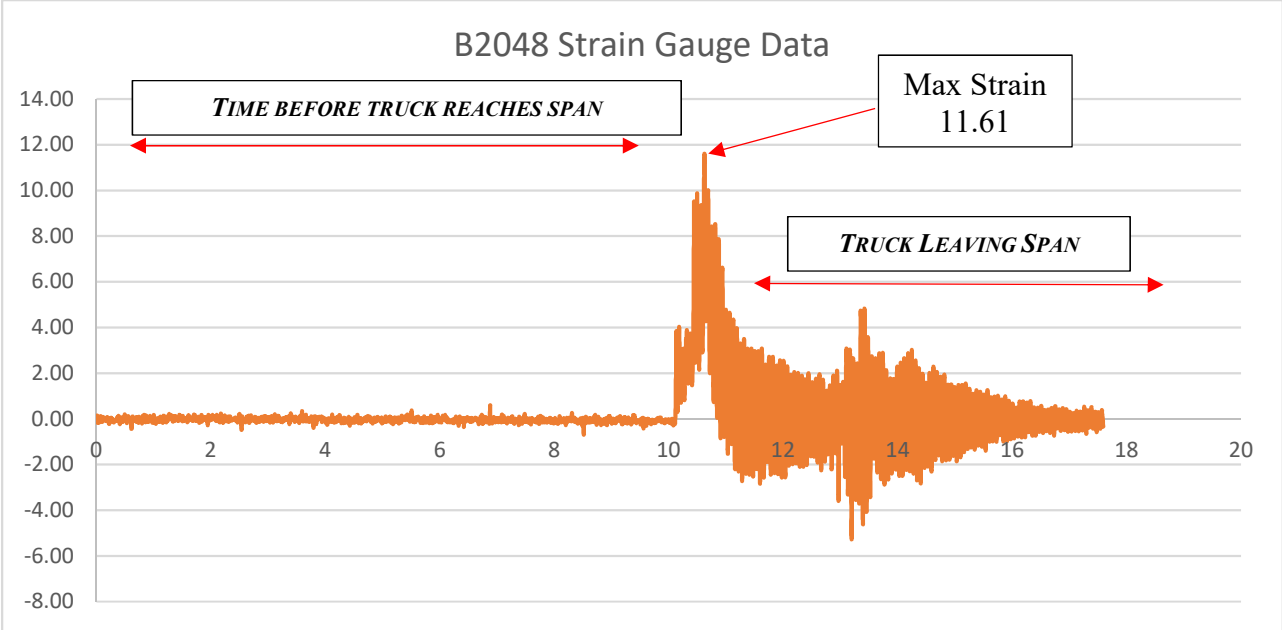

Figure 6.8 - B2048 Strain Gauge Data

6.2.2.3 - Comparison of 2016 versus 2018 Field Results

As we can see from the above tables, for both testing runs the maximum strain was observed during the 30mph test. For the calibration and analysis this data will be utilized. For the floor beams again the 30mph test, yielded the highest results therefore, these values will be utilized during the load rating analysis. It should be noted that the loading of the truck in 2016 was 27.1 kips while the loading of the truck in 2018 was 31 kips, a 14.4% increase in loading. This can be the reason why the results obtained in 2018 were overall higher than that in 2016. A table containing the max strains for each of the two tests are shown below.

Table 6.8 - Max Stain Comparison 2016 vs 2018

Year	Run	Fascia Girder	Floor beam
2018	30 mph (2nd run)	22.43	13.11
2016	30 mph	17.96	11.15

Based on the above table, we see an increase in maximum strain by 24.88% for the fascia girder. This, is likely due to a combination in increase in loading between the two tests and the different number of truck axles. Additionally, for the floor beam we see only a 17.5% increase in strain, this could be due to again the increase in weight during the two tests. Additionally, visual inspections performed during the testing revealed no significant changes to the tested members. Therefore, once can conclude that the members tested did not deteriorate further during the two-year gap of testing.

6.3 – Finite Element Modeling

This subsection reviews the finite element calibration model development, and the live load results obtained through the various models developed.

6.3.1 – Finite Element Calibration

Following the structural health monitoring phase of this project, the next step was to develop a finite element model suitable for further analysis. Since various load cases would be utilized the goal was to develop a model which yielded results like the field data obtain. Key points such as maximum strain and shape of the graph would be observed to determine whether the model was calibrated correctly or not. Due to the nature of the ABAQUS programing it was expected that the FEM would be linear and would not totally mimic the field data.

Therefore, two load cases were developed for input into ABAQUS. These load cases matched the truck loads used during 2016 and 2018. Since the maximum strain was observed on the thru girder at mid span on the bottom flange, this area was utilized as the basis of comparison. These results are shown in the below two figures.

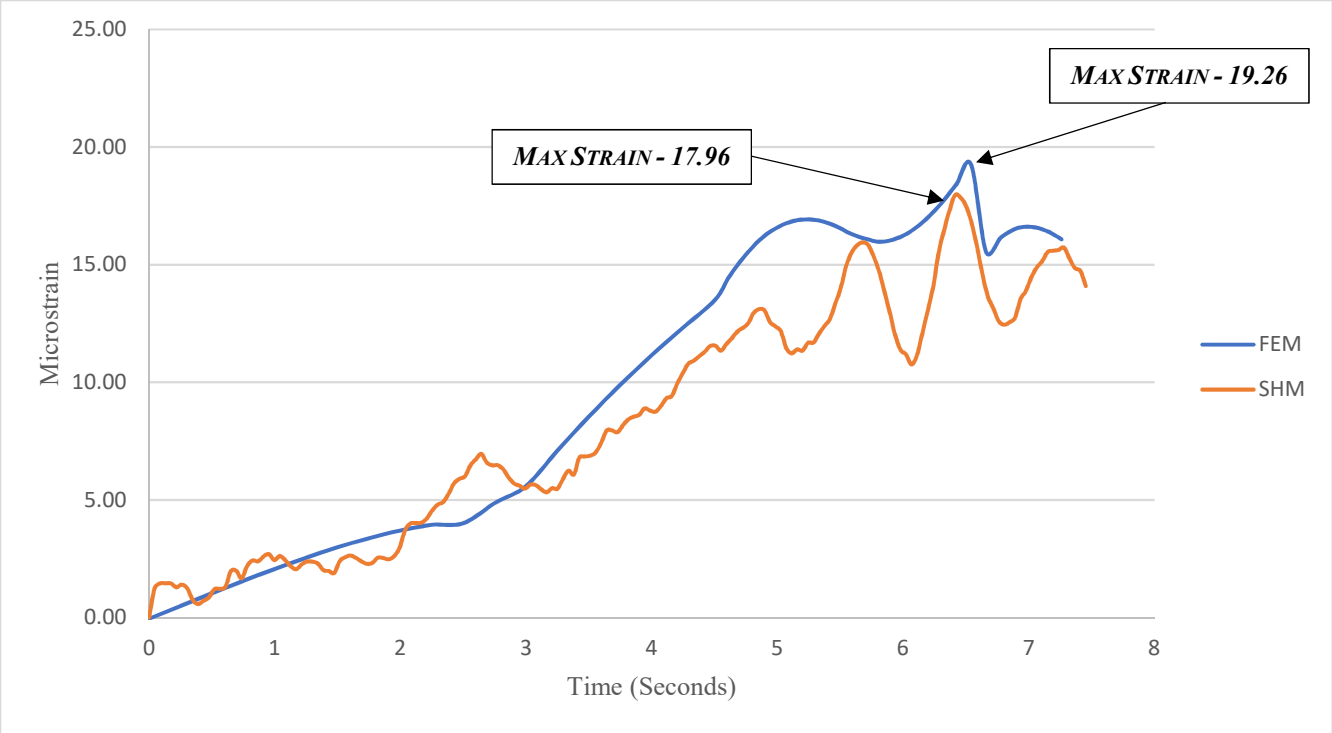

Figure 6.9 - 2016 Calibration Fascia Girder

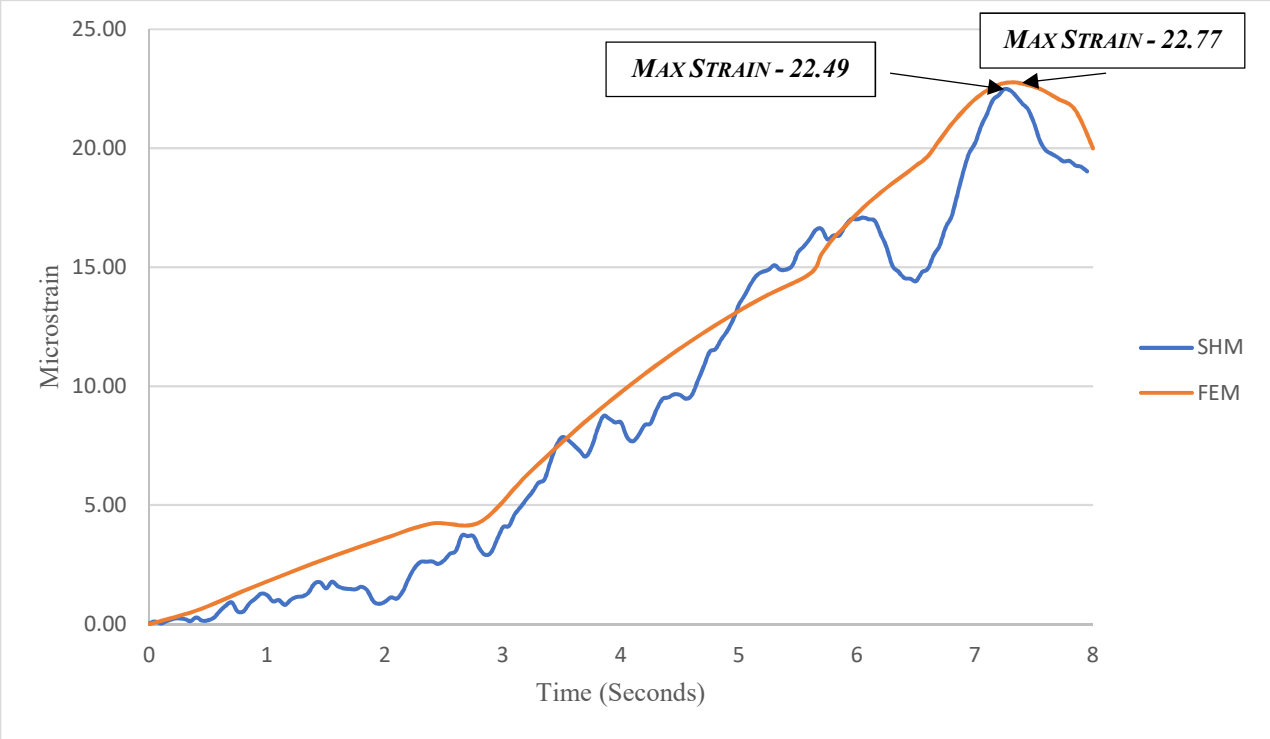

Figure 6.10 - 2018 Calibration Fascia Girder

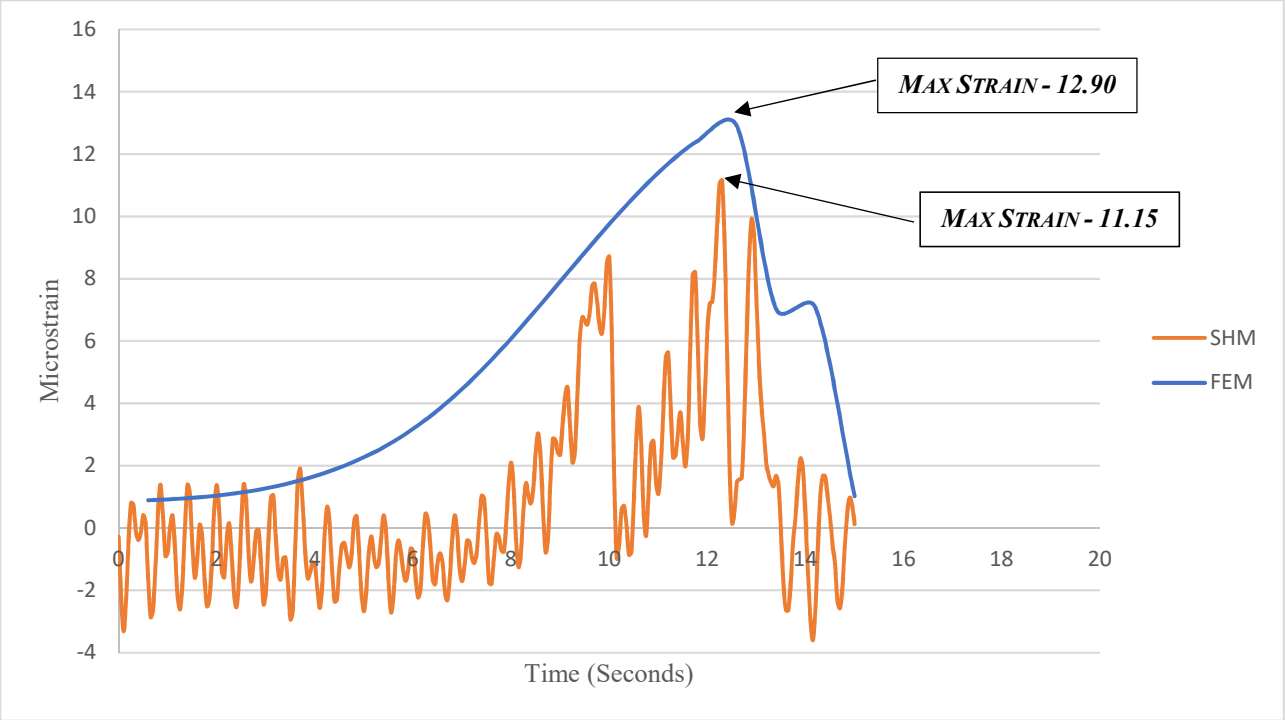

Figure 6.11 - 2016 Calibration Floor Beam

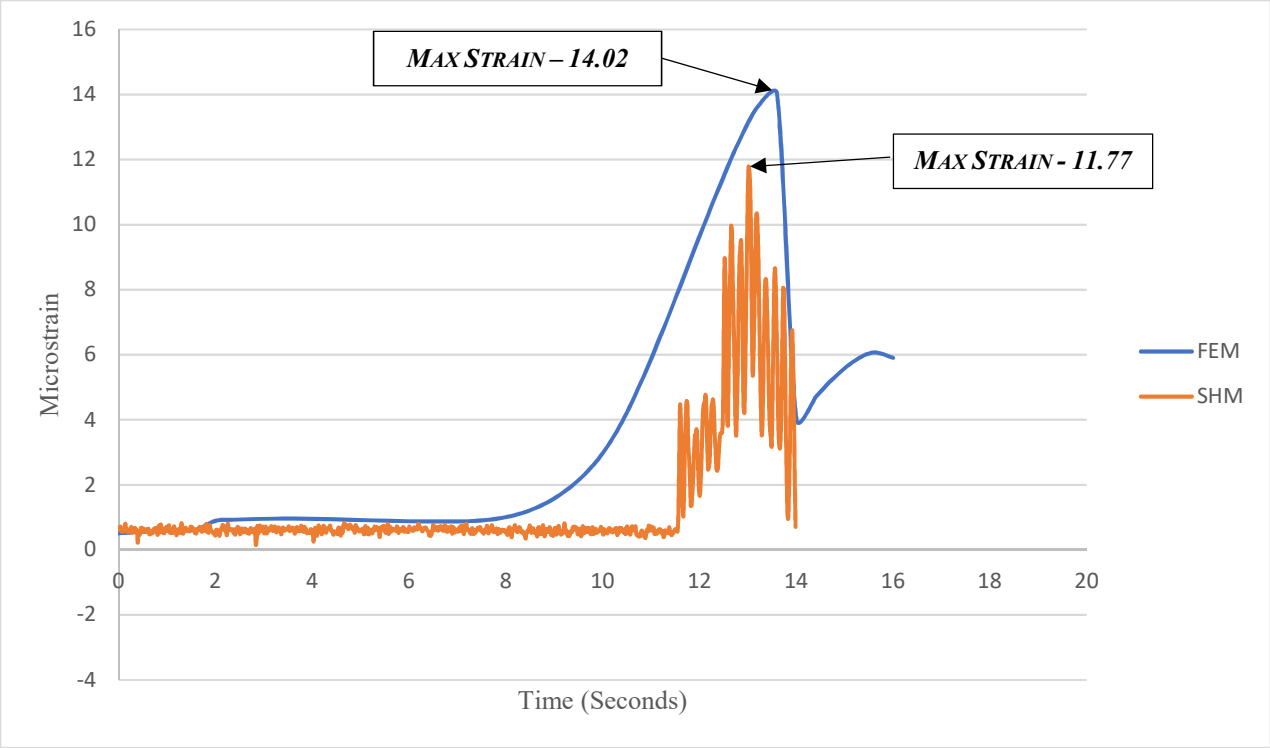

Figure 6.12 - 2018 Calibration Floor Beam

The above two figures are for the floor beams. For these members, strain gauges were only attached to the bottom flange at mid span. Finite element results were obtained at an identical location to the field gauges. These results were plotted and compared directly against the field data obtained as shown in the below two figures.

Following this, as another means of checking the model versus the field data, maximum strains were obtained and compared. The results are shown in the below table with percent differences.

Table 6.9 - Maximum Strain Comparison

Year	Area	FEM	SHM	Difference
2016	Fascia Girder	19.26	17.96	7.23%
2018	Fascia Girder	22.77	22.49	1.25%
2016	Floor Beam	12.90	11.15	13.6%
2018	Floor Beam	14.02	11.77	16%

Per the table in all cases the finite element model was found to be more conservative than the field data. Additionally, per review of the four graphs above, the finite element model results resemble the shape of the field data especially in the areas where max strain is observed.

However, for the floor beam the FEM model is found to be considerably more conservative than the thru girder. This can be due to the fact that the floor beam is a secondary member and the method of analysis via FEM is more conservative than what was obtained in the field.

Also, the FEM model may not account for additional methods of load distribution that is seen in the field. Finally, the method of repair to the floor-beam and contribution from the existing steel may not also be fully accounted for resulting in a lower strain being obtained from the structural health monitors.

In each of the four cases shown above, the graphs provide a good representation of how the beams react to different loads. Additionally, in the case of the thru girders the difference between the field data and finite element results is less than 10% for maximum strain. Therefore, it can be concluded that the model developed is calibrated.

6.3.2 – Finite Element Results

The next phase was to develop the various finite element models and load cases to be tested. As discussed, for the fascia girder three finite element model scenarios were created including:

- As-Built Condition (1939) - Finite Element Model I
- As-Inspected Condition (2018) - Finite Element Model II
- As-Predicted Condition (2029) - Finite Element Model III

For the floor beam a similar methodology was followed. However, since the floor beams were already repaired in 2016, the following three models were developed for analysis.

- As-Built Condition (1939) - Finite Element Model I
- As-Inspected Condition (2018) - Finite Element Model II
- As-Inspected Deteriorated Condition (2013) - Finite Element Model III

As for live load, several load case scenarios were inputted as follows:

- 2016 Truck Load (15 Tons)
- 2018 Truck Load (15 Tons)
- HS-20 Loading (36 Tons)
- Maximum Load Obtained from WIM sensors (44 Tons)

These trucks were inputted into the original model, to determine which yielded higher max-strain results, specifically at the fascia girder. Based off this information the other models were analyzed compared against to this higher load.

6.3.3 – Finite Element Fascia Girder Results

The first model analyzed was the 2018 Model (Model I) which had been calibrated. Below are figures provided for the HS-20 and maximum WIM load. All results can be found in the appendix. It should be noted that although the span is simply supported due to the configuration of the deck located at floor beam 5, the live load is immediately transferred over to the following span. Therefore, our FEM output does not hit zero when the truck leaves the span.

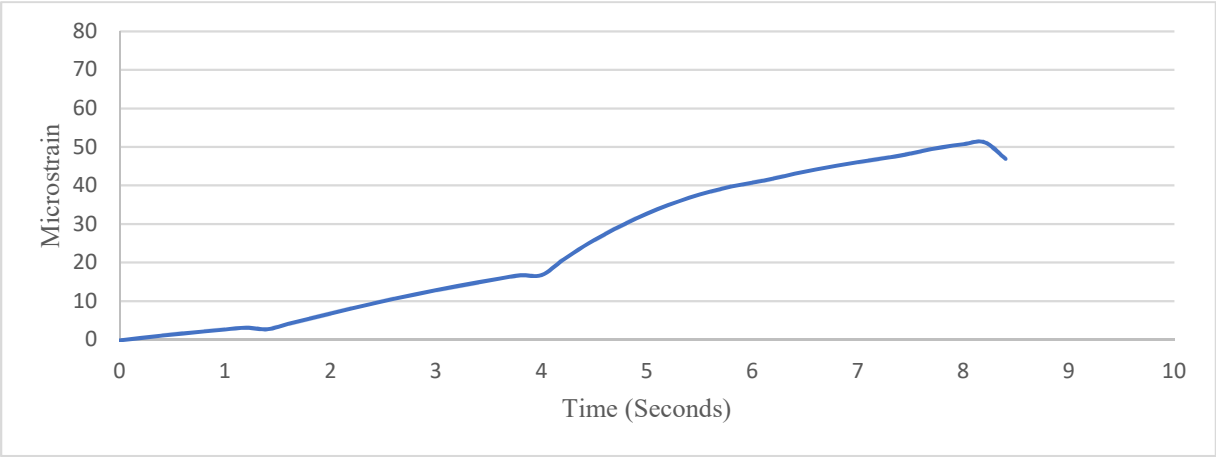

Figure 6.13 - HS-20 Loading for Model I

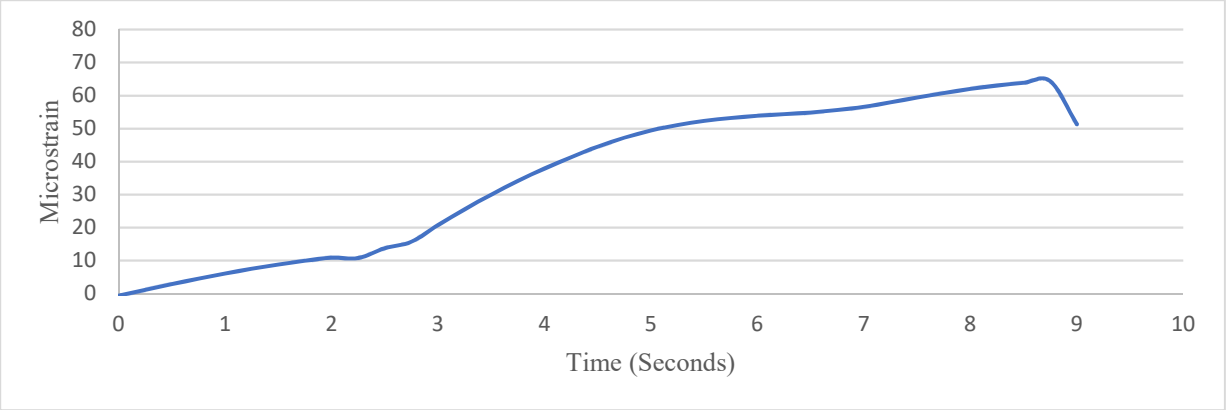

Figure 6.14 - Maximum WIM Load for Model I

The maximum strain results obtained from the FEM model for the above load cases are shown below in the below table.

Table 6.10 - Maximum Strain Obtained from Finite Element Model I (2018 Model)

Truck	GVW	Max Strain
2016	14 Tons	19.26
2018	15 Tons	22.77
HS-20	36 Tons	51.23
Max WIM Load	43 Tons	64.37

The second model analyzed was the 1939 as-built model. The section properties of this model match those on the original as-built drawings. It was predicted that the maximum strains for this model should be less than the 2018 model due to its condition. Only the HS-20 and max WIM load was analyzed under this scenario. The results are shown in the below figures.

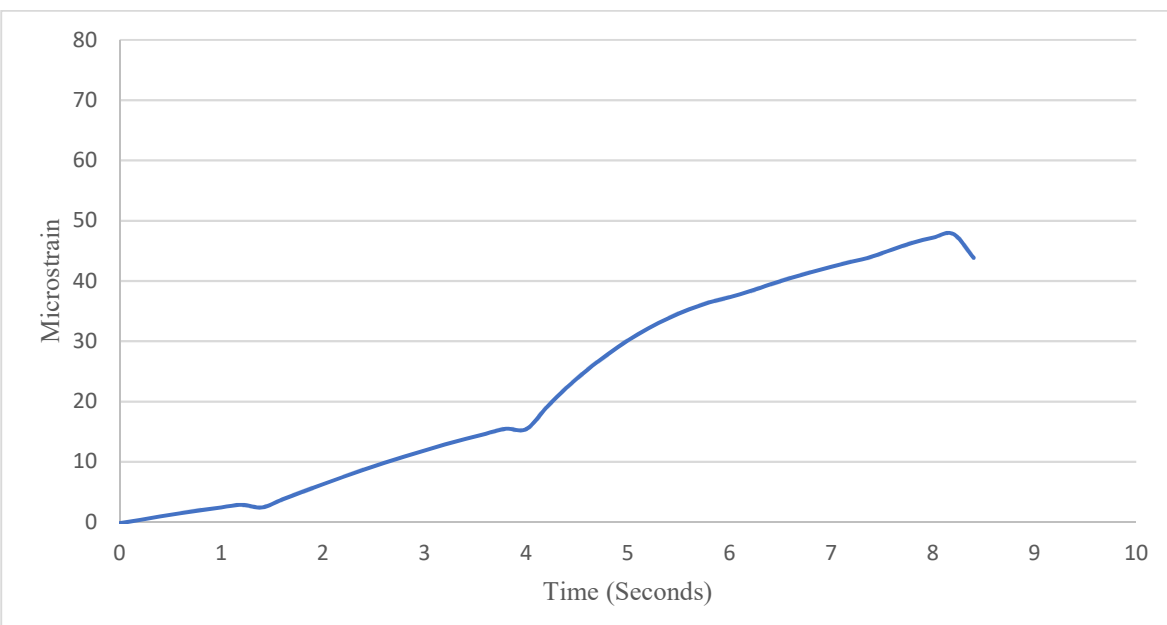

Figure 6.15 - 1939 Model - HS-20 Load for Model II

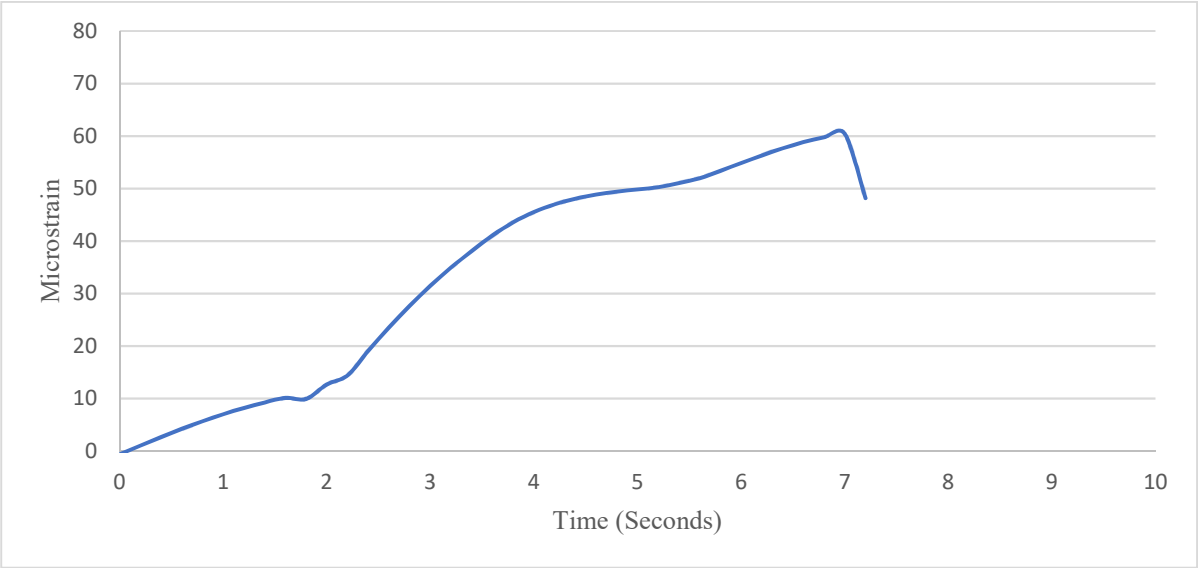

Figure 6.16 - 1939 Model - Max WIM Load for Model II

Additionally, maximum strains were obtained and can be found in the below table. As we can see from the results, the maximum strain is less than what was obtained from the 2018 model meeting our initial prediction.

Table 6.11 - Maximum Strain Obtained from Finite Element Model II (1939 Model)

Truck	GVW	Max Strain
HS-20	36 Tons	47.80
Max WIM Load	43 Tons	60.42

The final model analyzed was the 2029 Corrosion Prediction Model. The section properties of this model match those calculated using the original section properties minus the section loss due to corrosion. The results are shown in the below figures and tables.

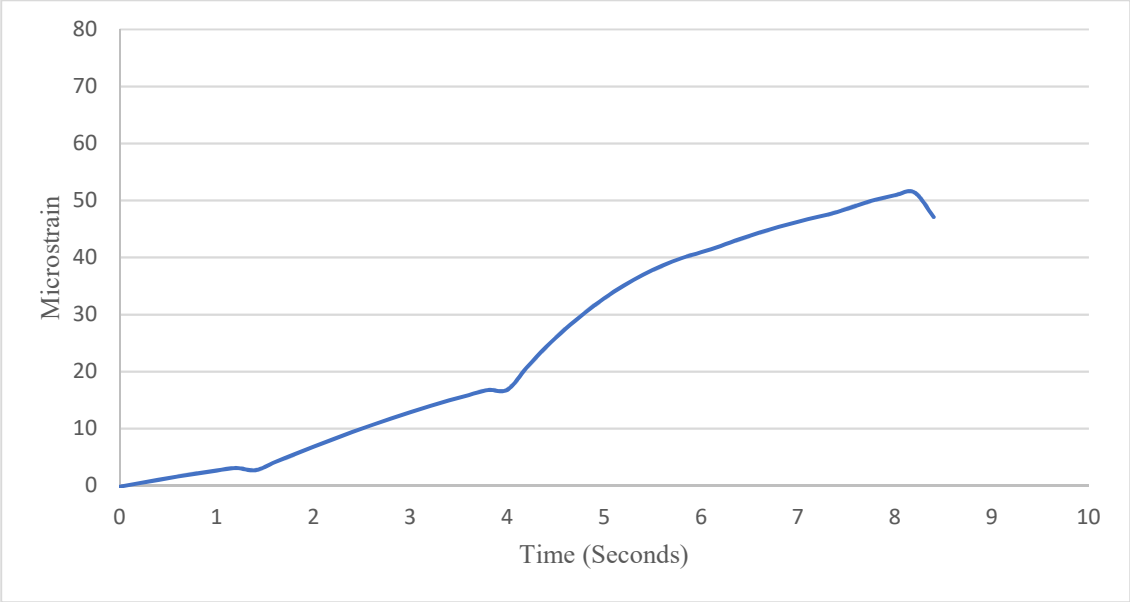

Figure 6.17 - 2029 Model - HS-20 Load for Model III

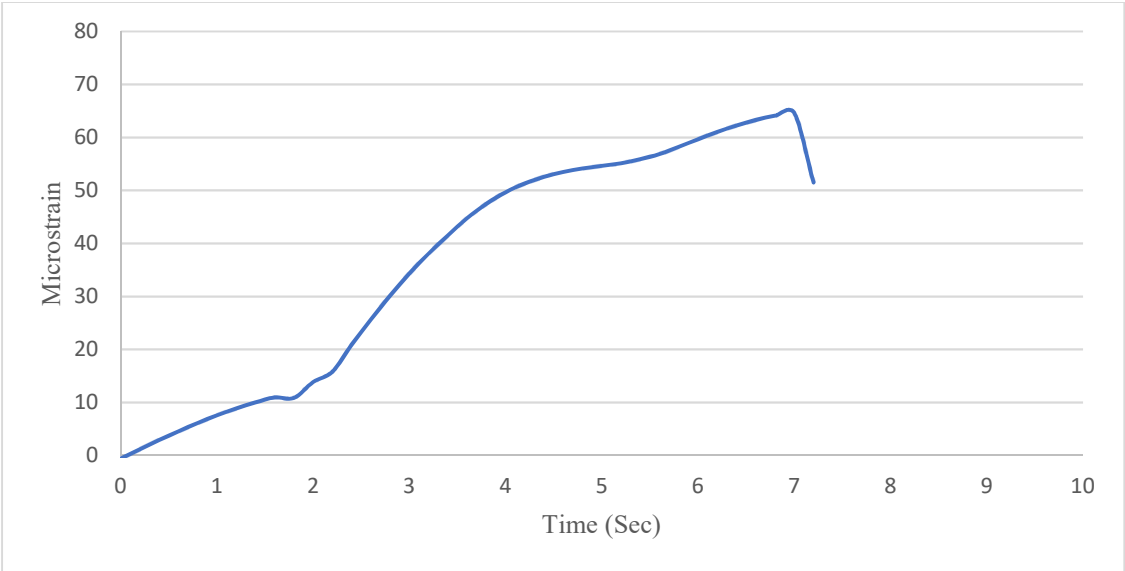

Figure 6.18 - 2029 Model - Max WIM Load for Model III

Table 6.12 - Maximum Strain Obtained from Finite Element Model (2018 Model)

Truck	GVW	Max Strain
HS-20	36 Tons	51.42
Max WIM Load	43 Tons	64.60

As we can see from the results, the maximum strain is greater than what was obtained from the 2018 model. While the increase in maximum strain is minimal, this validates the conclusion that ABAQUS may be utilized to create load prediction models to better analyze complex structures. A table summarizing the results for the three cases and their maximum strains are shown below:

Table 6.13 - Summary Table for Maximum Strains Obtained for Models I through III

Truck	GVW	2018 Max Strain	1939 Max Strain	2029 Max Strain
HS-20	36 Tons	51.23	47.80	51.42
Max WIM Load	43 Tons	64.37	60.42	64.60

6.3.4 – Finite Element Floor Beam Results

Following the analysis of the fascia girder, the next step was to analyze the floor beam. As discussed previously, three finite element models were ultimately developed for the floor beam.

The first model, was based off the 2018 As-Inspected Condition (FEM Model I). The second model was based off the 1939 As-Built Drawings (FEM Model II). While the final model was based of the 2013 As-Inspected Condition.

For the 2013 As-Inspected condition (FEM Model III), due to the severe section loss, holes in the floor beam needed to be modeled. Initially, this was done by significantly reducing the section properties to attempt to mimic what was noted in the field. However, this method was refined further by reducing the overall Modulus of Elasticity of the member in conjunction with reducing the overall section.

Additionally, as discussed in the previous section, four load cases were inputted including the 2016, 2018, HS-20 and Maximum WIM Load. The output of these all these results are shown below and in the appendix.

For the Finite Element graphs it should that the portion which includes the time in which the truck is not over the floor beam has been included (see Figure 6.19 as an example below). This resulted in the microstrain to be less than four and around zero. Similarly, like the fascia girder, due to the fact that the span abruptly ends due to load transferring to the machine room following floor-beam 5, our graph does not conclude at zero.

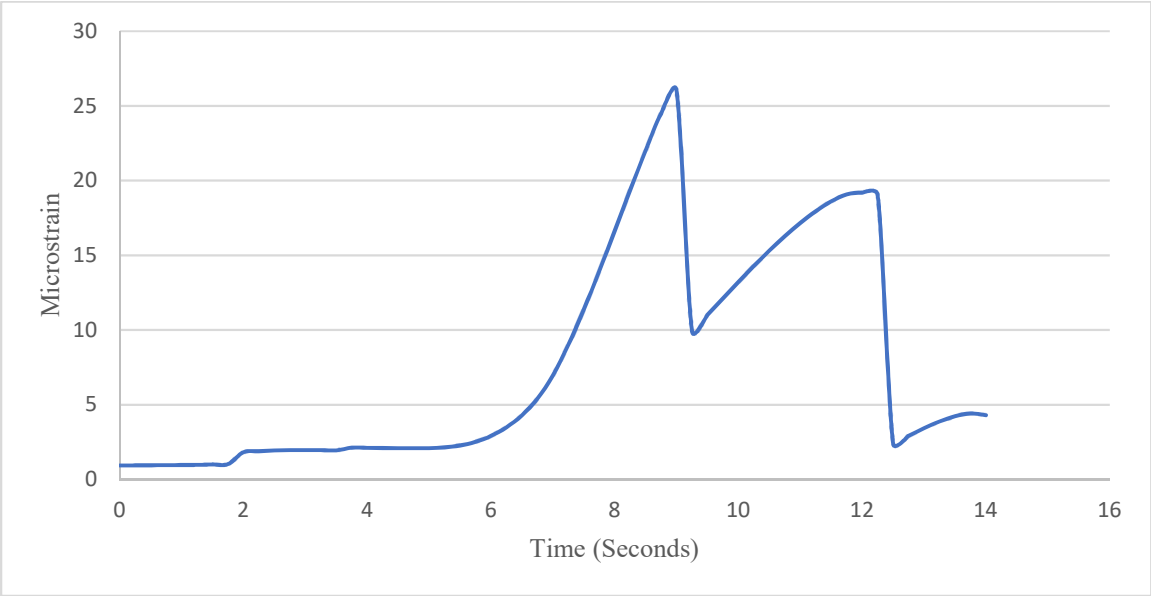

Figure 6.19 - 2018 Model - HS-20 Load

The maximum strain results obtained from the FEM model for the above load cases are shown below. It should be noted that these strains are significantly less than the fascia girder. This is expected as the floor beam, while seeing the maximum shear of the span, is considered a secondary member.

Table 6.14 - Maximum Strain Obtained from Finite Element Model I (2018 Model)

Truck	GVW	Max Strain
2016	14 Tons	12.90
2018	15 Tons	14.02
HS-20	36 Tons	26.02
Max WIM Load	43 Tons	36.07

The second model analyzed was the 1939 as-built model. As the 2018 model accounted for the repaired condition which reinforced the existing with a higher yield steel it was predicted that the maximum strains should be less. All four load cases were analyzed under this scenario. The results for the HS-20 Load is shown below in addition to a table which includes the observed maximum strains for each of the four cases. As we can see the maximum strains are higher than those observed for the 2018 model satisfying this condition.

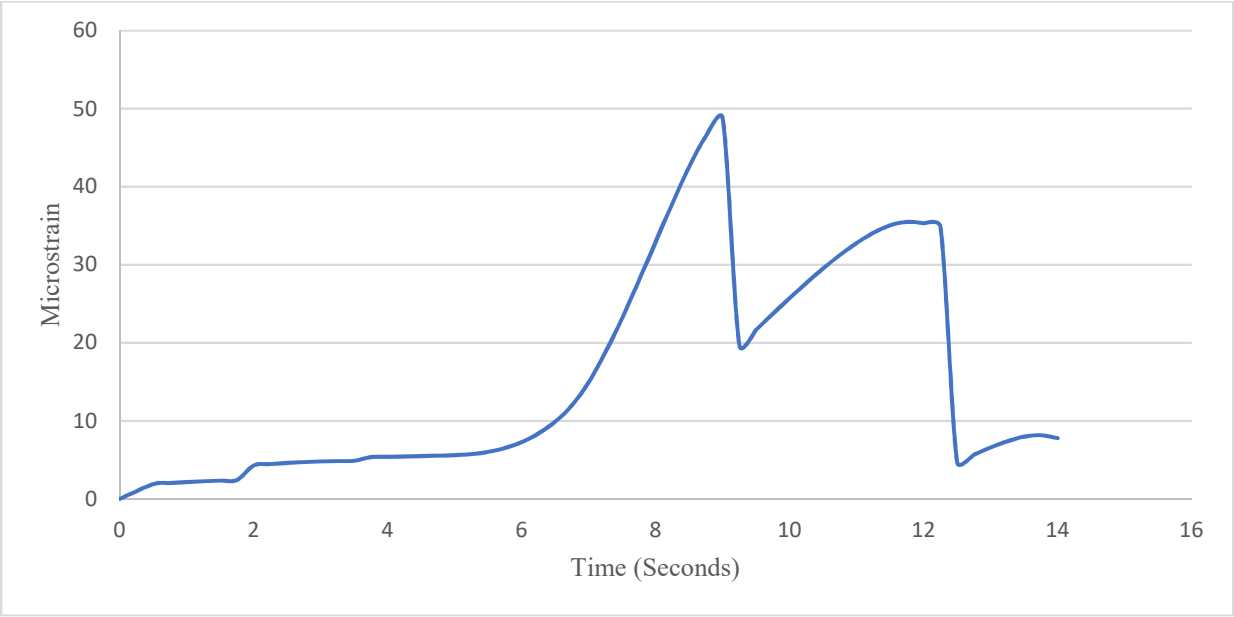

Figure 6.20- 1939 Floor beam -HS-20 Truck

Table 6.15 - Maximum Strain Obtained from Finite Element Model II (1939 Model)

Truck	GVW	Max Strain
2016	14 Tons	24.02
2018	15 Tons	25.91
HS-20	36 Tons	48.78
Max WIM Load	43 Tons	68.81

The final model created and analyzed was the 2013 Deteriorated Model. As stated above, the section properties of this model closely match inspection data obtained during 2013 when the floor beams were in much need of repair. An initial model was developed which reduced the section properties to match what was in the field. The results taken from this model is shown in Table 6.16.

Table 6.16 - Initial Maximum Strain Obtained from Finite Element Model III (2013 Model)

Truck	GVW	Max Strain
2016	14 Tons	44.71
2018	15 Tons	44.97
HS-20	36 Tons	89.88
Max WIM Load	43 Tons	123.55

To model the holes in the web, this initial model was refined. As stated previously, this was achieved by reducing the modulus of elasticity of the floor beam. The results taken from this model are shown below in Table 6.17. As discussed further in this section the Rating Factors obtained appeared to be more in line with what was observed in the field, therefore the results in Table 6.17 were used for further analysis.

Table 6.17 - Final Maximum Strain Obtained from Finite Element Model III (2013 Model)

Truck	GVW	Max Strain
2016	14 Tons	82.80
2018	15 Tons	94.68
HS-20	36 Tons	169.07
Max WIM Load	43 Tons	315.52

The goal of this model was not only to predict what the actual strain on the member was prior to repair, but also validate whether the 5-ton posting was acceptable. By doing this we can make similar assumptions and follow a similar methodology for other complex bridges in a deteriorated state. The results for HS-20 load and the maximum strains for each case are shown below.

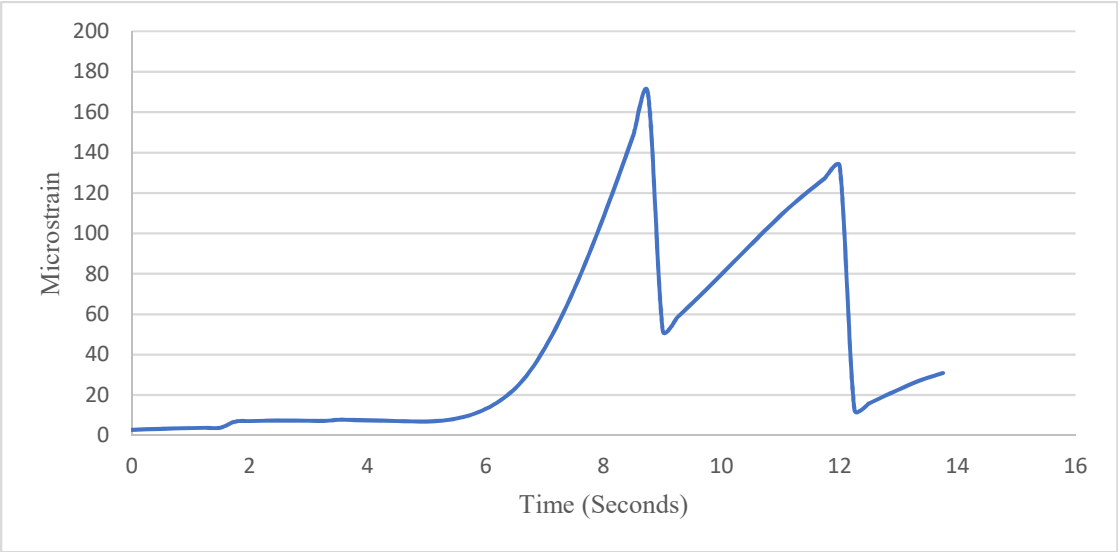

Figure 6.21 - Finite Element Model III (2013 Model) Floor beam -HS-20 Truck

As we can see from Figure 6.21, one telling point is the curvature of the graph. Because the section modulus of the beam has been reduced significantly, that causes the almost abrupt rise in microstrain. This is opposed to the results obtained as a part of Finite Element Models I

and II, in which the microstrain is increased almost gradually. Again, this relates to the fact that stress is being induced more abruptly due to the lower section modulus. A side-by-side presentation of the strains is provided table 6.18 below.

Table 6.18 - Microstrain for Finite Element Models I through III

	Microstrain Obtained from Model		
Truck Type	2018 Condition	1939 Condition	2013 Condition
2016 Truck	12.9	24.02	82.8
2018 Truck	14.02	25.91	94.68
HS-20 Truck	26.02	48.78	169.07
Max WIM Truck	36.07	68.81	315.52

A comparison between the Finite Element Models III and I, III and II, as well as, I and II are compared below in table 6.19, 6.20, and 6.21.

Table 6.19 - Microstrain Comparison for Finite Element Models I and II

Truck Type	2018 Condition	1939 Condition	% Difference
2016 Truck	12.9	24.02	60%
2018 Truck	14.02	25.91	60%
HS-20 Truck	26.02	48.78	61%
Max WIM Truck	36.07	68.81	62%

Table 6.20 - Microstrain Comparison for Finite Element Models I and III

Truck Type	2018 Condition	2013 Condition	% Difference
2016 Truck	12.9	82.8	146%
2018 Truck	14.02	94.68	148%
HS-20 Truck	26.02	169.07	147%
Max WIM Truck	36.07	315.52	159%

Table 6.21 - Microstrain Comparison for Finite Element Models II and III

Truck Type	1939 Condition	2013 Condition	% Difference
2016 Truck	24.02	82.8	110%
2018 Truck	25.91	94.68	114%
HS-20 Truck	48.78	169.07	110%
Max WIM Truck	68.81	315.52	128%

As we can see from tables 6.19 through 6.21, the maximum strain is much greater for Model III than what was obtained from Model I. This makes sense as the floor beam was heavily reinforced due to the 2016 repairs. These results validate the conclusion that ABAQUS may be utilized to create resistance prediction models to better analyze complex structures. From this the results obtained can be utilized as a form of refined analysis to obtain the appropriate Rating Factors for each member.

6.4 – Load Rating Results

Utilizing the information obtained from the finite element modeling, and the WIM sensors, there is enough information to perform all the load ratings required for analysis and comparison of the S-31 fascia girder and floor beam. The following subsection will cover the fascia girder followed by the floor beam. For each, results for the LRFR and LFR are computed and compared. Additionally, for the floorbeam we will look at changes in ratings per condition and look to see what the load rating would have been.

6.4.1 – S-31 Fascia Girder

The first member analyzed was the fascia girder. As discussed previously, three overall conditions were analyzed for the fascia girder. Dead Loads remained consistent for the three cases and were calculated based off the 1939 as-built drawings.

6.4.1.1 – LRFR Analysis

As there was no wearing surface or Permanent Loads the LRFR Load Rating Equation was simplified to the following form:

$$RF = \frac{C-(\gamma_{DC})(DC)}{(\gamma_{LL})(LL+IM)} \quad (6.1)$$

Based on the above equation, the first step was to determine the Capacity and Dead Load for input into the respective load rating equation. These results for capacity of each of the cases noted above, can be found within the below tables. Specifics regarding how each of the specific values were calculated can be found in the appendix of this dissertation. Note, that the Dead Load for all three condition cases stays the same and calculations regarding that can also be found in the appendix as well.

Table 6.22 - Fascia Girder Resistance for each Condition Case

Type	Rn	ØcØs	C	Unit
1939 As-Built Condition	11,998.00	0.85	10,198.00	Kip-FT
2018 As-Inspected Condition	11,564.00	0.85	9,829.00	Kip-FT
2029 Predicted Condition	10,478.00	0.85	8,906.00	Kip-FT

As steel coupon tests were not available consultation of the 2018 MBE was required to determine the yielding stress of steel. Using Table 6A.6.2.1.1 a minimum yielding stress of 33 KSI was selected as the steel of the oceanic was fabricated in 1939 and fell within the 1936 to 1963 category. Additionally, investigation of the structural steel shop drawings revealed that the steel fabricated met A7-36 standards which normally had a 36 KSI yielding stress associated with it. Therefore, this yielding stress selected is reasonable. This table from the 2018 MBE has been included below in Table 6.23.

Table 6.23 - 2018 MBE Table 6A.6.2.1-1

Year of Construction	Minimum Yield Point or Minimum Yield Strength, F_y, ksi	Minimum Tensile Strength, F_u, ksi
Prior to 1905	26	52
1905 to 1936	30	60
1936 to 1963	33	66
After 1963	36	66

As for applied factors, under the LRFR, per the MBE a Dead Load Factor of 1.25 was utilized. As for resistance factors a combined factor of 0.85 (both condition and system) was ultimately used since the bridge was classified as non-redundant and fracture critical which yielded a factor of 0.85. As discussed previously, live loads were calculated one of three ways for this project when applicable. For FEM and SHM, the max strains obtained were converted over to live-load moment and plugged into the load rating equation. A breakdown of the live loads calculated as a part of this project can be found in the appendix. For the FEM and SHM results a multiple presence factor of 1.2 was applied.

As for the Live Load Factors the under the LRFR the MBE was closely followed. However, a separate category using the new site-specific factor was also created which is allowed for by the MBE. Under this category a sub-category was created which utilized the unrestricted live load factor. All live load factors utilized can be found in the Table 6.24.

Table 6.24 - Live Load Factors

Live Load Safety Factor		
Type	Value	Reason
γLL	1.75	Inventory
γLL	1.35	Operating
γLL	1.30	WIM
γLL	0.79	WIM*

*Unrestricted Factor as calculated by C6A.4.4.2.3a

With this information, we were able to compute the respective rating factors for each of the three cases and for each live load scenario. The first condition tested was the 2018 condition. The results can be found in the following tables below.

Table 6.25 - 2018 Traditional Approach Load Rating Results

Truck Type	Traditional Method			
	INV	OP	WIM	WIM*
HS-20 Truck	1.05	1.36	1.41	1.92
2018 Truck	5.11	6.63	6.88	9.37
2016 Truck	6.13	7.95	8.26	11.25
Max WIM Load	1.90	2.46	2.55	3.48

Table 6.26 - 2018 Finite Element Modeling Load Rating Results

Truck Type	Finite Element Modeling			
	INV	OP	WIM	WIM*
HS-20 Truck	4.28	5.55	5.76	7.85
2018 Truck	9.63	12.48	12.96	17.66
2016 Truck	11.38	14.75	15.32	20.88
Max WIM Load	3.41	4.41	4.58	6.25

Table 6.27 - 2018 Structural Health Monitoring Load Rating Results

Truck Type	Experimental			
	INV	OP	WIM	WIM*
2018 Truck	9.77	12.67	13.16	21.65
2016 Truck	12.21	15.82	16.43	27.04

As we can see from the results above, the traditional approach yields the most conservative results. Additionally, we can see a close correlation between the experimental load rating results and the finite element modeling load rating results. Based on this, it can be concluded that the fascia girder does not require repair or strengthening.

The next case was to analyze the as-built condition. The purpose of this was to create a model which matched the original as-built drawings so that a comparison could be made between

the current condition and the original design condition. The traditional Load Rating Results and FEM results can be found in the below two tables:

Table 6.28 - 1939 As-Built Condition Traditional Load Rating Results

Truck Type	Traditional Method			
	INV	OP	WIM	WIM*
HS-20 Truck	1.12	1.45	1.51	2.48
2018 Truck	5.46	7.08	7.35	12.10
2016 Truck	6.55	8.50	8.82	14.52
Max WIM Load	2.03	2.63	2.73	4.49

Table 6.29 - 1939 As-Built Condition Finite Element Load Rating Results

Truck Type	FEM			
	INV	OP	WIM	WIM*
HS-20 Truck	4.90	6.35	6.60	10.86
Max WIM Load	3.88	5.03	5.22	8.59

Based on this information certain comparisons were made to see the significance of change in Load rating in relation to the condition of the fascia girder deteriorating over time. A comparison was made using the traditional HL-20 Loading and the Max WIM Load. These comparisons can be found in Tables 6.30 and 6.31:

Table 6.30 - 1939 vs 2018 Traditional Load Rating Result Comparison

Truck Type	1939 (Traditional)				2018 (Traditional)			
	INV	OP	WIM	WIM*	INV	OP	WIM	WIM*
HS-20 Truck	1.12	1.45	1.51	2.48	1.05	1.36	1.41	1.92
Max WIM Load	2.99	3.88	4.03	4.49	1.90	2.46	2.55	3.48

Table 6.31 - 1939 vs 2018 FEM Load Rating Result Comparison

Truck Type	1939 (FEM)				2018 (FEM)			
	INV	OP	WIM	WIM*	INV	OP	WIM	WIM*
HS-20 Truck	4.90	6.35	6.60	10.86	4.28	5.55	5.76	7.85
Max WIM Load	3.88	5.03	5.22	8.59	3.41	4.41	4.58	6.25

As we can see from the above comparisons, when comparing the FEM to classic one observes a large variation between ratings. This indicates to us that the load is not being truly

distributed in ways in which the fascia girder traditionally would experience the load. Therefore, this change can be attributed to internal structural redundancy not normally accounted for when traditionally designing or analyzing a beam. A conclusion that can be drawn from this is that when analyzing a complex structure, the traditional method could be utilized as a means of identifying members for further study using either finite element modeling, or structural health monitoring.

The final condition which was studied was the 2029 Predicted Corroded Condition. As stated previously, the model reflects section properties calculated based off using the Komp Corrosion prediction equation described in Chapter 5 and reviewed in Chapter 2. The following results were obtained using this approach and shown in Tables 6.32 and 6.33.

Table 6.32 - 2029 Predicted Condition Traditional Load Rating Results

Truck Type	Traditional Method			
	INV	OP	WIM	WIM*
HS-20 Truck	0.87	1.12	1.17	1.92
2018 Truck	4.23	5.49	5.70	9.37
2016 Truck	5.08	6.58	6.84	11.25
Max WIM Load	1.57	2.04	2.12	3.48

Table 6.33 - 2029 Predicted Condition Traditional Load Rating Results

Truck Type	FEM			
	INV	OP	WIM	WIM*
HS-20 Truck	3.53	4.58	4.75	7.82
Max WIM Load	2.81	3.64	3.78	6.22

As we can see the results in both the FEM and Traditional way of analysis yield results which show a decrease in rating factor. However, when compared to the original as-inspected rating factor we only see a slight reduction. When compared to the 1939 as-built rating for HS-20 and the Max WIM load, the change is more significant; this is shown in Table 6.34.

Table 6.34 - 1939 vs 2029 Load Rating Comparison

Truck Type	1939		2029	
	INV	OP	INV	OP
HS-20 Truck	1.12	1.45	0.87	1.12
Max WIM Load	2.03	2.63	1.57	2.04

6.4.1.2 – LFR Analysis

As the LFR equation does not formally account for wearing surface or other permanent loads, the equation unlike the LRFR equation could not be simplified. Therefore, the equation stayed consistent. Using the 2018 MBE, the values of A1 and A2 were as follows:

Table 6.35 - Permanent Load Safety Factors

Type	Value	
A1	1.30	DC
A2	2.17	INV
A2	1.30	OP

Member capacities were previously calculated under Section 7.5.1.1 but did not have the condition or system factors applied to them. Therefore, the capacity of the members was in accordance with the safety factors applied under the AASHTO and AISC Design code. The capacity of the fascia girder under each condition is shown in the below table:

Table 6.36 - Fascia Girder Member Capacity

Condition	C	Unit
1939 As-Built Condition	11,998.00	Kip-FT
2018 As-Inspected Condition	11,564.00	Kip-FT
2029 Predicted Condition	10,478.00	Kip-FT

As for live load, the lives load calculated previously under Section 7.5.1.1 were utilized. Since these live loads included impact. The Load Rating Equation for LFR was modified as follows:

$$RF = \frac{C - A_1 D}{A_2 L}$$

As discussed, the MBE under Section 6B does not allow or call for the use of Site Specific WIM Data, analysis by field testing, or a refined method of analysis such as finite element modeling. Results were not included for field testing or were loads modified due to the site-specific factor. Finite element results were inputted, but only as a means of comparison.

Based on this information, rating factors were computed for each of the three conditions, and various load case scenarios. Since the purpose of this exercise is to compare the results to the LRFR results, the rating factors were not converted over to tons. For the 2018 as-inspected condition, the rating factors were calculated as follows:

Table 6.37 - 2018 As-Inspected LFR Load Rating Results Traditional Method

Truck Type	Traditional Method	
	Inventory	Operating
HS-20 Truck	1.09	1.82
2018 Truck	2.56	4.28
2016 Truck	2.94	4.90
Max WIM Load	1.97	3.30

Table 6.38 - 2018 As-Inspected LFR Load Rating Results Finite Element Modeling

Truck Type	FEM	
	Inventory	Operating
HS-20 Truck	4.73	7.90
2018 Truck	12.58	21.01
2016 Truck	10.64	17.77
Max WIM Truck	3.77	6.28

Following the 2018 as-inspected condition, load ratings were performed for the 1939 condition and 2029 predicted condition. Methodology for these two methods was identical to the to what was previously performed. The results for each of these conditions are shown in the following tables.

Table 6.39 - 1939 As-Built LFR Load Rating Results Traditional Method

Truck Type	Classical	
	Inventory	Operating
HS-20 Truck	1.16	1.93
2018 Truck	2.72	4.55
2016 Truck	3.12	5.21
Max WIM Load	2.10	3.50

Table 6.40 - 1939 As-Built LFR Load Rating Results FEM Method

Truck Type	FEM	
	Inventory	Operating
HS-20 Truck	4.73	7.90
Max WIM Load	3.77	6.28

Table 6.41 - 2029 Predicted Condition LFR Load Rating Results Traditional Method

Truck Type	Classical	
	Inventory	Operating
HS-20 Truck	0.92	1.53
2018 Truck	2.16	3.61
2016 Truck	2.48	4.13
Max WIM Load	1.66	2.78

Table 6.42 - 2029 Predicted Condition LFR Load Rating Results FEM Method

Truck Type	FEM	
	Inventory	Operating
HS-20 Truck	3.75	6.27
Max WIM Load	2.99	4.99

6.4.1.3 – LFR vs. LRFR

Following the LFR analysis, the next step was to compare the results of the LRFR Analysis to the LFR analysis. This was done only for the 2018 as-inspected condition, as the conclusions drawn from this comparison would be similar to the other two scenarios. For this comparison, the traditional approach, and FEM approach results were compared. The Traditional approach side-by-side comparison can be found below:

Table 6.43 - LRFR vs LFR Traditional Approach (2018 Condition)

Truck Type	LRFR Method				LFR Method	
	INV	OP	WIM	WIM*	INV	OP
HS-20 Truck	1.05	1.36	1.41	1.92	1.09	1.82
2018 Truck	5.11	6.63	6.88	9.37	2.56	4.28
2016 Truck	6.13	7.95	8.26	11.25	2.94	4.90
Max WIM Load	1.90	2.46	2.55	3.48	1.97	3.30

As we can see from the above table, the LRFR Inventory and LFR Inventory are very similar for HS-20 Design Loading and are also similar for Max Wim Loading scenarios as well, but not for LFR. This is broken out further into the table below.

Table 6.44 - LRFR vs LFR Heavier Load Comparison (2018 Condition)

Truck Type	LRFR Method				LFR Method	
	INV	OP	WIM	WIM*	INV	OP
HS-20 Truck	1.05	1.36	1.41	1.92	1.09	1.82
Max WIM Load	1.90	2.46	2.55	3.48	1.97	3.30

As we can see from the above table, the Inventory Ratings under the three conditions noted above are within less than 5% of each other. The operating ratings, however, vary consistently at around 33.5%. The WIM results however, when restricted reduce this difference to approximately 29.4%. This is because the change from operating to WIM is only 0.5. However, when unrestricted the WIM results provide the least conservative rating factor and is in fact better than what operating offers.

FEM results were also compared, but in two ways. The first is shown below which shows a direct comparison of LRFR to LFR both using live load data obtained from the FEM.

Table 6.45 - LRFR vs LFR Finite Element Modeling (2018 Condition)

Truck Type	LRFR Method				LFR Method	
	INV	OP	WIM	WIM*	INV	OP
HS-20 Truck	5.14	6.66	6.91	7.85	4.45	7.43
2018 Truck	11.55	14.98	15.55	17.66	11.84	19.77
2016 Truck	13.66	17.71	18.39	20.88	10.02	16.72
Max WIM Load	4.09	5.30	5.50	6.25	3.54	5.91

While the above methods show that the operating is less conservative than what is provided in the LFR, the results based off the Site-Specific Factor is more in line. Additionally, if you look at the WIM* (Unrestricted Live Load Factor based on WIM Results) results, you will note that unrestricted the LRFR method provides the best results for cases analyzed under all conditions. This means that use of the WIM sensors to develop a Site-Specific Factor provide a direct benefit. It should be noted that the above differences are similar to those computed under the traditional method.

The second form of comparison is in direct accordance with the 2018 MBE. In this case FEM results are only used for the LRFR method, and not used for the LFR. For the LFR only the traditional results were included. This comparison is shown in the below table. As we can see, when using the 2018 Code as interpreted, the flexibility of using refined analysis in conjunction with the site-specific factor, the LRFR results yield better Ratings overall than the LFR and is clearly the preferred method.

Table 6.46 - LRFR vs LFR per 2018 MBE (2018 Condition)

Truck Type	LRFR Method (FEM)				LFR Method	
	INV	OP	WIM	WIM*	INV	OP
HS-20 Truck	5.14	6.66	6.91	7.85	1.09	1.82
2018 Truck	11.55	14.98	15.55	17.66	2.56	4.28
2016 Truck	13.66	17.71	18.39	20.88	2.94	4.90
Max WIM Load	4.09	5.30	5.50	6.25	1.97	3.30

6.4.2 – Floor Beam Analysis

The first step was to determine the Capacity and Dead Load for input into the respective load rating equation. These results for each of the cases noted above, can be found within the below tables. A full breakout of all calculations can be found in the appendix.

Table 6.47 - Member Resistance for each Condition Case

Type	Rn	ØcØs	C	Unit
2016/2018 Repaired Condition	451.00	0.85	383.00	Kips
1939 As-Built Condition	269.00	0.85	228.00	Kips
2013 Deteriorated Condition	104.00	0.85	88.00	Kips

The capacity of the floor beam was determined utilizing the Section 6 of the AASHTO LRFD 8th Edition, while the dead load was calculated using the as-built plans provided from 1939. The focus of our analysis pertained to this mode of failure because the priority notice issued in 2013 for floor beam 9 was for shear. Initially, moment was analyzed but it was determined that in a deteriorated condition was still not the controlling mode of failure.

Similarly, as for applied factors, under the LRFR, per the MBE a Dead Load Factor of 1.25 was utilized. As for resistance factors a combined factor of 0.85 (both condition and system) was ultimately used since the bridge was classified as non-redundant and fracture critical which yielded a factor of 0.85. Like the fascia girder, for floor beam 9, the live loads were calculated either one of three ways for this project when applicable.

For the traditional approach, AISC Table 4-23 on page 3-228 provides guidance on how to determine the maximum shear load on a simply supported beam carrying a moving concentrated load. For this approach, moment shear diagrams were developed for each of the different load types and the maximum shear at floor beam 9 was determined accordingly.

For FEM and SHM, the max strains obtained, were converted over to shear force and plugged into the load rating equation. Unlike, the fascia girder, to find the maximum shear induced on the floor beam, a different set of equations needed to be utilized as described previously.

Like the fascia girder, a separate category using the new site-specific factor was also created. These are the same factors that were utilized in the previous section. With this information, we were able to compute the respective rating factors for each of the three cases and for each live load scenario. The first condition tested was the 2018 as-inspected condition. Like the fascia girder for the SHM results, only the 2016 and 2018 trucks were analyzed. The results can be found in the following tables below.

Table 6.48 - Traditional Approach Load Rating Results (2018 As-Inspected Condition)

Truck Type	Classical			
	INV	OP	WIM	WIM*
HS-20 Truck	3.62	4.69	4.87	8.01
2018 Truck	6.71	8.70	9.04	14.87
2016 Truck	7.52	9.75	10.12	16.66
Max WIM Load	2.58	3.34	3.47	5.70

Table 6.49 - FEM Model Load Rating Results (2018 As-Inspected Condition)

Truck Type	FEM			
	INV	OP	WIM	WIM*
HS-20 Truck	9.92	12.86	13.36	21.98
2018 Truck	18.41	23.87	24.79	40.79
2016 Truck	20.01	25.94	26.94	44.33
Max WIM Load	7.16	9.28	9.63	15.85

Table 6.50 - SHM Load Rating Results (2018 As-Inspected Condition)

Truck Type	Experimental			
	INV	OP	WIM	WIM*
2018 Truck	22.24	28.83	29.93	49.26
2016 Truck	23.15	30.01	31.17	51.29

Like the fascia girder, we can see from the results above, the traditional approach yields the most conservative results, with the least conservative results being the experimental data. This is important as these results pertain to Shear. Additionally, we can see a close correlation between the experimental load rating results and the finite element modeling load rating results.

One of the main reasons the load rating for the FEM Model is well above 1.00 is likely due to the inherent structural redundancy of the floor beam system that is not accounted for in traditional design methods. By treating the floor beam system three-dimensionally, we can account for redundancy normally not considered. This is important as this conclusion should be considered when analyzing structures of a similar configuration. When looking at the experimental data in relation to the traditional approach, we see that they are almost 3.7x greater than the traditional results. This could be because when designing or analyzing a rehabilitated member, the existing steel is generally ignored. However, we can see from above the corroded steel, and more importantly the existing angles are in fact contributing to the overall stability and shear resistance of the member.

The next case was to analyze the as-built condition. The purpose of this was to create a model which matched the original as-built drawings so that a comparison could be made between the current condition, the original design condition and the 2013 deteriorated condition to determine if further considerations could be made to rehabilitated members. The traditional Load Rating Results and FEM results can be found in the Tables 6.51 and 6.52 shown below.

Table 6.51 - Traditional Approach Load Rating Results (1939 As-Built Condition)

Truck Type	Classical			
	INV	OP	WIM	WIM*
HS-20 Truck	1.91	2.48	2.57	4.24
2018 Truck	3.55	4.60	4.78	7.87
2016 Truck	3.98	5.16	5.35	8.81
Max WIM Load	1.36	1.77	1.83	3.02

Table 6.52 - FEM Approach Load Rating Results (1939 As-Built Condition)

Truck Type	FEM			
	INV	OP	WIM	WIM*
HS-20 Truck	7.16	9.28	9.64	15.86
2018 Truck	14.54	18.84	19.57	32.20
2016 Truck	13.48	17.47	18.14	29.85
Max WIM Load	5.07	6.58	6.83	11.24

As we can see from the above two tables, we again see a large difference between the FEM Model Load Rating Results and the traditional approach. Additionally, we see a decrease in rating factor which is due to the decrease in overall section, and reduction in yielding stress from 50 KSI to 36 KSI. This exercise is important as it serves as a basis to work off of for the following model.

The case analyzed was the 2013 deteriorated condition of the floor beam. As discussed previously, section loss for the FEM model was taken as an average like the traditional approach. The load rating results for this case can be found in the below tables:

Table 6.53 - Traditional Approach Load Rating Results (2013 Deteriorated Condition)

Truck Type	Classical			
	INV	OP	WIM	WIM*
HS-20 Truck	0.37	0.48	0.50	0.83
2018 Truck	0.69	0.90	0.93	1.54
2016 Truck	0.78	1.01	1.05	1.72
Max WIM Load	0.27	0.35	0.36	0.59

Table 6.54 - FEM Approach Load Rating Results (2013 Deteriorated Condition)

Truck Type	FEM			
	INV	OP	WIM	WIM*
HS-20 Truck	1.73	2.24	2.33	3.83
2018 Truck	3.09	4.00	4.16	6.84
2016 Truck	3.53	4.58	4.75	7.82
Max WIM Load	0.93	1.20	1.25	2.05

As we can see from the above table, under the traditional approach the load rating in the deteriorated condition has a rating factor well below 1.00 for most load cases. This is good to know, as it is consistent with the findings found in the 2013 NBIS report. It also validates the decision to issue the 5-ton priority notice. However, when modeled via FEM, the load ratings for all scenarios has a rating factor above 1.00 particularly for the design loading. Based off this refined analysis it appears that the 5-ton down posting was not required.

This is likely due to the fact, that the structural redundancy of the system distributes the load in such a way that that the floor beam is not experiencing the full effect of the max shear induced. It is possible that the majority of the shear load in this location is being taken by the fascia girder. It is also possible, that elements such as the angles and the stiffeners are also taking the load.

Regardless, this explains while the bridge was able to operate safely between the time when the issue was discovered until it was repaired. This also assists in proving to us that when dealing with a complex structure or a fracture critical member, the traditional approach may not yield the best result since it does not account for contributing factors such as redundancy or alternative load paths.

6.4.2.2 – LFR Analysis

Like the fascia girder, the floor beam 9 was analyzed using the LFR equation referenced in the previous section. Using the 2018 MBE, the values of A1 and A2 were identical as well. Member capacities were previously calculated under Section 7.5.2.1 but did not have the condition or system factors applied to them. Therefore, the capacity of the members was in accordance with the safety factors applied under the AASHTO and AISC Design code. The capacity of the fascia girder under each condition is shown in the below table:

Table 6.55 - Fascia Girder Member Capacities used for the LFR Methodology

Condition	C	Unit
2018 As-Inspected Condition	451.00	Kips
1939 As-Built Condition	269.00	Kips
2013 Priority Repair Condition	104.00	Kips

As for live load, the lives load calculated previously under Section 7.5.2.1 were utilized. Based on this information, rating factors were computed for each of the three conditions, and various load case scenarios. Since the purpose of this exercise is to compare the results to the LRFR results, the rating factors were not converted over to tons. For the 2018 as-inspected condition, the rating factors were calculated as follows:

Table 6.56 - 2018 As-Inspected LFR Load Rating Results Traditional Method

Truck Type	Classical	
	INV	OP
HS-20 Truck	2.30	3.84
2018 Truck	3.50	5.84
2016 Truck	6.50	10.85
Max WIM Load	7.28	12.15

Table 6.57 - 2018 As-Inspected LFR Load Rating Results Finite Element Modeling

Truck Type	FEM	
	INV	OP
HS-20 Truck	9.60	16.03
2018 Truck	17.82	29.75
2016 Truck	19.37	32.33
Max WIM Load	6.93	11.56

Following the 2018 as-inspected condition, load ratings were performed for the 1939 Condition and 2013 Deteriorated Condition. Methodology for these two methods was identical to the approach used in previously. The results for each of these conditions are shown Tables 6.58 through 6.61 below.

Table 6.58 - 1939 As-Built LFR Load Rating Results Traditional Method

Truck Type	Classical	
	INV	OP
HS-20 Truck	1.89	3.15
2018 Truck	3.50	5.85
2016 Truck	3.92	6.55
Max WIM Load	1.34	2.24

Table 6.59 - 1939 As-Built LFR Load Rating Results FEM Method

Truck Type	FEM	
	INV	OP
HS-20 Truck	3.73	6.23
2018 Truck	7.58	12.66
2016 Truck	7.03	11.74
Max WIM Load	2.65	4.42

Table 6.60 - 2013 Condition LFR Load Rating Results Traditional Method

Truck Type	Classical	
	INV	OP
HS-20 Truck	0.42	0.71
2018 Truck	0.79	1.31
2016 Truck	0.88	1.47
Max WIM Load	0.30	0.50

Table 6.61 - 2013 Condition LFR Load Rating Results FEM Method

Truck Type	FEM	
	INV	OP
HS-20 Truck	1.96	3.27
2018 Truck	3.50	5.85
2016 Truck	4.01	6.69
Max WIM Load	1.05	1.75

6.4.2.3 – LFR vs. LRFR

Following the LFR analysis, the last step was to compare the results of the LRFR Analysis to the LFR Analysis. This was done only for the 2018 As-Inspected condition, as the conclusions drawn from this comparison would be relative to the other two scenarios. For this comparison, the traditional approach, and FEM approach results were each compared. The traditional approach side-by-side comparison can be found in the table below:

Table 6.62 - LRFR vs LFR Traditional Approach (2018 Condition)

Truck Type	LRFR Method				LFR Method	
	INV	OP	WIM	WIM*	INV	OP
HS-20 Truck	3.62	4.69	4.87	8.01	1.96	3.27
2018 Truck	6.71	8.70	9.04	14.87	3.50	5.85
2016 Truck	7.52	9.75	10.12	16.66	4.01	6.69
Max WIM Load	2.58	3.34	3.47	5.70	1.05	1.75

As we can see from above when dealing with shear, the LRFR Inventory and LFR Inventory are very similar for HS-20 Design Loading and are also similar for max WIM loading scenario as well. This is broken out into the table below. Like the fascia girder, when unrestricted the WIM results provide the least conservative rating factor of all options.

Like the fascia girder a second form of comparison was performed in direct accordance with the 2018 MBE. In this case FEM results are only used for the LRFR method, and not used for the LFR. For the LFR only the traditional results were included. This comparison is shown in the below table. As we can see, when using the 2018 Code as interpreted, the flexibility of using refined analysis in conjunction with the site-specific factor, the LRFR results again yield better Ratings overall than the LFR and is clearly the preferred method.

Table 6.63 - LRFR vs LFR per 2018 MBE (2018 Condition)

Truck Type	LRFR Method (FEM Results)				LFR Method	
	INV	OP	WIM	WIM*	INV	OP
HS-20 Truck	9.92	12.86	13.36	21.98	2.30	3.84
2018 Truck	18.41	23.87	24.79	40.79	3.50	5.84
2016 Truck	20.01	25.94	26.94	44.33	6.50	10.85
Max WIM Load	7.16	9.28	9.63	15.85	7.28	12.15

6.5 – Discussion of Results

Based on a review of the comparisons drawn above for both the fascia girder and the floor beam, the LRFR method provides more flexibility and more realistic results than the LFR method does. This is because the LRFR method allows the use of refined analysis, site-specific live load factor, and experimental field data while the 2018 MBE does not allow for this under the LFR method. Even when using FEM data for both the LFR and LRFR method, it can be observed that the results obtained are more in factor of the LRFR method especially once code restrictions pertaining to the site-specific factor is removed. Once can conclude that when dealing with complex bridges, while at first glance the LFR method provides a conservative means in calculation, the LRFR method is more favorable once an owner exercises these other code provisions provided to them.

CHAPTER 7

SUMMARY AND CONCLUSIONS

The objective of this dissertation was to develop a procedure for evaluation of complex bridges. This dissertation also includes a direct comparison of the LRFR and LFR methods specifically. This study contained both an analytical and experimental approach. Under the analytical portion a finite element model was developed, in addition to traditional calculations. On the experimental end, this study included the installation of weigh-in-motion sensors and structural health monitors.

The case study for this project was the Oceanic Bridge, a complex structure due to its dual leaf bascule movable span. The bridge serves as an applicable case study due to its age, complexity, and varying condition. The primary area of focus of the project was located at Spans 28 and 30. The members analyzed were the main thru girder which tied in directly to the bascule span and a floor beam at the outer end of the span.

Based off the research performed, a major conclusion drawing from the comparison of the LRFR and LFR methods is that the LRFR provided more better results when analyzing a complex structure. Under a side-by-side comparison using classical analysis techniques inventory ratings were found to be within 5% of each other. However, they varied for Operating. When the operating rating was modified for site specific data, the rating factors yield reasonable results which closely matched the LRFR method. Additionally, when the WIM factor minimum restriction was removed, the rating factor was found to be the most conservative.

When using the full scope of the 2018 MBE, the LRFR methodology provided is clearly the preferred method for complex bridges when compared to the LFR method. This is because the 2018 MBE allows for the use of refined analysis, site-specific live load factors, and the use of experimental data for the LRFR method, while it does not for the LFR method. When compared the LRFR method provides better ratings in all cases then the LFR. This flexibility in which the 2018 MBE allows under the LRFR method is something the LFR cannot provide. Additionally, benefits such as condition and system factors cannot be applied under the LFR and wearing surface loads are not broken out separately. Therefore, it is recommended that the LRFR be utilized in conjunction with this site-specific factor going forward.

Additionally, it is recommended that for all complex bridges, WIM sensors be installed as a Site-Specific Factor will provide a realistic analysis of the rating factor for the structure. When applicable structural health monitors should be applied to critical members for further evaluation to determine their capacity. This small investment could save owners millions in unnecessary repairs. Additionally, the installation of WIM sensors provide data on specific truck loads which can be utilized for further analysis.

Based off these analyses and conclusions made above, it is recommended that Section 6.1.6 Evaluation of Complex Structures under the 2018 MBE should also be expanded to give more guidance to the load rating engineer. Currently, the language mentions special analysis methods and procedures. As we know complex structures generally come with a high cost, and numerous repairs or replacement may not financially feasible for some agencies. Therefore, prioritization is essential.

Furthermore, utilizing the research performed on S-31, when analyzing a complex bridge, especially one in a deteriorated state, and near the end of its service life, an owner can prioritize and identify areas of repairs using the following procedure:

1. Perform an in-depth inspection of the structure in accordance with NBIS Standards. During the inspection, identify all areas of deterioration and potential repair.
2. Perform Load Rating Calculations for all members of the complex structure. Load ratings should be performed in accordance with the 2018, NBIS and/or State Standards, whatever is most stringent. Load ratings should be done following the traditional approach to yield the most conservative values.
3. Based on these calculations, identify members with a rating factor of 1.0 or less for the HL-93/HS-20 Design Condition.
4. Review the inspection data and determine if any additional deterioration is noted which should be considered in the analysis.
5. Install weigh-in-motion sensors and determine the following:
    - Site-Specific Live Load Factor for the bridge
    - Maximum load seen at bridge
    - Average load seen at the bridge
6. Once the Site-Specific Factor has been determined, re-run the load ratings to determine if any of the potential members have a rating factor greater than 1.0. If they do, eliminate them from the potential pool of repairs.
7. Once all the members with a rating factor greater than 1.00 have been screened and removed from the pool of elements, for the remaining identified areas, install Strain Gauges on the members identified in the above steps and obtain field measured stresses.

8. Develop a finite element model for the bridge or specific spans needing analysis and calibrate it to match the measurements taken from the field.
9. Using the weigh-in-motion data input the maximum loading conditions into the finite element model and analyze it, as well as, average load to determine the rating factors of the members under analysis.
10. Using the finite element model in conjunction with the field data gathered, prioritize repairs based off new modified load ratings.
11. If possible, run a proof load tests for higher loads for validation.
12. If repairs are not financially feasible post the bridge in accordance with the experimental data received for the member in need of repair.

This procedure should be incorporated into the MBE as a method of identifying and addressing repairs for complex bridges. In addition to the above recommended method, additional conclusions based off the research performed as a part of the project include the following:

Bridge S-31 has additional capacity unaccounted for based off its internal redundancy. This is based off the experimental and finite element data gathered on the bridge in conjunction with the WIM data received. It is safe to assume that the posting of 15 tons is violated daily with more than 50% of the trucks passing over the bridge violating this restriction.

Regarding the impact of this research, while there has been research regarding monitoring and evaluating bridges, very few have been done for bridges in a deteriorated state or near the end of its service life. Additionally, very few analyze the bridge utilizing the LRFR method when it was originally designed for Working Stress and comparing it to the LFR Rating. Additionally, few studies focus on shear forces specifically within a stringer floor beam system.

This research assists in further understanding how a bridge designed for working stress reacts under the newer LRFR method and how it correlates to finite element and experimental data.

Additionally, this project provides insight in the evaluation of complex bridges. In many of the studies performed normally standard bridges have been evaluated and compared. This study utilizes a bridge which is complex in nature providing additional insight into internal redundancy and proposes a method of evaluating and prioritizing repairs. A method which will not only benefit the academic community, but the industry. Finally, very few projects, if any, have incorporated the use of weigh-in-motion sensors to assist in evaluating a structure as far as prioritizing repairs, and at the same time provide us insight into truck loads on a local roadway.

REFERENCES

[1.] AASHTO Manual for Bridge Evaluation Second Edition (2011), with 2016 Interims

[2.] AASHTO Manual for Bridge Evaluation Third Edition (2018)

[3.] AASHTO LRFD Bridge Design Specifications, 8th Edition, 2018

[4.] AASHTO Movable Bridge Evaluation and Maintenance Manual, 2nd Edition, 2016

[5.] U.S. Department of Transportation Federal Highway Administration Recording and Coding Guide for the Structure Inventory and Appraisal of the Nation's Bridges, Report No. FHWA-PD-96-001

[6.] ASCE 2017 Infrastructure Report Card, https://www.infrastructurereportcard.org

[7.] 14th Cycle Bridge Reevaluation Survey Report, Structure No. 1300-S31 on Bingham Avenue-Locust Point Road (CR8A) over the Navesink River (Oceanic Bridge) Rumson Borough, Middletown Township, Monmouth County, Prepared by S&R Engineers, P.C., 2013

[8.] 15th Cycle Bridge Reevaluation Survey Report, Structure No. 1300-S31 on Bingham Avenue-Locust Point Road (CR8A) over the Navesink River (Oceanic Bridge) Rumson Borough, Middletown Township, Monmouth County, Prepared by Michael Baker, 2015

[9.] 16th Cycle Bridge Reevaluation Survey Report, Structure No. 1300-S31 on Bingham Avenue-Locust Point Road (CR8A) over the Navesink River (Oceanic Bridge) Rumson Borough, Middletown Township, Monmouth County, Prepared by Michael Baker, 2017

[10.] A1512 Accelerometer, Bridge Diagnostic Group, Doc 201441, Rev A, 740 S. Pierce Avenue Unit 15, Louisville Colorado 80027, 2019

[11.] STS4 Wireless Structural Testing System, Bridge Diagnostic Inc, 1995 57th Court North, Suite 100, Boulder Colorado 80301, 2020

[12.] ST350 Strain Transducer, Bridge Diagnostic Group, 740 S. Pierce Avenue Unit 15, Louisville Colorado 80027, 2019

[13.] Moses, Fred and Verma, D., NCHRP Report 301 Load Capacity of Existing Bridges, 1987

[14.] Kulicki, J.M., Prucz, Z., Sorgenfrei, D.F., and Mertz, D.R., NCHRP Report 333 Guidelines for Evaluating Corrosion effects in Existing Steel Bridges, December 1990

[15.] Wassef, Wagdy G.; Kulicki, John M.; Nassif, Hani; Mertz, Dennis; and Nowak, Andrzej S. National Academies of Sciences, Engineering, and Medicine 2014. Calibration of AASHTO LRFD Concrete Bridge Design Specifications for Serviceability Report 12-83. Washington, DC: The National Academies Press. https://doi.org/10.17226/22407

[16.] Ghosn, Michel, and Moses, Fred, NCHRP Report 406 Redundancy in Highway Bridge Superstructures, 1998

[17.] Moses, Fred, NCHRP Report 454 Calibration of Load Factors for LRFR Bridge Evaluation, 2001

[18.] Mlynarski, Mark; Wassef, Wagdy G.; Nowak, Andrzej J.; NCHRP Report 700 A Comparison of AASHTO Bridge Load Rating Methods, 2011

[19.] Nowak, Andrzej, Live Load Model for Highway Bridges, Structural Safety, 13(1993)53-66 Elsevier, 1993

[20.] Nowak, Andrzej, Calibration of LRFD Code, Journal of Structural Engineering, Vol. 121, No. 8, 1995

[21.] Czarnecki, Artur and Nowak, Andrzej, S., Time-Variant reliability. Profiles for steel girder bridges, Science Direct, Structural Safety 30, 2008

[22.] Pelphrey Jordan, Higgins, Higgins, Christopher; Sivakumar, Bala; Groff, Richard; Hartman, Bert; Charbonneau, Joseph; Rooper, Jonathan; Johnson, Bruce; State Specific LRFR Live Load Factors Using Weigh-in-Motion Data, Journal for Bridge Engineering, Vol. 13, No. 4, 2008

[23.] Gao, Lubin, Load Rating Highway Bridges in the United States: The State of Practice, Structural Engineering International, 3/2013.

[24.] Uddin, Nasim; Zhao, Hua; Waldron, Christopher; Dong, Li; Greer, Amber; Weigh-in-Motion (WIM) Data for Site-Specific LRFR Bridge Load Rating, UTCA, Report Number 10204, 2011

[25.] Sanayei, Masoud; Reiff, Alexandra, J.; Brenner, Brian; Imbaro, Gregory R.; Load Rating of a Fully Instrumented Bridge: Comparison of LRFR Approaches, Journal of Performance of Constructed Facilities, 2015

[26.] Gunasekaran, Umarani; Ashokkumar, Kanchanadevi; Amaladosson, Teresa; Enid Rose, Load Rating for Bridges – Current Practices and Issues, Prague Development Center, ATI-Applied Technologies and Innovations, Volume 2, Issue 2, 2010

[27.] Deng, Yaohua and Phares, Brent, Automated bridge load rating determination using strain response due to ambient traffic trucks, Engineering Structures 117, 2016

[28.] Feldman Lisa; Jackson, Kristopher; Sparling Bruce; Sparks, Gordon, Comparison of load rating techniques for the Red Deer River Bridge, 2011

[29.] Seo, Junwon; Wan Hu, Jong; Lee Jaeha, Summary Review of Structural Health Monitoring Applications for Highway Bridges, Journal of Performance of Constructed Facilities, 2015

[30.] Seo, Junwon; Czaplewski, Taylor M.; Kimn, Jung-Han; Hatfield, Gary; Integrated Structural Health Monitoring Systems and Multi-Regression Models for Determining Load Ratings for Complex Steel Bridges, Measurement, 2015

[31.] Darmawan, M. Sigit; Refani, A.N.; Irmawan, M.; Bayuaji, R.; and Anugraha, R.B., Time Dependent Reliability Analysis of Steel I Bridge Girder Designed based on SNI T-02-2005 and SNI T-3-2005 Subject to Corrosion, Procedia Engineering, 2013

[32.] Phares, Brent; Wipf, Terry; Klaiber, F. Wayne; Abu-Hawash Ahmad; Bridge Load Rating using Physical Testing, 2003

[33.] Shipman, P.E., Finding Maximum Moment: Determining HL-93 Truck Position on Simple Spans, J. Bridge Eng., 2014

[34.] Kayser, Jack R., and Nowak, Andrzej S., Reliability of Corroded Steel Girder Bridges, Elsevier Science Publishers, 1989

[35.] Fontan, Mars., Corrosion Engineering 3rd Edition, McGraw Hill, 1987

[36.] Monmouth County Oceanic Bridge over North Shrewsbury River, P.W.A. Project NJ 1322-F, As-Built Construction Plans, as prepared by Morris Goodkind, and Ash-Howard-Needles & Tammen, 1938

[37.] Oceanic Bridge (S-31) Detour Plan as prepared by as prepared by the County of Monmouth Department of Public Works and Engineering Division of Traffic Safety, County Engineer, Joseph M. Ettore, PE, August 9, 2011

[38.] Structural Steel and Concrete Deck Repairs at Bridge S-31 on County Route 8A (Bingham Avenue) over the Navesink River, in the Township of Middletown and the Borough of Rumson, Monmouth County New Jersey, as prepared by the County of Monmouth Department of Public Works and Engineering Division of Traffic Safety, County Engineer, Joseph M. Ettore, PE, November 13, 2014.

[39.] Local Concept Development Study for Monmouth County Oceanic Bridge (S-31) on Bingham Avenue - Locust Point Road (CR8A) over the Navesink River , http://monmouthcountyoceanicbridge.com/ (2020)

APPENDIX

APPENDIX A

WEIGH-IN-MOTION DATA

This appendix contains analysis results for WIM data taken at Bridge S-31. Contained in this appendix is the data following the scrubbing process, statistical calculations, results, and appropriate tables and graphs.

A.1 – Overall Data

Table A.1 - Overall WIM Data Results

Start Date	4/24/2019	
End Date	8/22/2019	
Number of Trucks	5,069	Trucks
Number Exceeding 15 Ton Posting	347	Trucks
ADTT	45	Trucks/Day
Average Speed	31.24	MPH
Minimum Load	8	Kips
Maximum Load	88	Kips
Average GVW	18.26	Kips
Standard Deviation	8.04	Kips

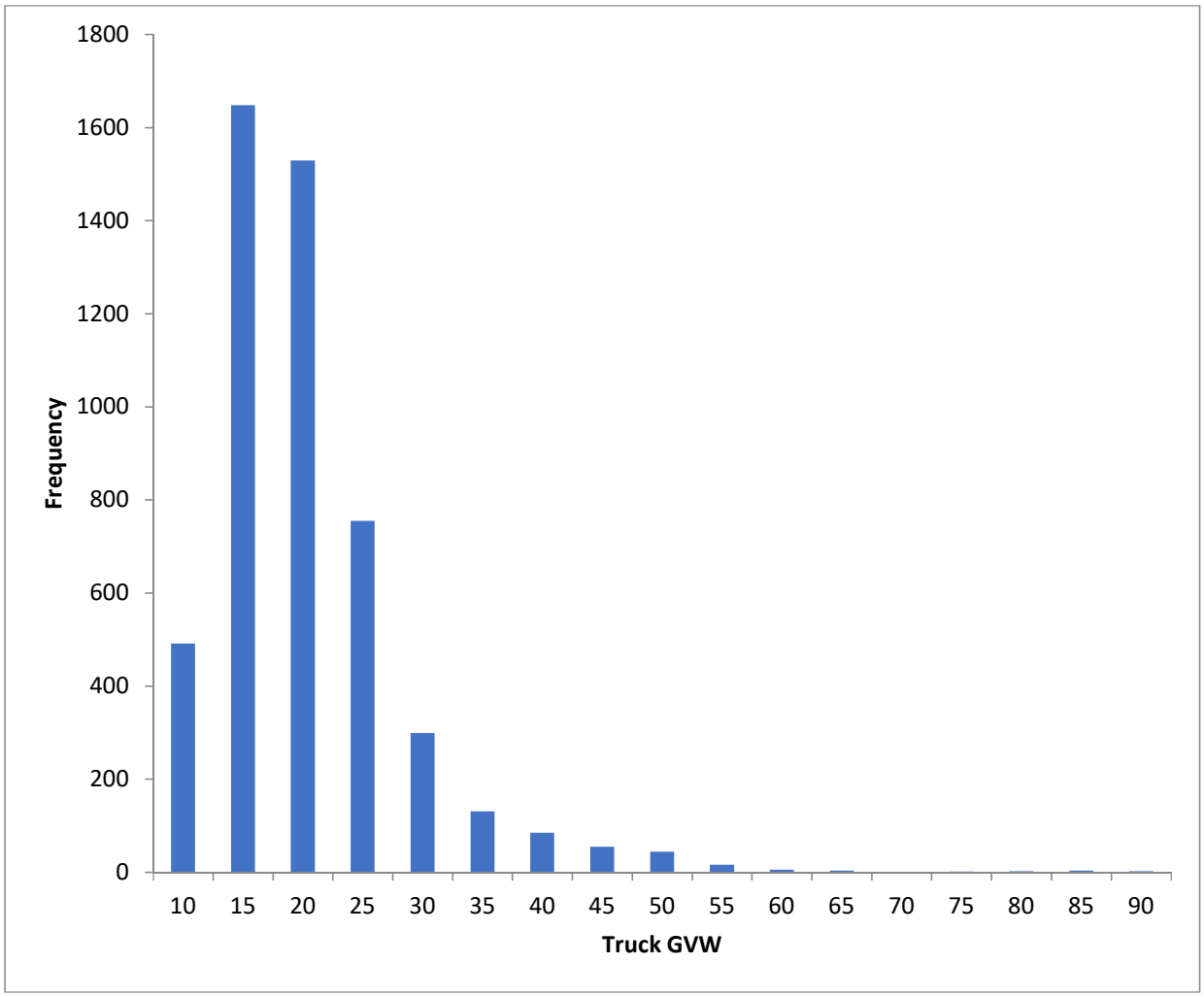

Figure A.1 - Histogram of Overall Truck Data

Table A.2 - Frequency Table for Overall Truck Data

GVW (Kips)	*Frequency*
<10	491
10 - 15	1648
15- 20	1529
20- 25	755
25 - 30	299
30 - 35	131
35 - 40	85
40 - 45	55
45 - 50	44
50 - 55	16
55 - 60	5
60 - 65	3
65 - 70	0
70- 75	1
75- 80	2
80 - 85	3
85 - 90	2
Total Trucks	5069

A.2 – Short Term Site-Specific Factor Calculation

A.2.1 – Short Term Site-Specific Factor Calculation - Overall Truck Data

Table A.3 - Site-Specific Factor with 2 Axle Data

20% Cutoff	26.39	Kips
Average Weight (W)	26.39	Kips
Standard Deviation	5.19	Kips

Table A.4 - Site Specific Factor Calculation

γ_L	0.462	(One Lane)
γ_L	0.512	(Two Lanes or More)
γ_L	**1.3**	per C6A.4.4.2.3a-1

A.2.1 – Short Term Site-Specific Factor Calculation - Without 2 Axle Trucks

Table A.5 - Filtered WIM Data Results

Start Date	4/24/2019	
End Date	8/22/2019	
Number of Trucks	645	Trucks
Number Exceeding 15 Ton Posting	293	Trucks
Minimum Load	13	Kips
Maximum Load	88	Kips
Average GVW	31.39	Kips
Standard Deviation	1.30	Kips

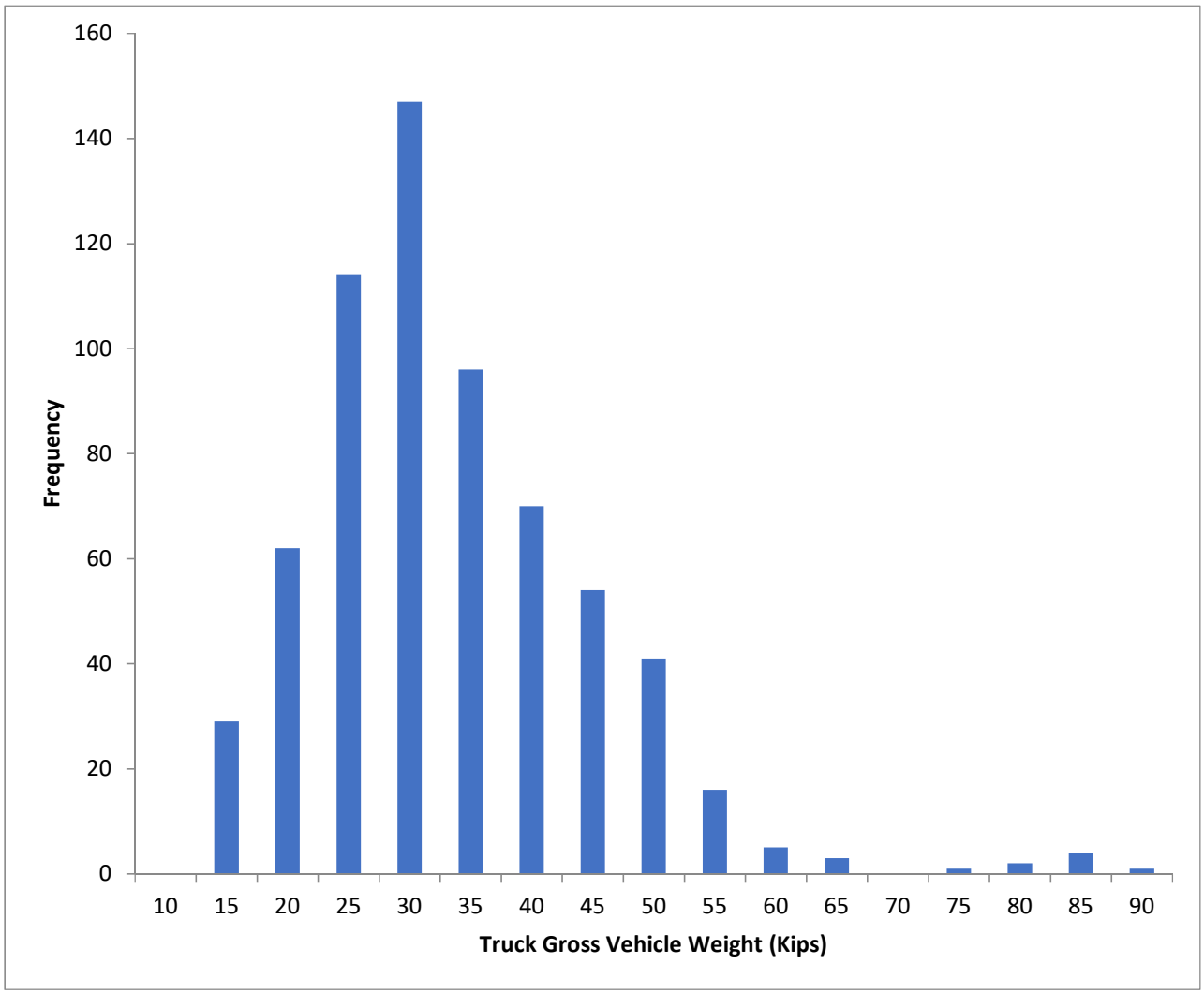

Figure A.2 - Histogram of Truck Data without 2-Axle Trucks

Table A.6 - Frequency Table for Truck Data without 2-Axle Trucks

GVW (Kips)	*Frequency*
<10	0
10 - 15	29
15- 20	62
20- 25	114
25 - 30	147
30 - 35	96
35 - 40	70
40 - 45	54
45 - 50	41
50 - 55	16
55 - 60	5
60 - 65	3
65 - 70	0
70- 75	1
75- 80	2
80 - 85	4
85 - 90	1
Total Trucks	645

Table A.7 - Sample Statistical Data

20% Cutoff	40	Kips
Average Weight (W)	41.36	Kips
Standard Deviation	1.30	Kips

Table A.8 - Site Specific Factor Calculation

γ_L	0.637	(One Lane)
γ_L	0.650	(Two Lanes or More)
γ_L	**1.3**	per C6A.4.4.2.3a-1

A.3 – 5-year Lmax Calculation and Supporting Data

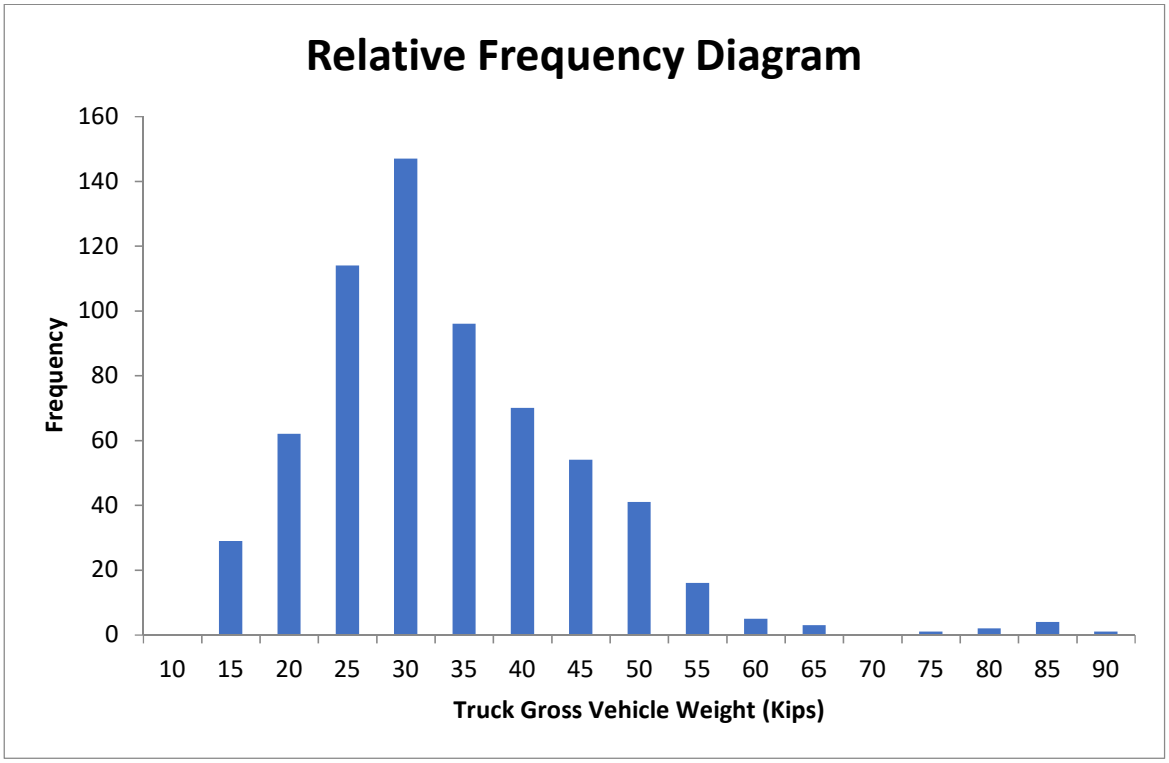

Figure A.3 - Relative Frequency Histogram

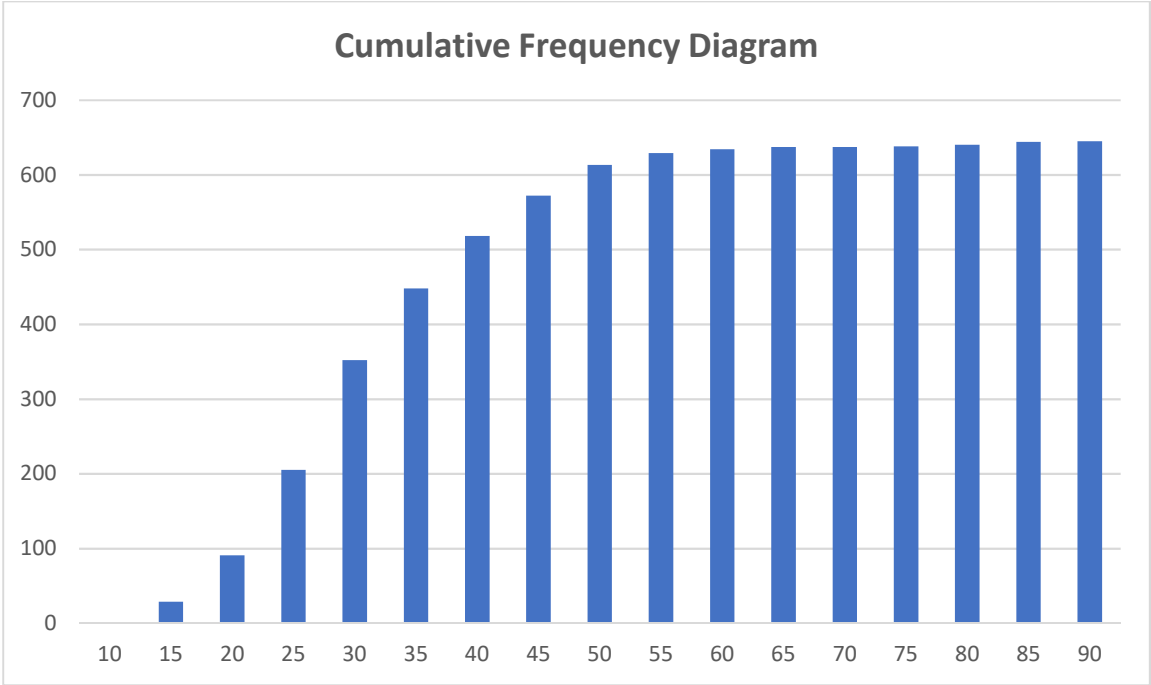

Figure A.4 - Cumulative Frequency Histogram

Table A.9 - Frequency Tables

Frequency Tables			
GVW	*Relative Frequency*	*GVW*	*Cumulative Frequency*
10	0	10	0
15	29	15	29
20	62	20	91
25	114	25	205
30	147	30	352
35	96	35	448
40	70	40	518
45	54	45	572
50	41	50	613
55	16	55	629
60	5	60	634
65	3	65	637
70	0	70	637
75	1	75	638
80	2	80	640
85	4	85	644
90	1	90	645
Total	645		

Table A.10 - Calculated Parameters for Lmax

Category	Value	Unit
Sample Mean	59.03	Kips
Sample Standard Deviation	11.98	Kips
Variance	143.56	Kips
Coefficient of Variation	20.30	Percent
95th Percentile	50	Kips

Table A.11 - Calculated Variables for Live Load Factor and Lmax

m (slope)	0.083
n (intercept)	-4.926
μ Event	59.025
σ Event	11.981797
μ N	104.089
α N	0.360
Lmax (kips)	105.693

Table A.12 - Sample Truck Data for Lmax

Truck	GVW
1	50
2	50
3	50
4	50
5	50
6	50
7	50
8	50
9	51
10	51
11	51
12	51
13	51
14	51
15	52
16	52
17	52
18	52
19	53
20	53
21	53
22	54
23	54
24	55
25	56
26	57
27	57
28	57
29	59
30	63
31	63
32	63
33	71
34	79
35	79
36	82
37	84
38	84
39	85
40	86

Table A.13 - Live Load Factor Calculation

Variable	Calculated LL Factor	# Lanes	AASHTO Minimum Factor	Live Load Factor Used
γL	0.79	Two Lanes	1.3	1.3
γL	1.59	One Lane	1.8	1.8

APPENDIX B

STRUCTURAL HEALTH MONITORING

This appendix contains the results obtained from the 2016 and 2018 Structural Health Monitoring at Bridge S-31.

B.1 – 2016 Field Test

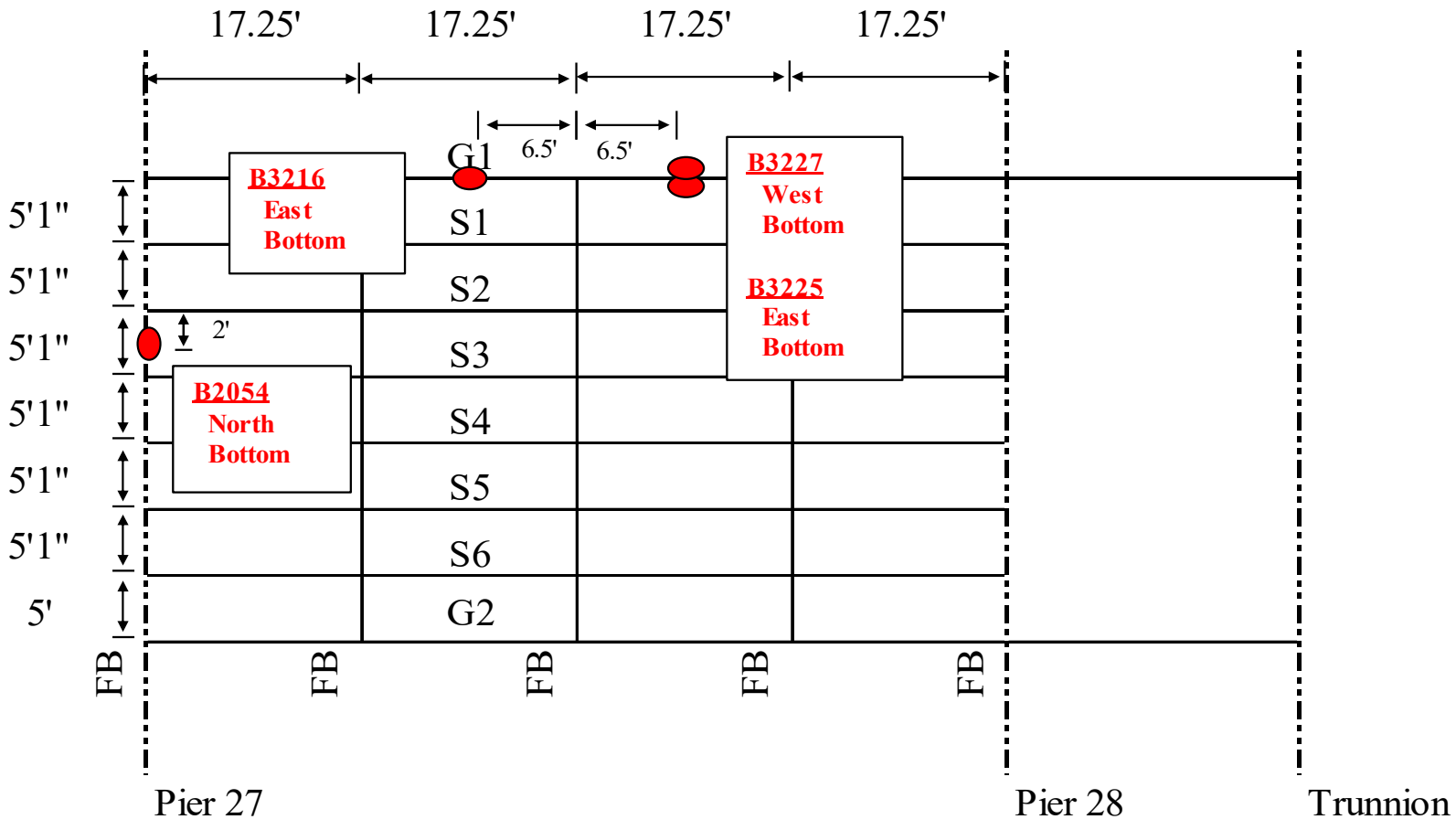

Figure B.1 - 2016 Sensor Plan

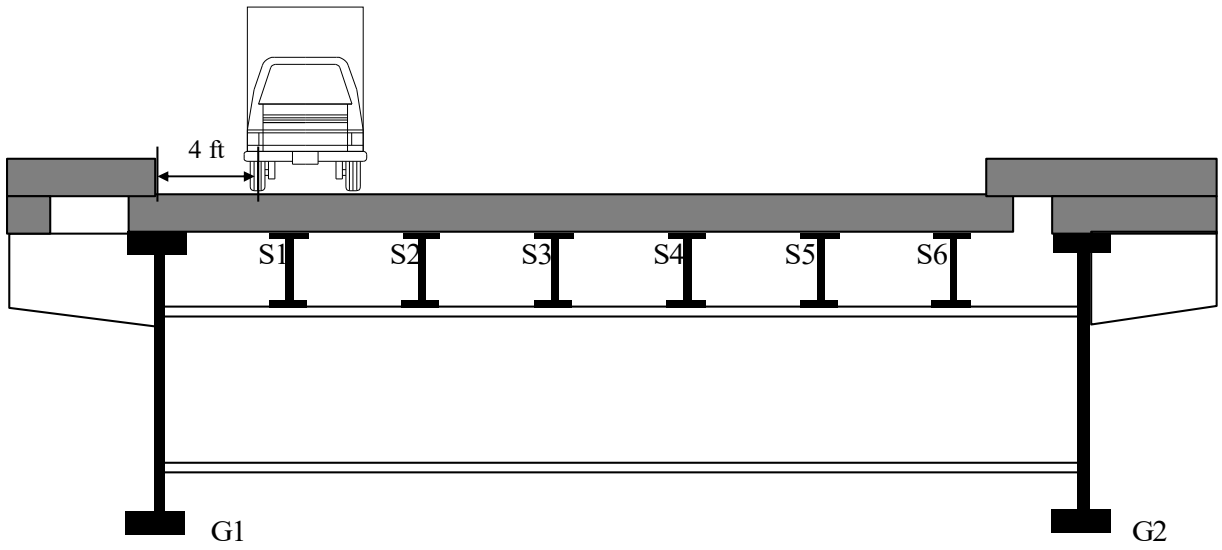

Figure B.2 - Testing Cross Section

Table B.1 - 2016 Maximum Strains Observed (30 MPH)

Sensor	B3225	B3227	B3216	B2054
MPH	30	30	30	30
Time	49.96	49.96	49.96	49.96
Max Strain	15.641	17.963	12.933	5.605

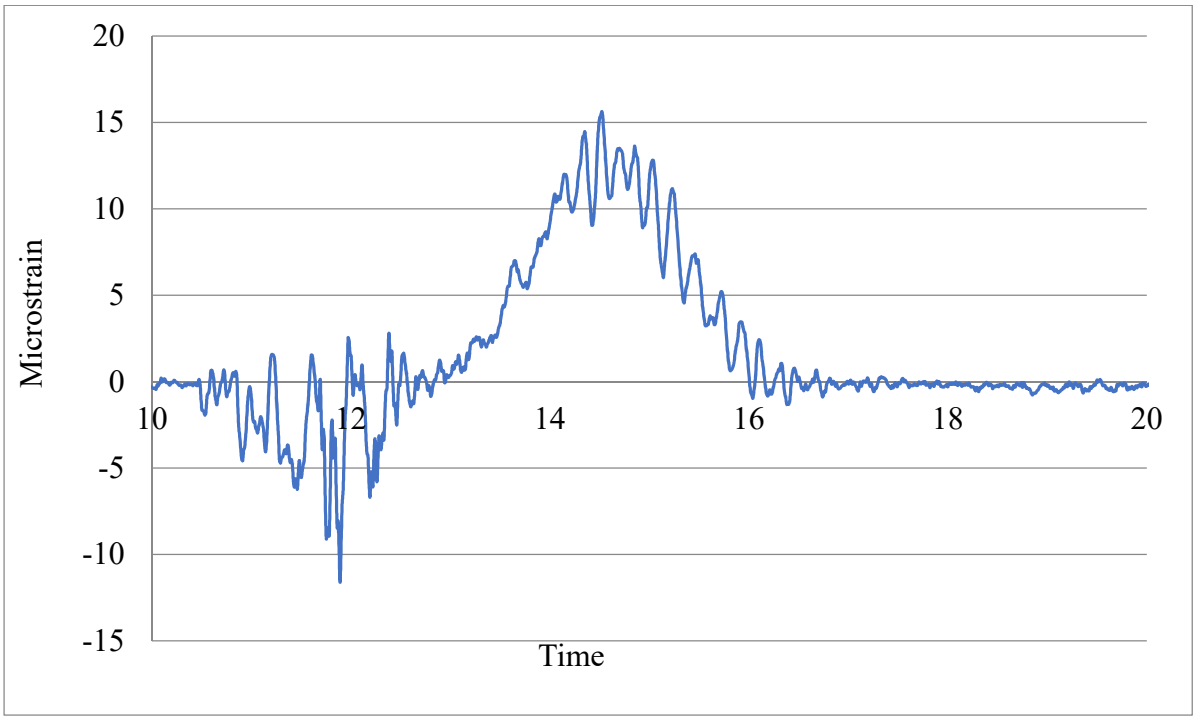

Figure B.3 - Sensor B3225 Results (30 Mph Test)

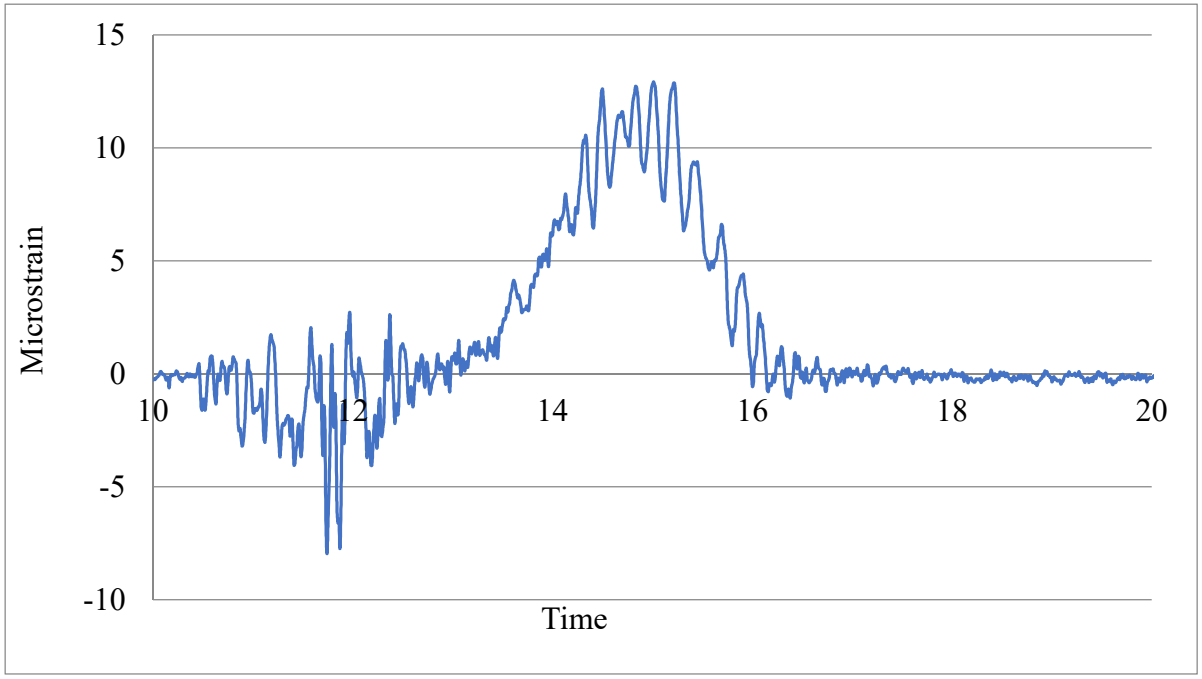

Figure B.4 - Sensor B3216 Results (30 Mph Test)

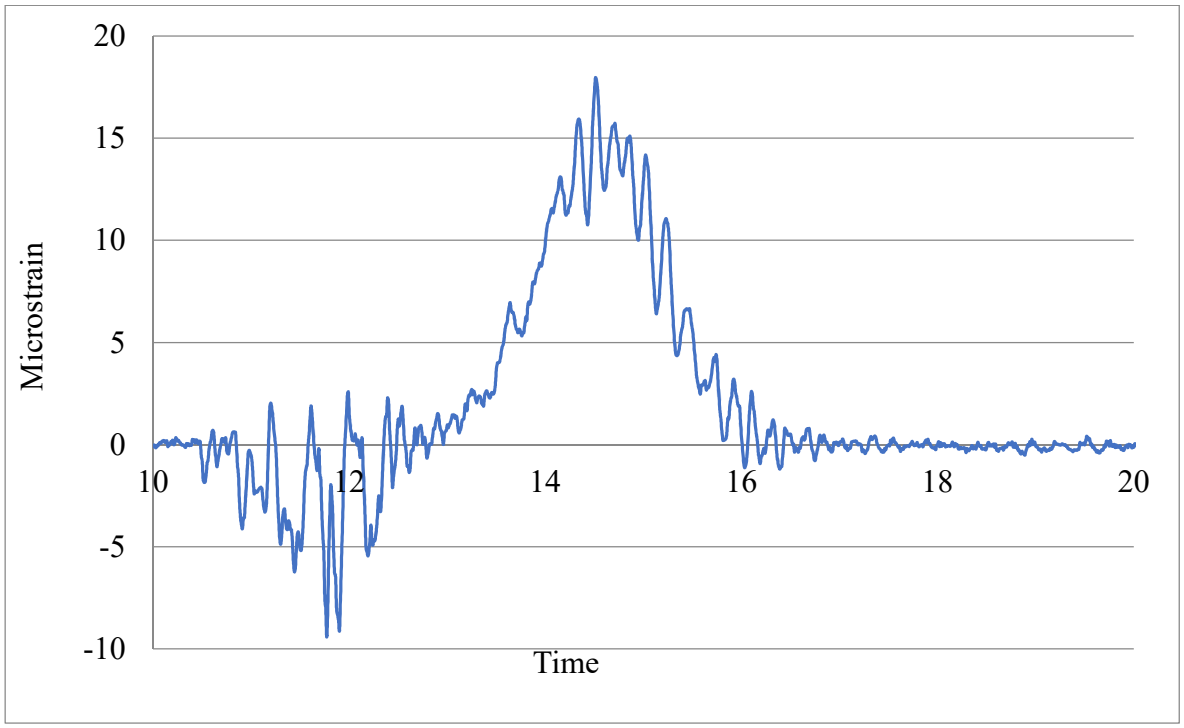

Figure B.5 - Sensor B3225 Results (30 Mph Test)

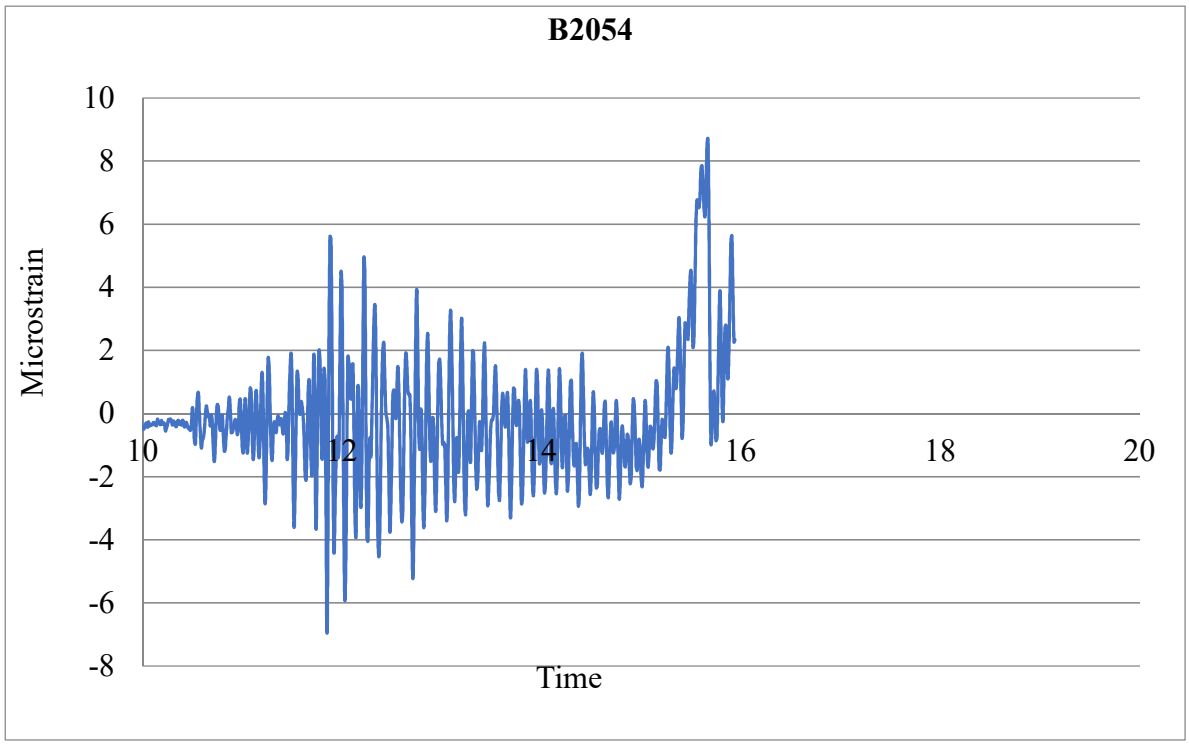

Figure B.6 - Sensor B2054 Results (30 Mph Test)

B.2 – 2018 Field Test

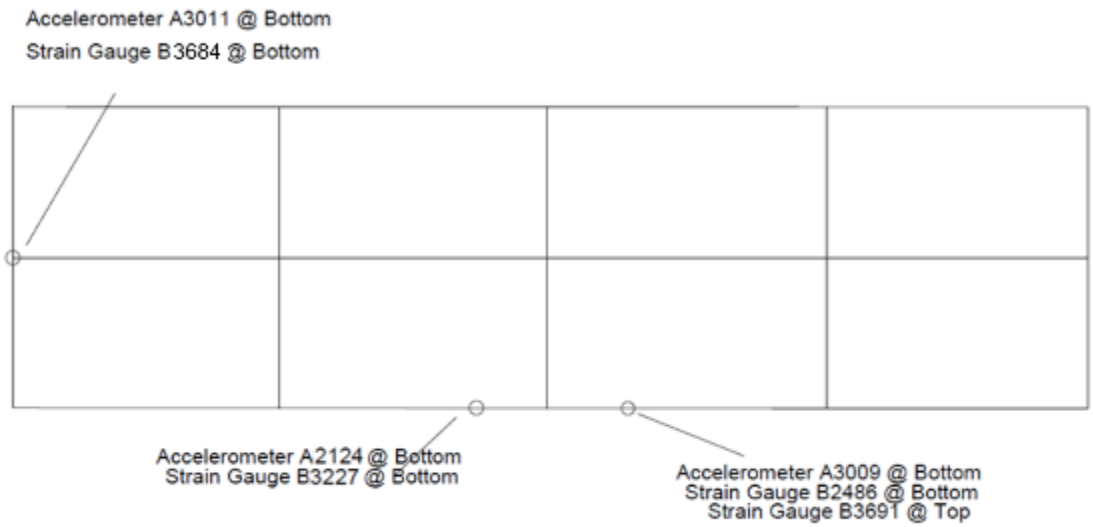

Figure B.7 - Sensor Plan North Span

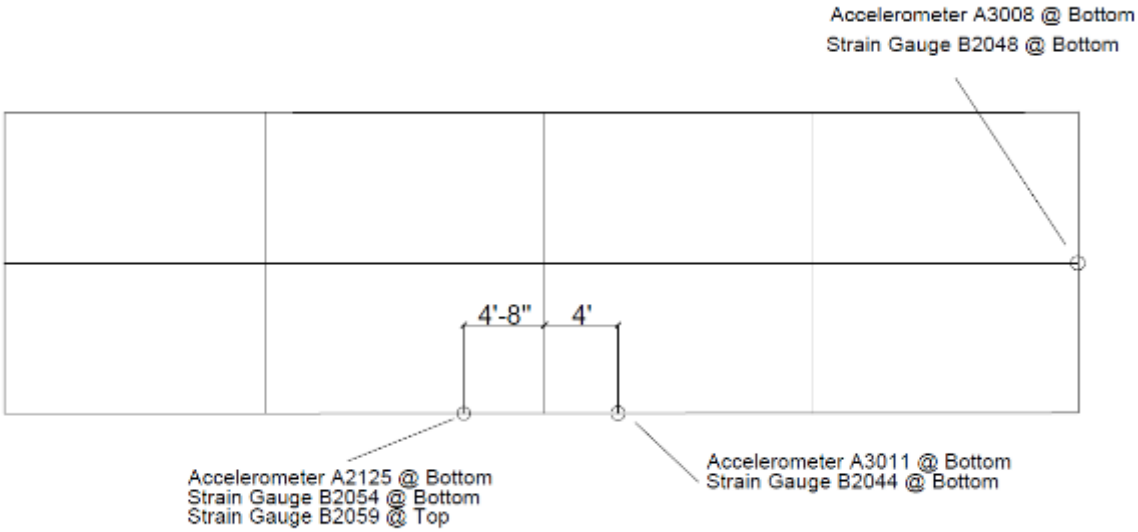

Figure B.8 - Sensor Plan South Span

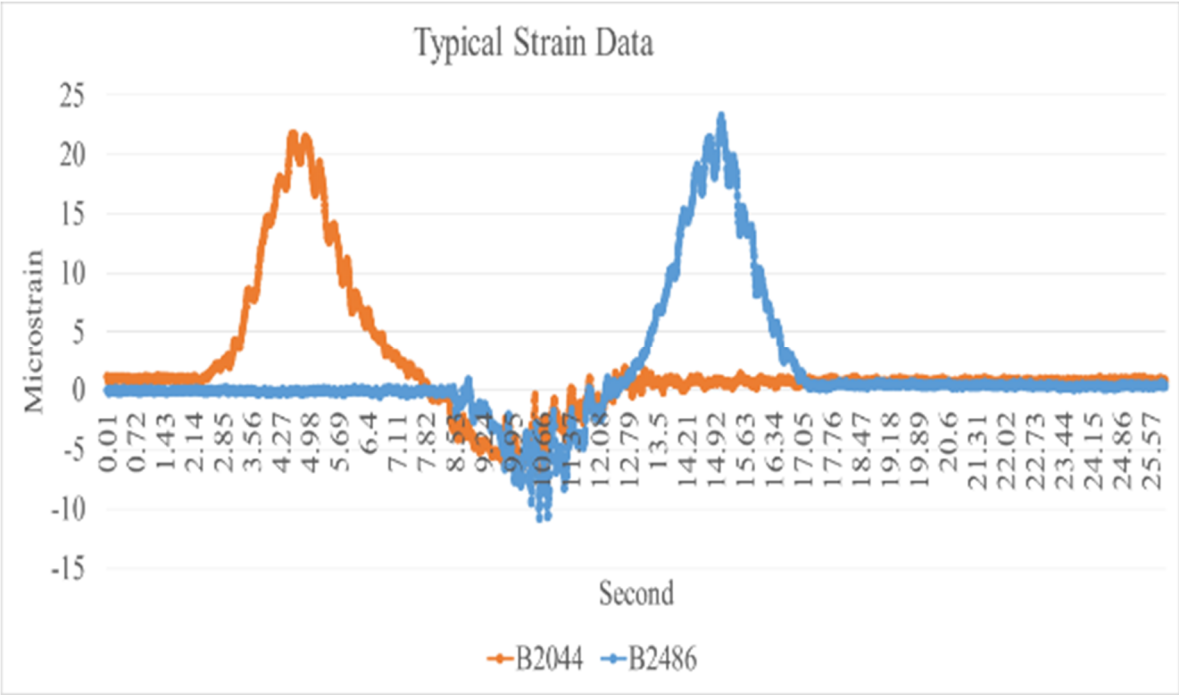

Figure B.9 - Strain Gauge Sensor Results B2044 and B2486 (30 MPH Test)

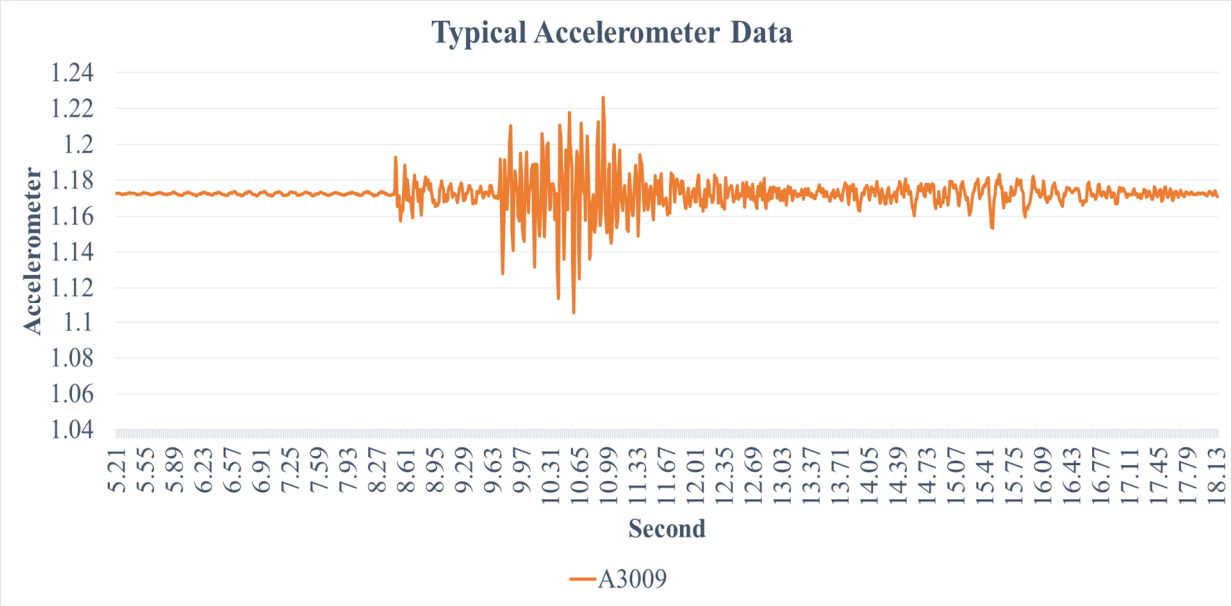

Figure B.10 - Accelerometer Results Sensor Results A3009 (30 MPH Test)

Table B.2 - Static Test North Span Results (Max Strain)

Runs	B3684 (Bot)	Time	B3227 (Bot)	Time	B2486 (Bot)	Time	B3691 (Top)	Time
Static North 1	7.00	16.4	14.65	14.35	21.16	13.33	0.488	13.48
Static North 2	9.08	17.9	13.84	15.15	19.30	14.75	0.629	14.98

Table B.3 - Static Test South Span Results (Max Strain)

Runs	B2048 (Bot)	Time	B2044 (Bot)	Time	B2054 (Bot)	Time	B2059 (Top)	Time
Static South 1	6.48	14.4	20.397	19.275	12.644	24.30	-1.073	24.30
Static South 2	5.22	11.85	18.862	15.425	10.739	16.45	-0.111	15.75

Table B.4 - Dynamic Test North Span Results (Max Strain)

Runs	B3684 (Bot)	Time	B3227 (Bot)	Time	B2486 (Bot)	Time	B3691 (Top)	Time
10 mph	7.10	16.73	14.51	15.39	22.76	15.06	1.46	10.81
20 mph	7.30	19.12	14.12	18.54	20.66	18.17	1.96	15.71
30 mph	8.28	27.32	14.50	26.75	21.81	26.71	1.70	24.48
30 mph (2nd run)	9.82	24.47	15.47	23.72	22.07	23.69	1.84	21.5

Table B.5 - Dynamic Test South Span Results (Max Stain)

Runs	B2048 (Bot)	Time	B2044 (Bot)	Time	B2054 (Bot)	Time	B2059 (Top)	Time
10 mph	9.81	3.4	21.72	4.57	13.34	5.24	-1.99	5.89
20 mph	9.47	11.31	22.70	12.19	13.02	12.61	-1.95	12.98
30 mph	11.77	20.38	22.33	21.21	12.14	21.64	-2.16	21.92
30 mph (2nd run)	11.61	17.59	22.43	18.39	13.11	18.76	-2.02	19.08

APPENDIX C

INSPECTION PHOTOS

This appendix contains select inspection photos taken from various field inspections of Bridge S-31.

Figure C.1 - 2013 Deteriorated Floorbeam (Center Panels)

Figure C.2 - 2013 Deteriorated Floorbeam (Panels 2 and 3)

Figure C.3 - 2013 Deteriorated Floorbeam (Looking North)

Figure C.4 - 2015 Repaired Floorbeam (Looking East)

Figure C.5 - Repaired Floorbeam (Looking North)

Figure C.6 - Fascia Girder at Bascule Pier (Looking North)

Figure C.7 - Fascia Girder Midspan Corrosion (Looking East)

Figure C.8 - West Fascia Girder (Looking South)

Figure C.9 - Fascia Girder (Interior View) Corrosion on Bottom Flange

Figure C.10 - Fascia Girder Repair at Bascule Pier during 2015 Rehabilitation

APPENDIX D

AS-BUILT DRAWINGS

This appendix contains information taken from As-Built Drawings which assisted in developing the Finite Element Model for the Flanking Span and determining the resistance of members evaluated.

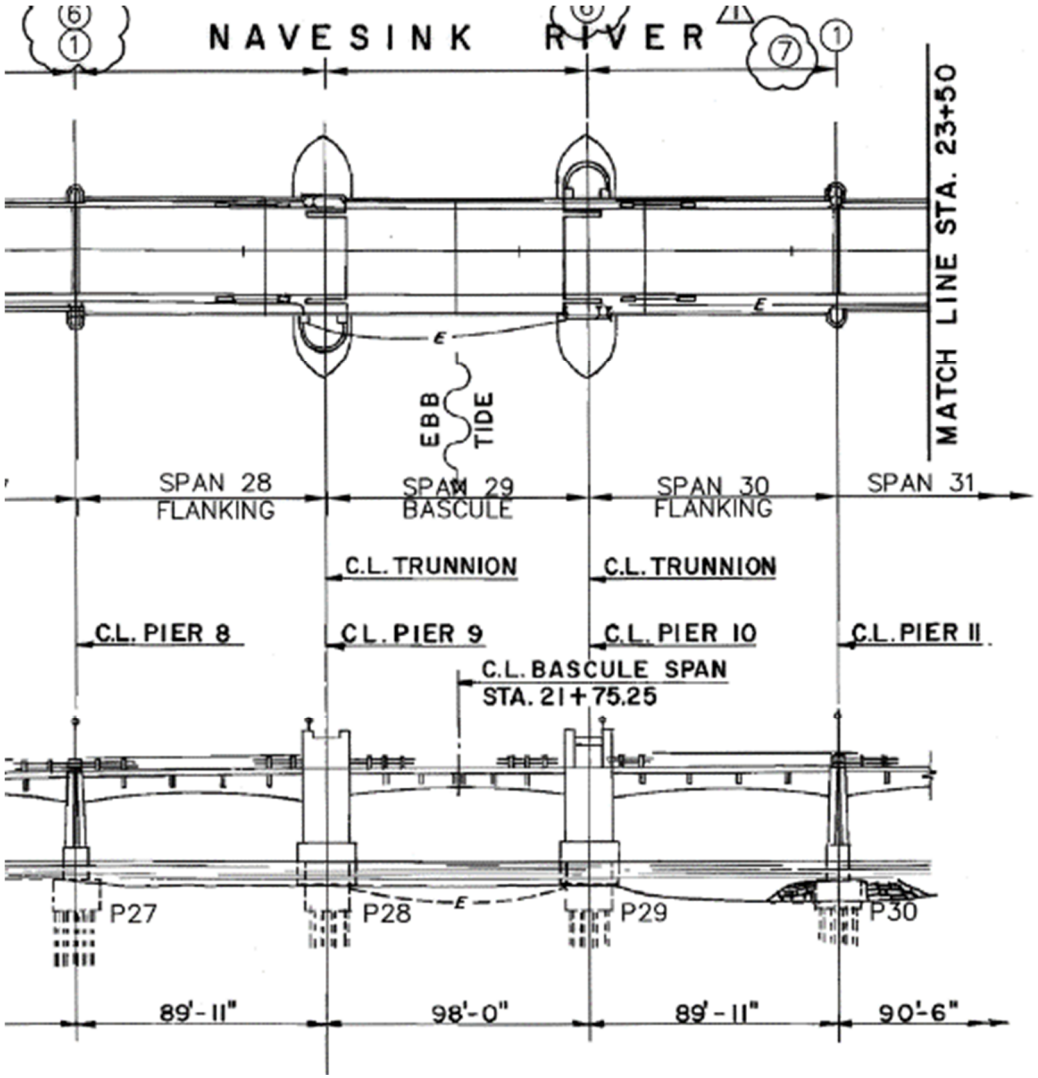

Figure D.1 - General Plan View and Elevation of S-31 Main Spans (2014 Repair Plans)

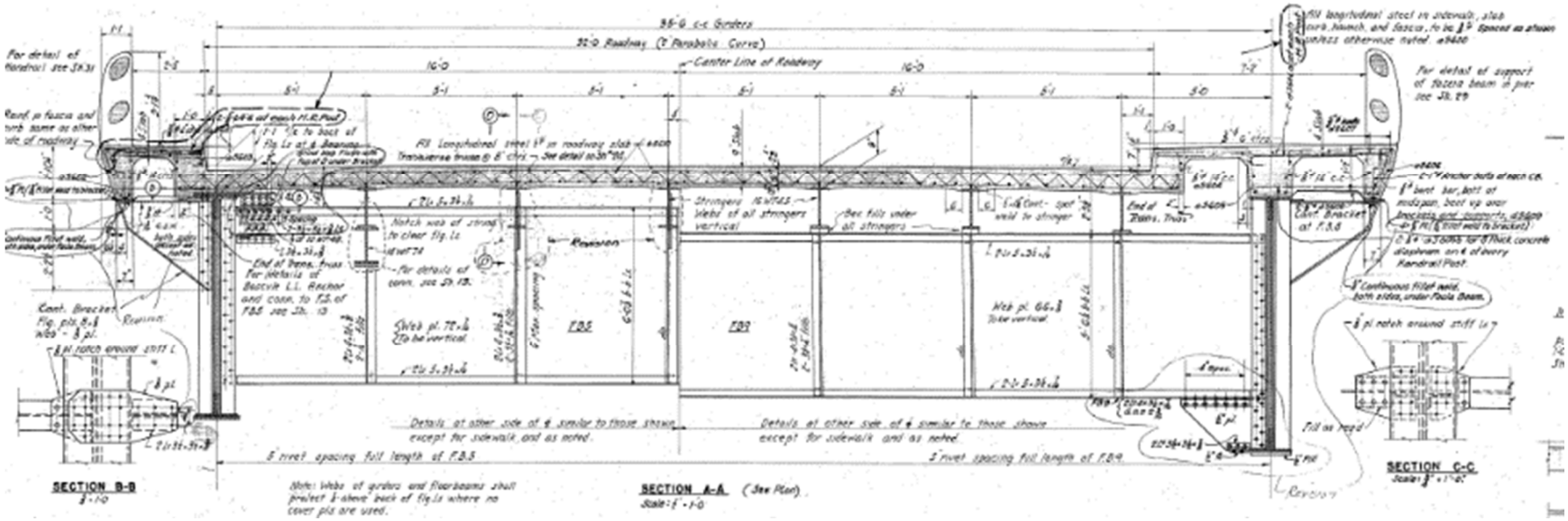

Figure D.2 - Typical Cross Section of Main Floor Beam (1939 As-Built Plans)

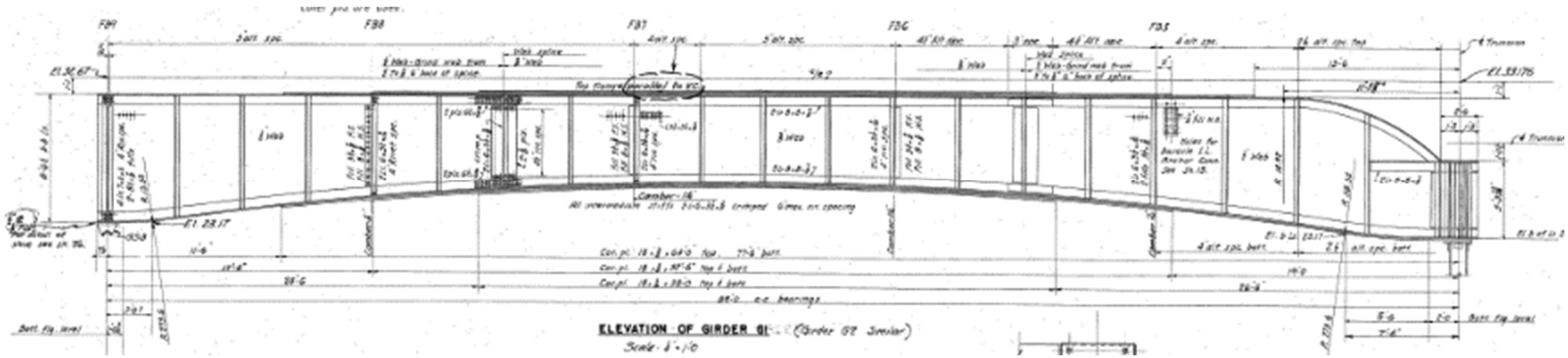

Figure D.3 - Elevation View of Fascia Girder (1939 As-Built Plans)

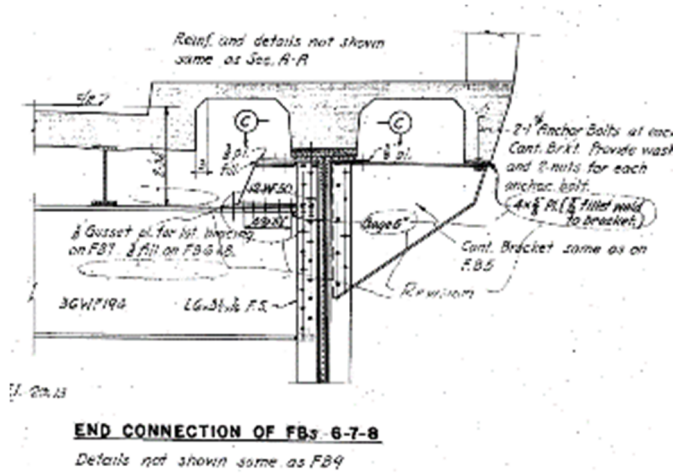

Figure D.4 - Detail of Interior Floor Beam at Flanking Span (1939 As-Built Plans)

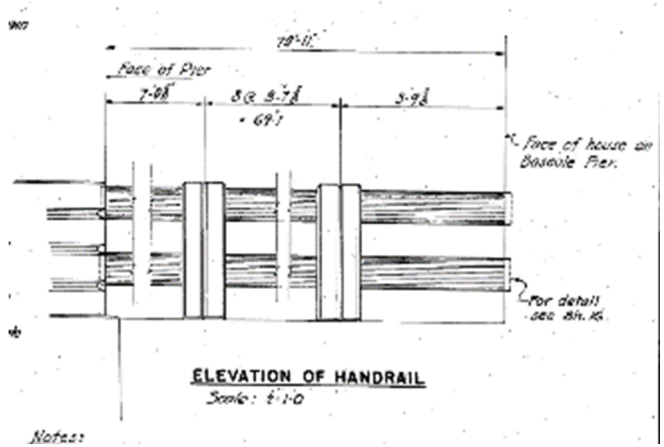

Figure D.5 - Detail of Parapet at Flanking Span (1939 As-Built Plans)

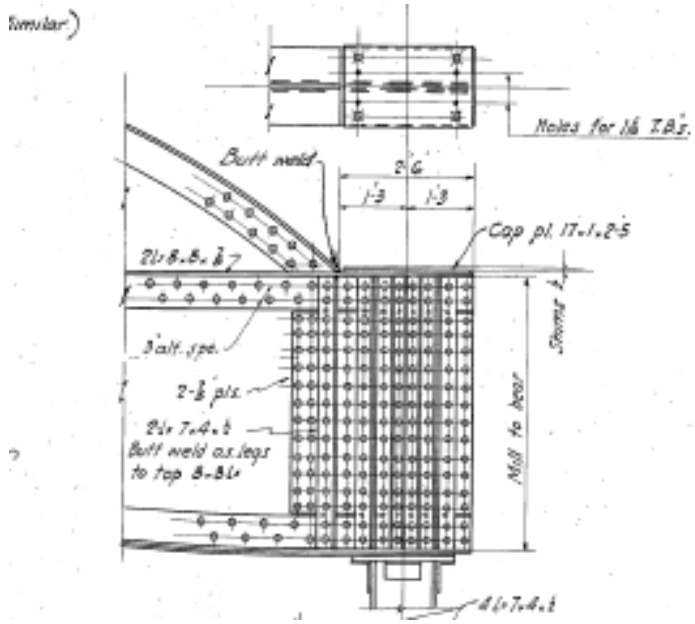

Figure D.6 - Detail of Connection to Main Trunnion Column (1939 As-Built Plans)

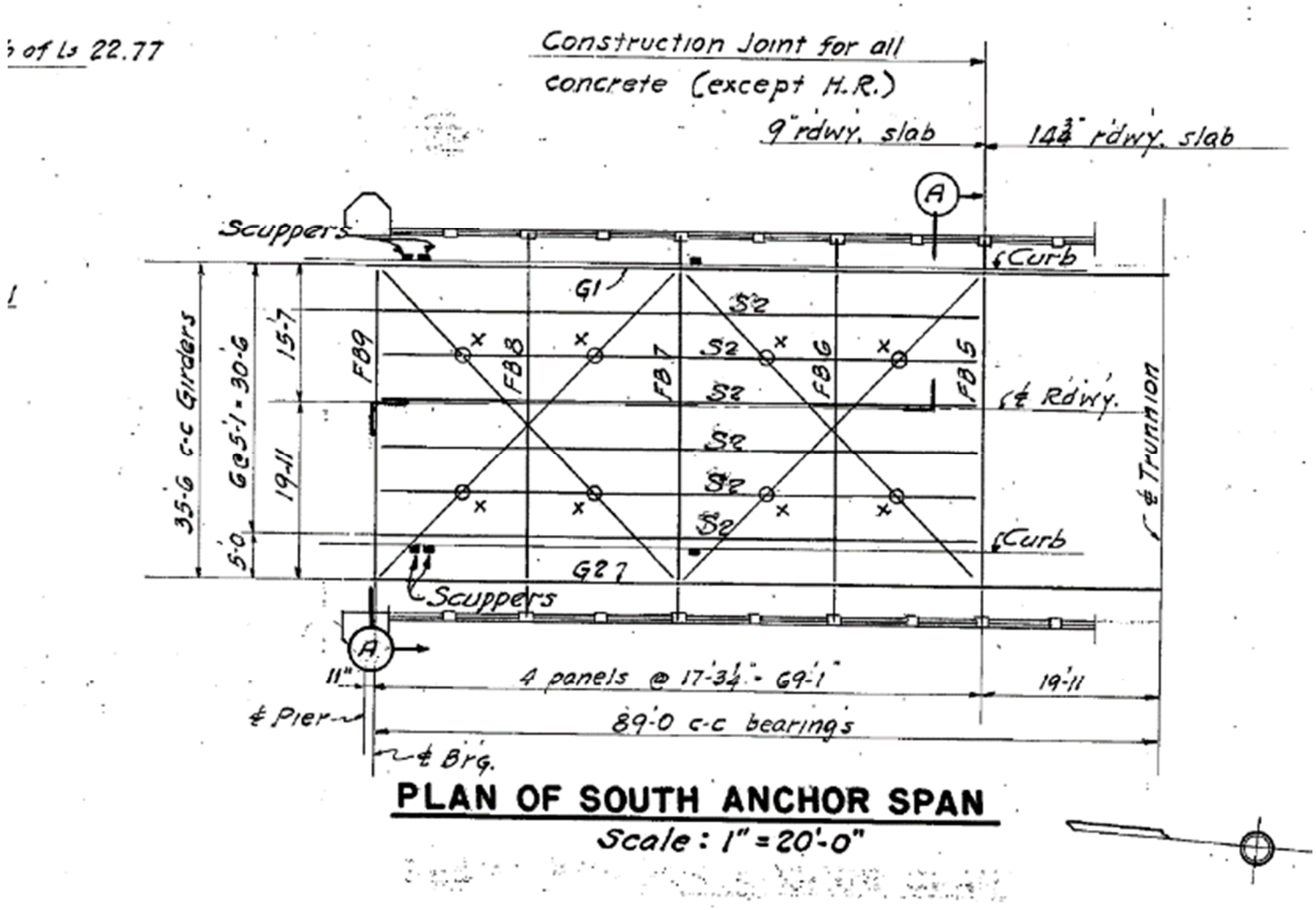

Figure D.7 - Framing Plan of Flanking Span (1939 As-Built Plans)

Figure D.8 - Floor Beam Deterioration, Elevation View (2014 Repair Plans)

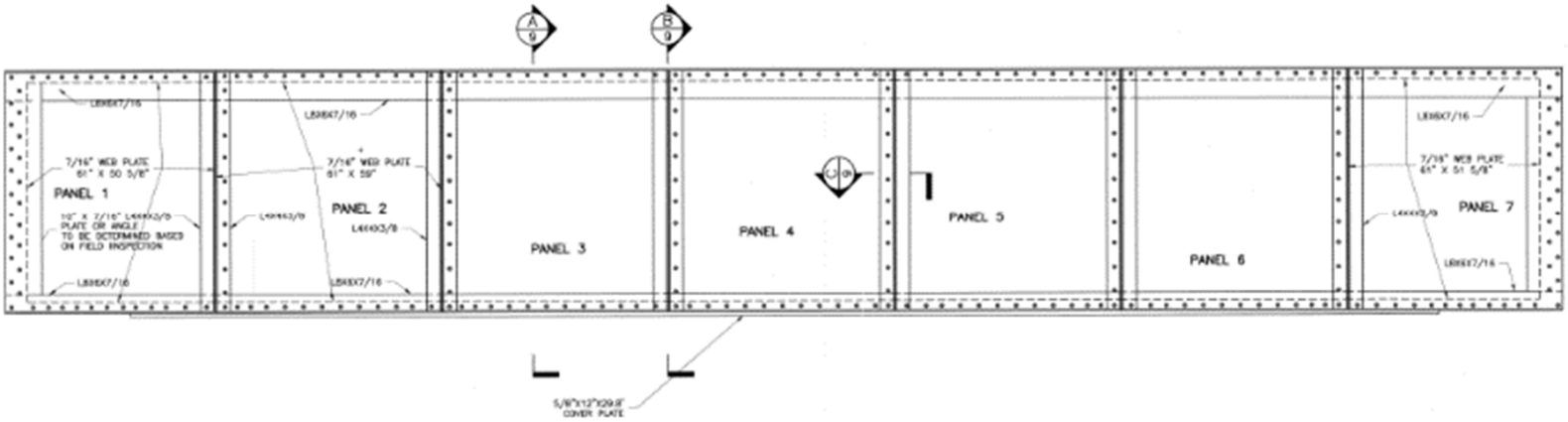

Figure D.9 - Floor Beam Repair, Elevation View (2014 Repair Plans)

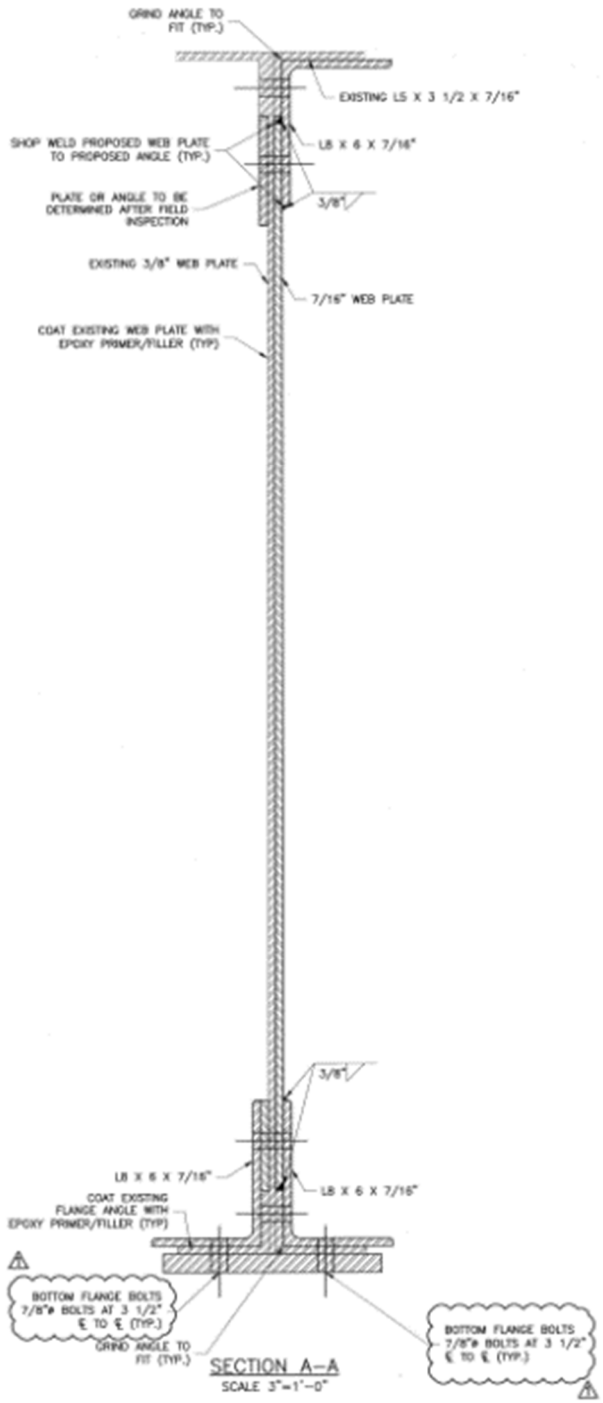

Figure D.10 - Floor Beam Repair, Detail (2014 Repair Plans)

APPENDIX E

FINITE ELEMENT MODEL RESULTS

This appendix contains results obtained from the Finite Element portion of this project.

E.1 – Fascia Girder Calibration Model and Results (All Models)

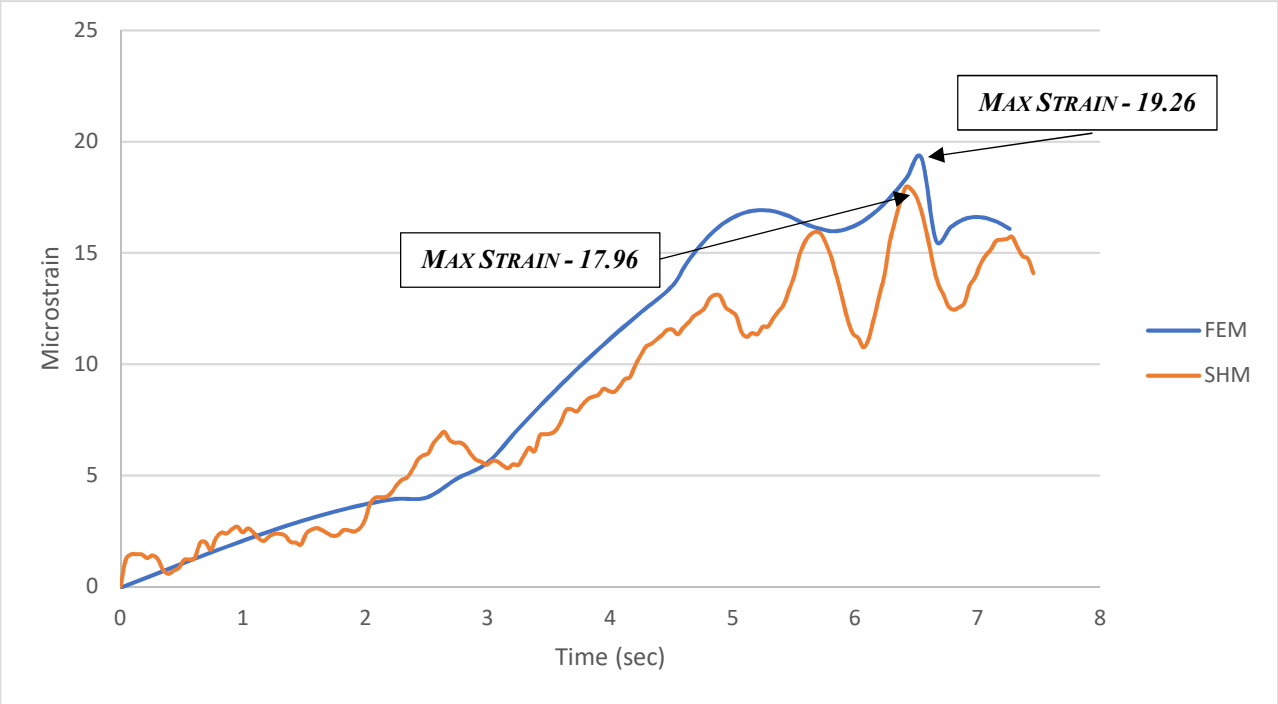

Figure E.1 - 2016 Calibration Fascia Girder (2018 Model)

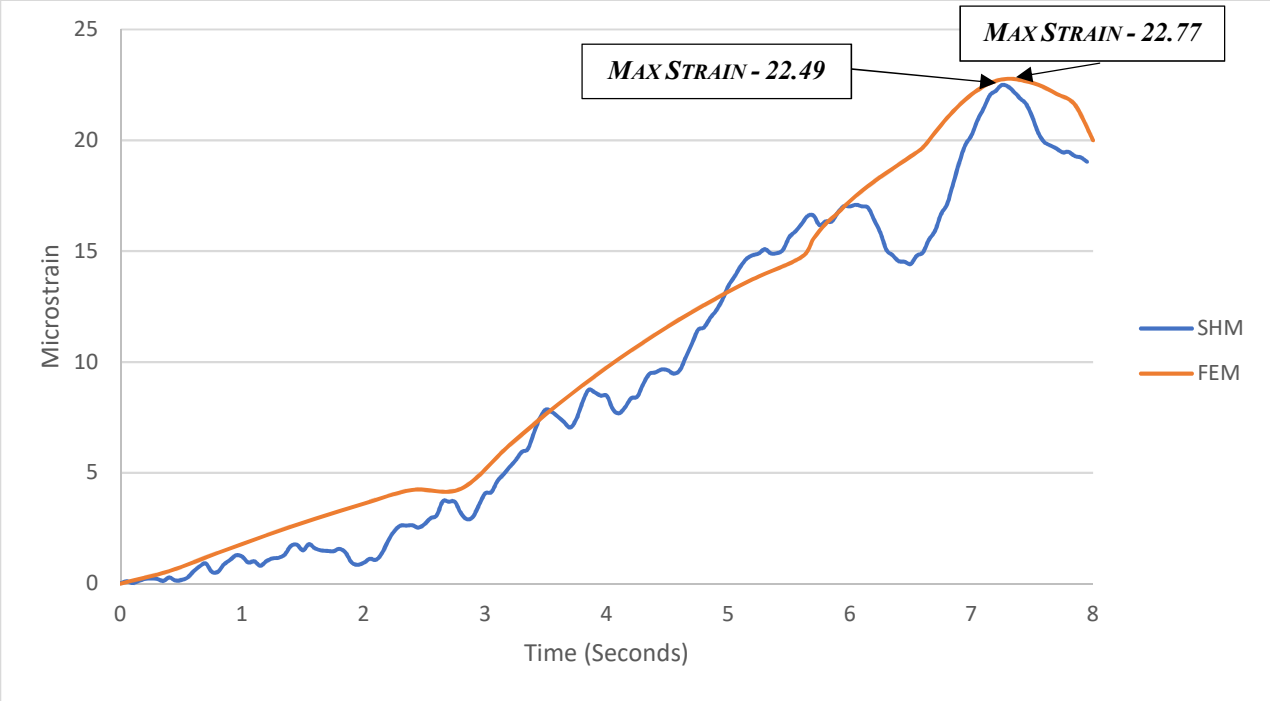

Figure E.2 - 2018 Calibration Fascia Girder (2018 Model)

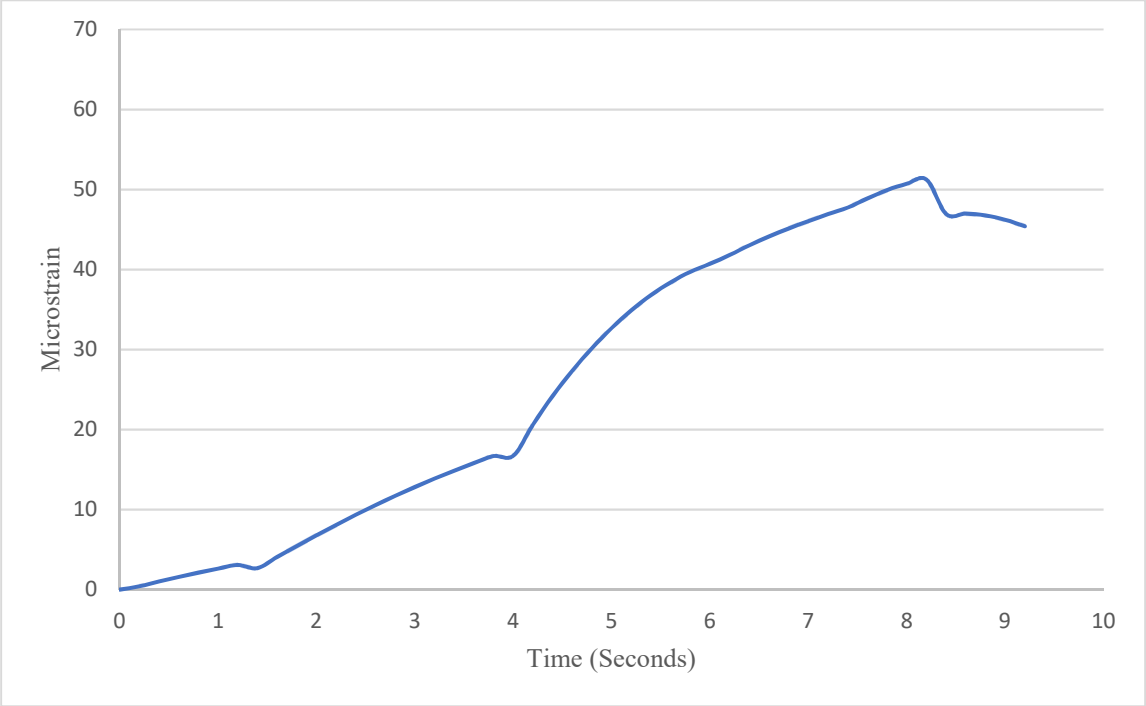

Figure E.3 - HS-20 FEM Results (2018 Model)

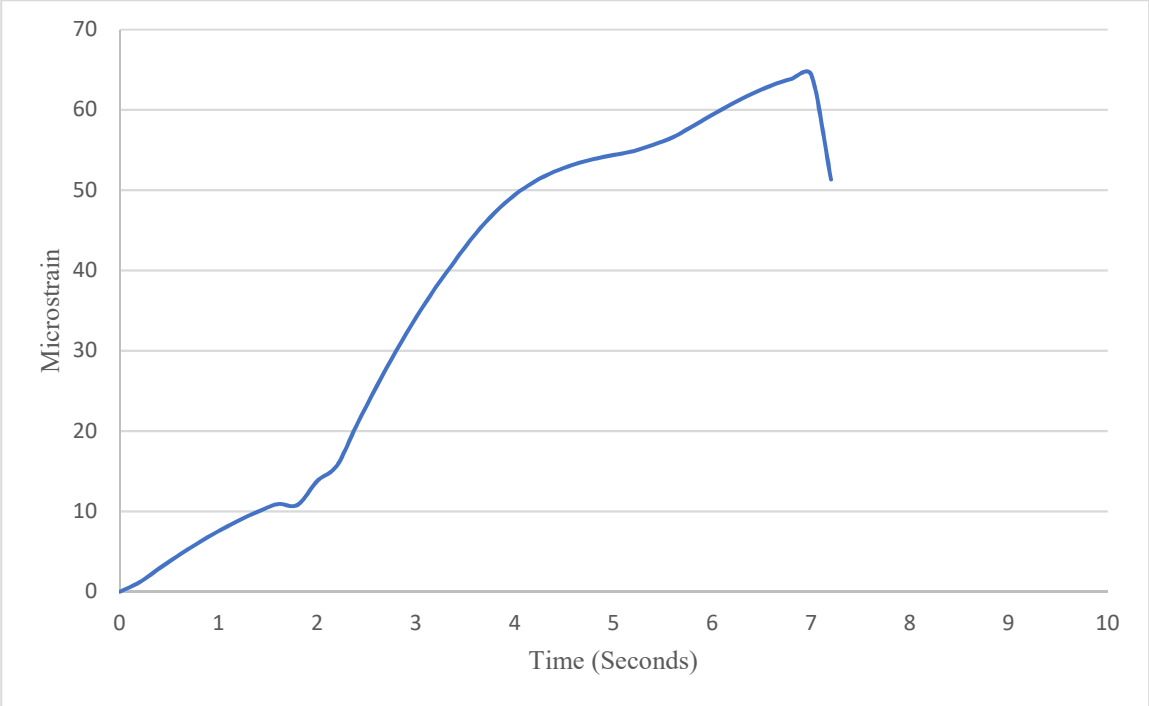

Figure E.4 - Maximum WIM Load FEM Results (2018 Model)

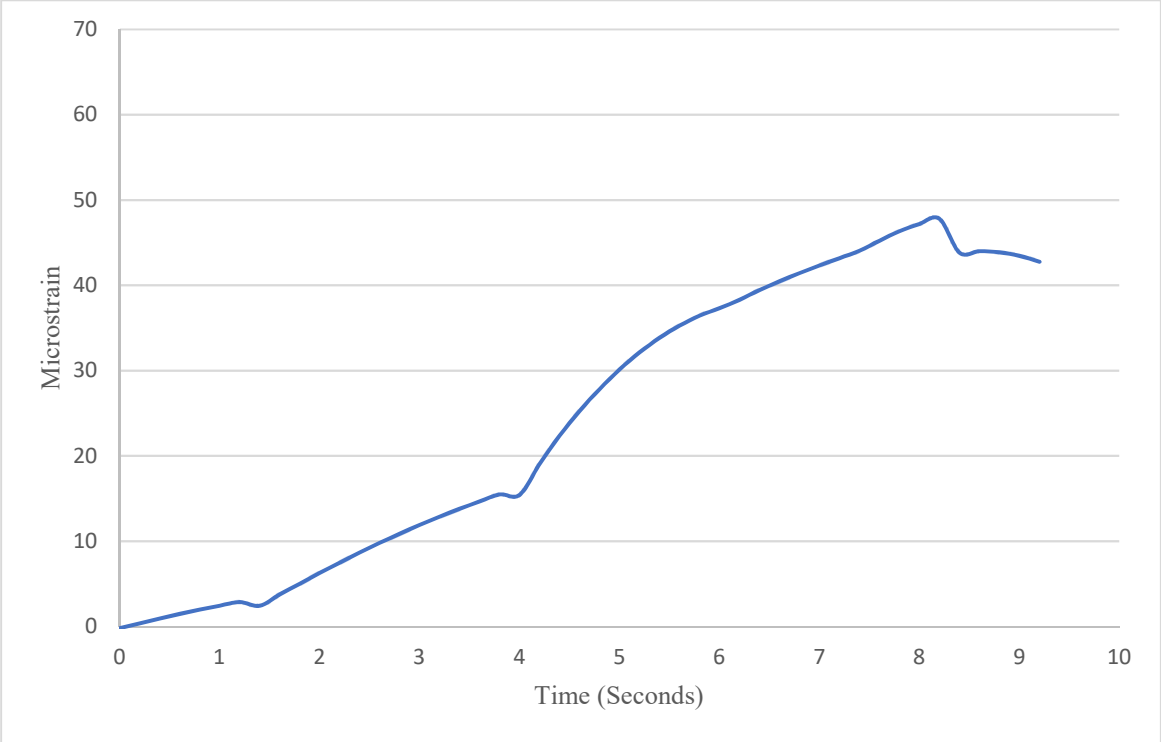

Figure E.5 - HS-20 FEM Results (1939 Model)

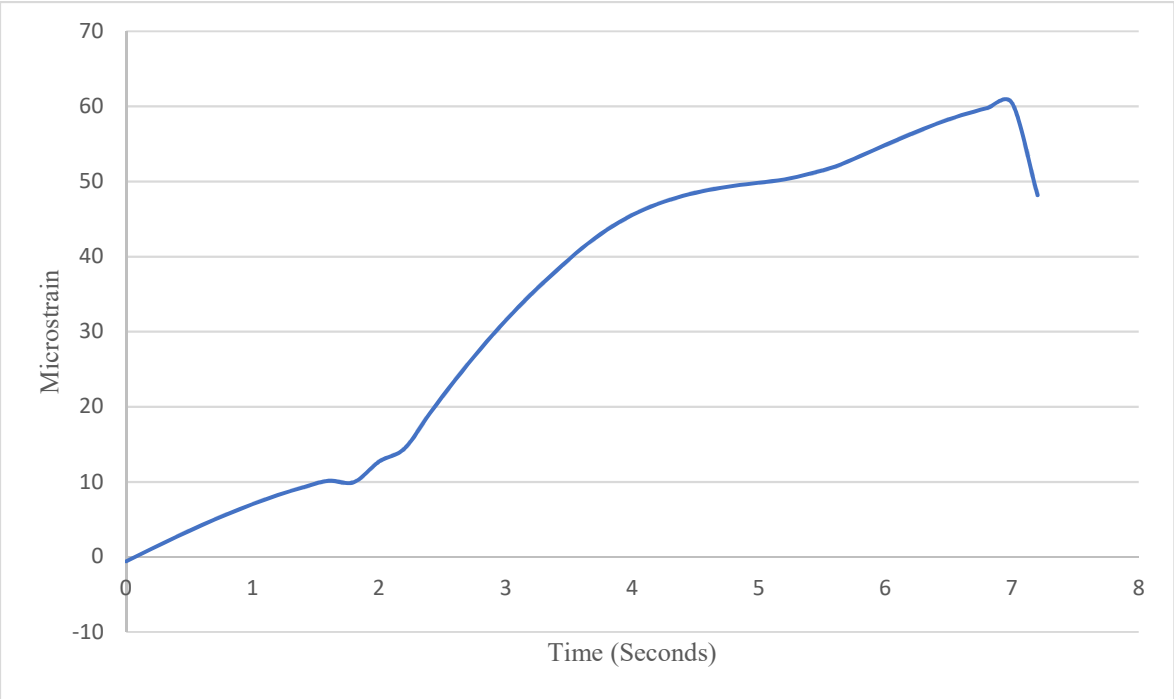

Figure E.6 - Max WIM Load FEM Results (1939 Model)

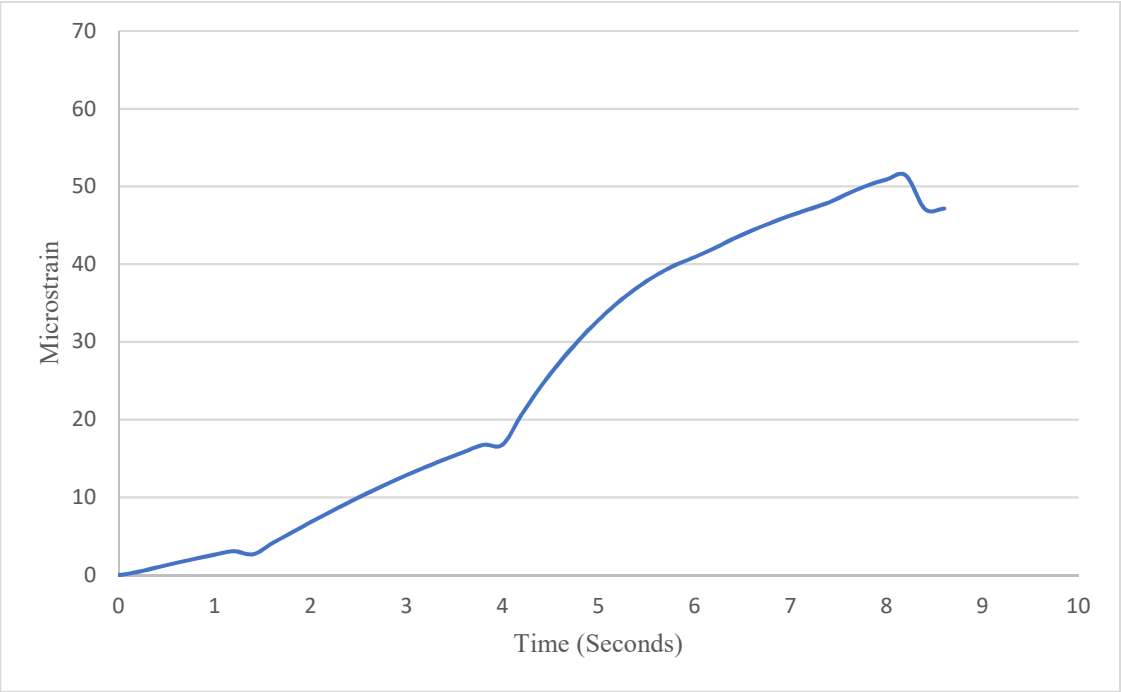

Figure E.7 - HS-20 FEM Results (2029 Model)

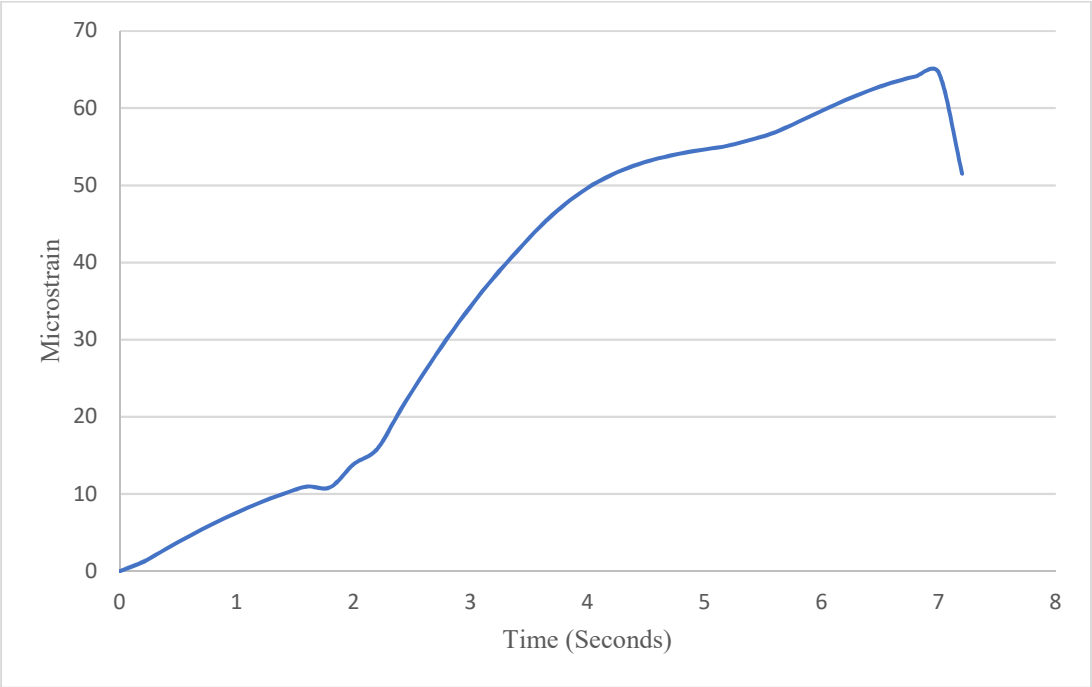

Figure E.8 - HS-20 FEM Results (2029 Model)

E.2 – Floor Beam Calibration Model and Results (All Models)

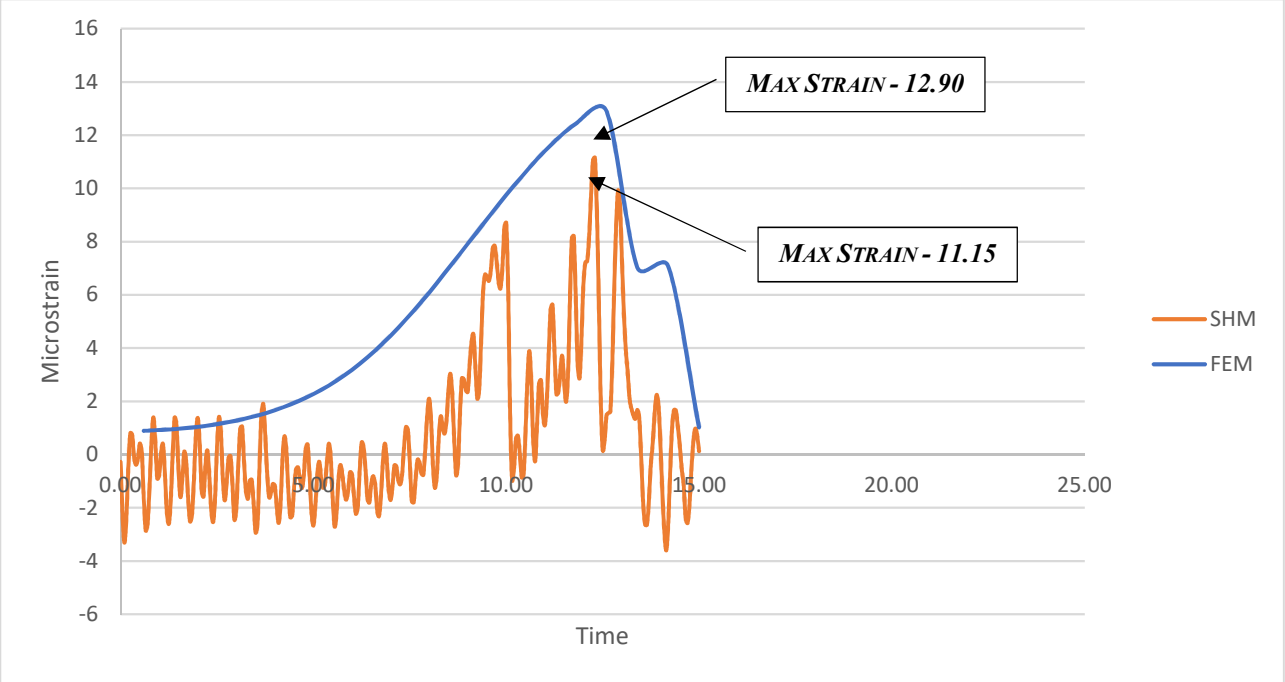

Figure E.9 - 2016 Calibration Floor Beam

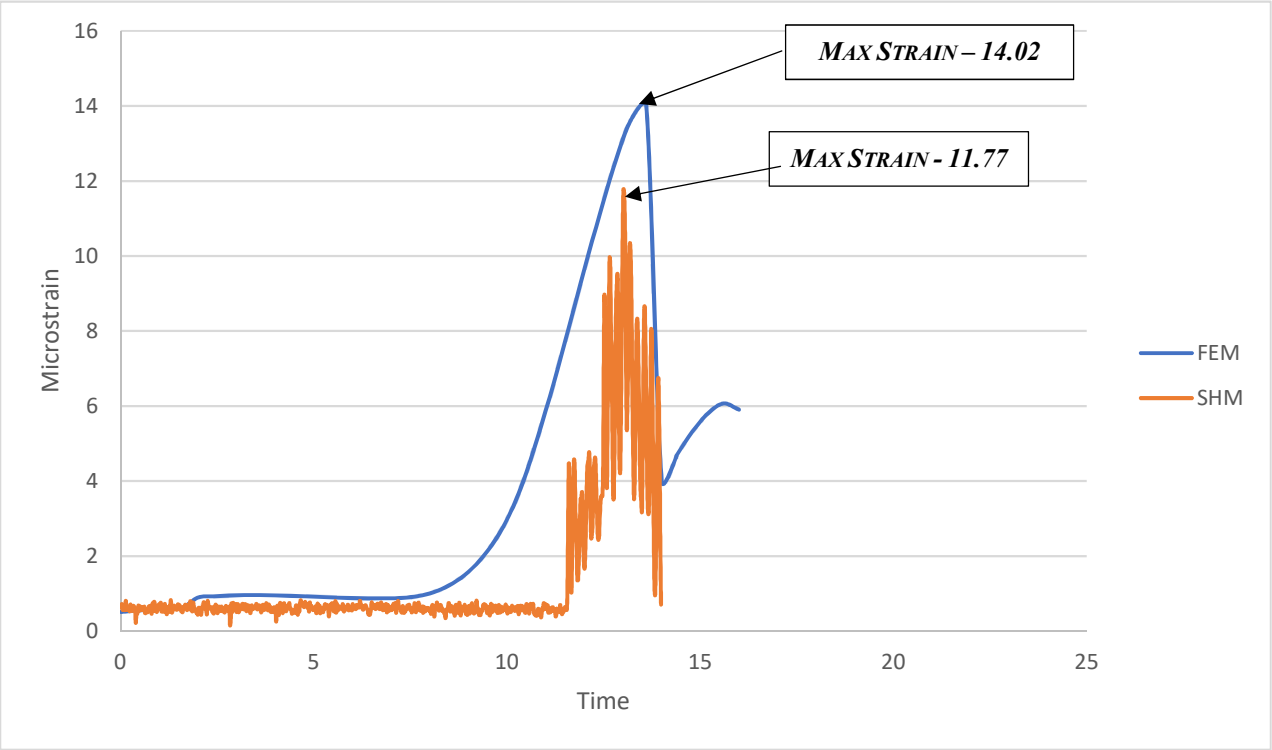

Figure E.10 - 2018 Calibration Floor Beam

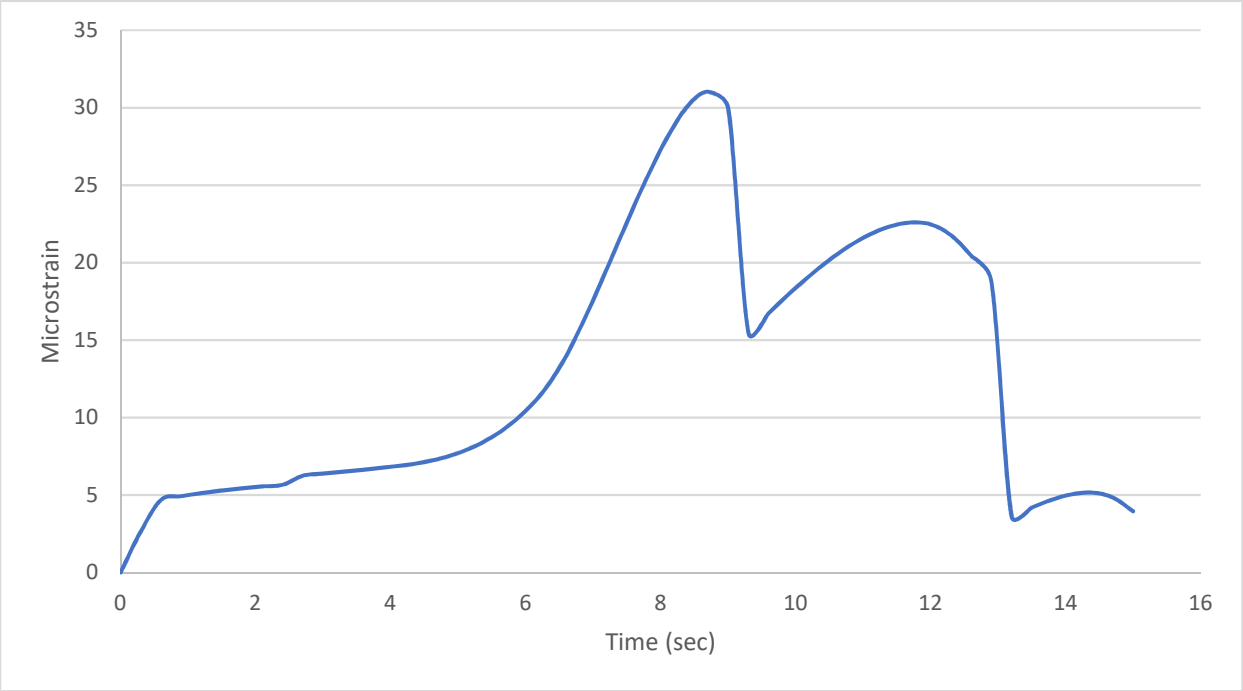

Figure E.11 - HS-20 FEM Results (2018 Model)

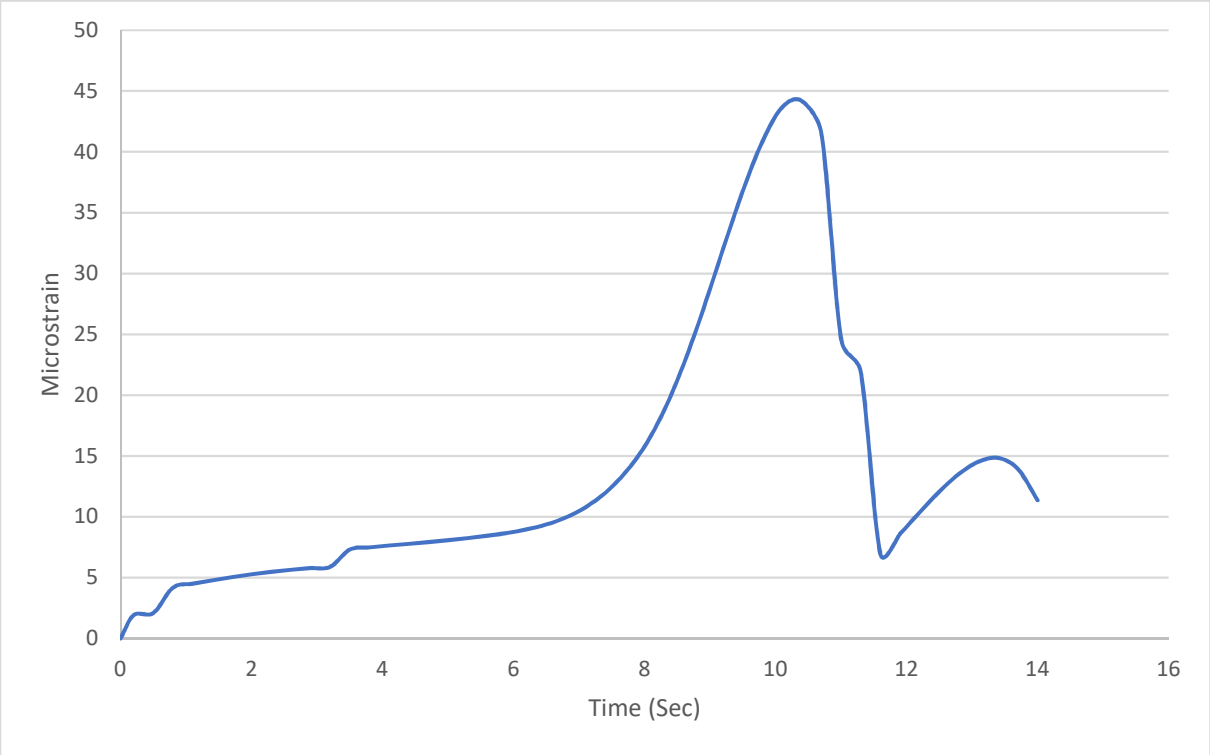

Figure E.12 - Max WIM Load FEM Results (2018 Model)

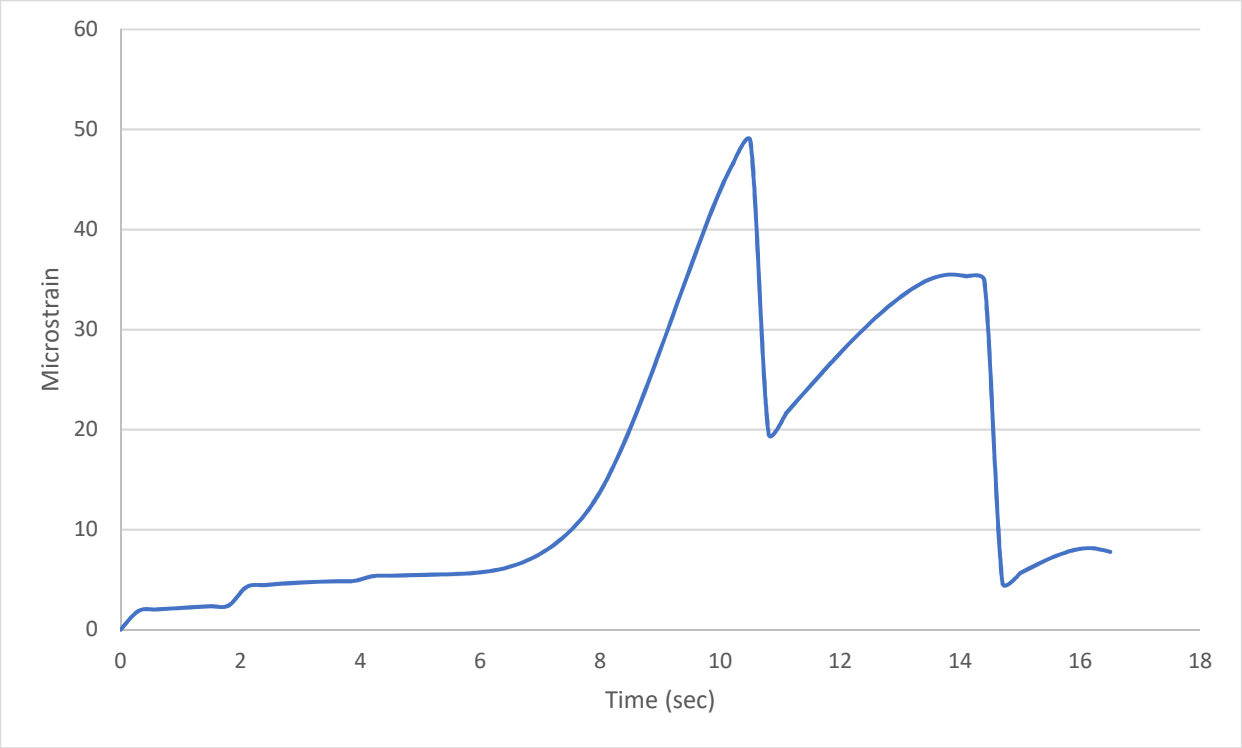

Figure E.13 - HS-20 FEM Results (1939 Model)

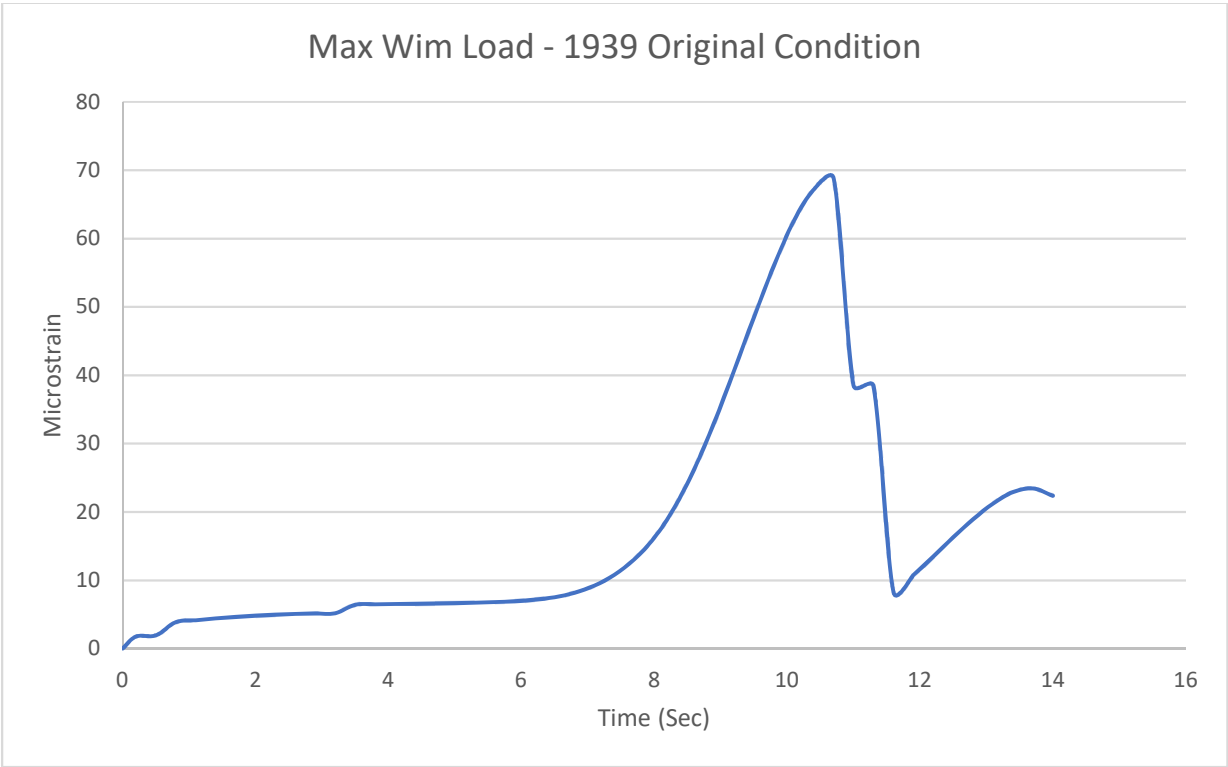

Figure E.14 - Max WIM Load FEM Results (1939 Model)

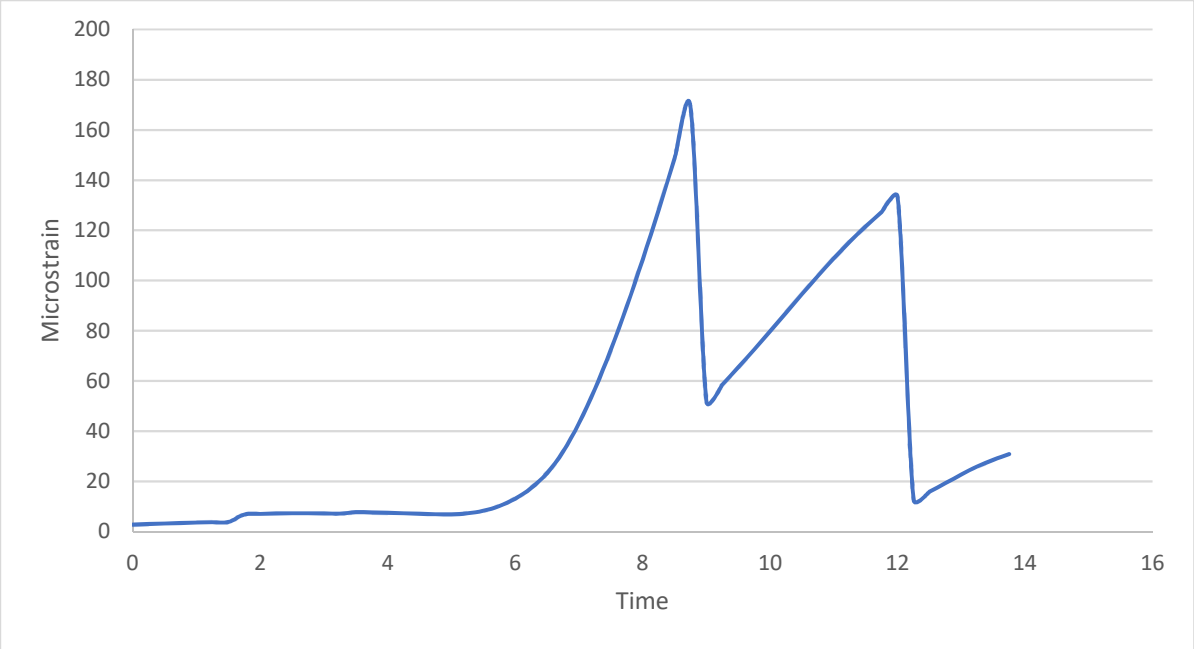

Figure E.15 - HS-20 Load FEM Results (2013 Model)

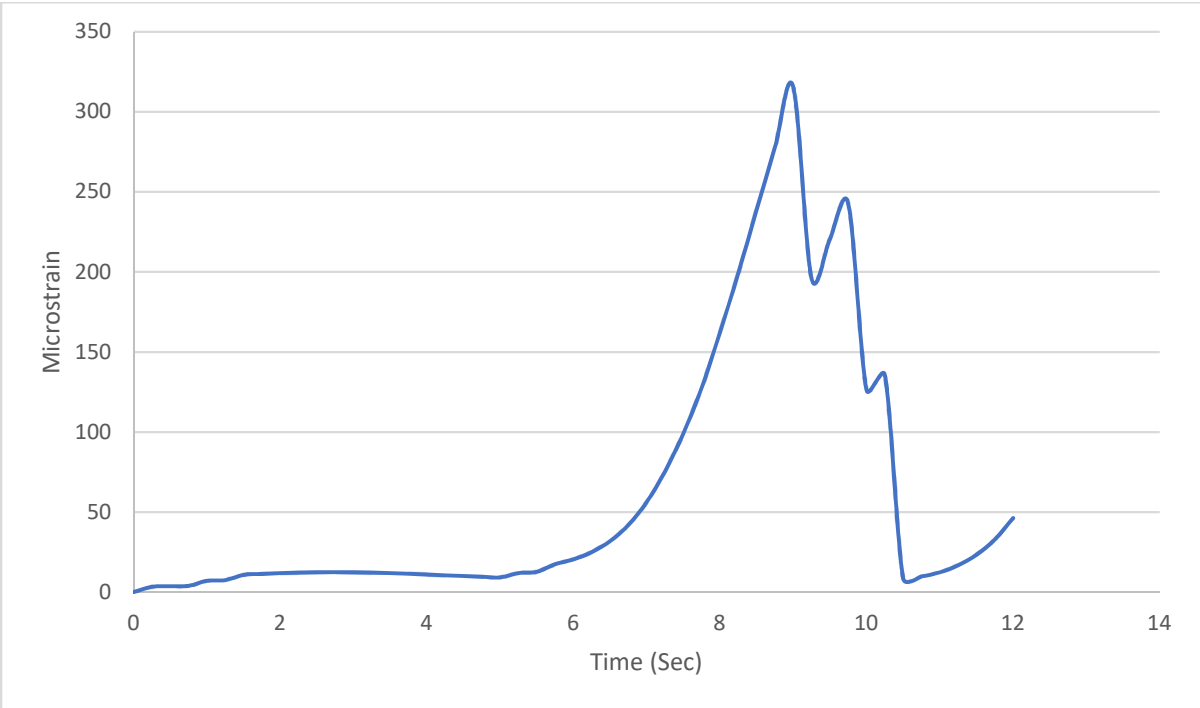

Figure E.16 - Max WIM Load FEM Results (2013 Model)

APPENDIX F

LOAD RATING CALCULATIONS AND RESULTS

F.1 – Fascia Girder Load Rating Calculations

F.1.1 – Fascia Girder Load Rating Calculations (LRFR Method)

Table F.1 - LRFR Member Resistance

Type	Rn	ØcØs	C	Units
1939 As-Built Condition	11,998.00	0.85	10,198.00	Kip-FT
2018 As-Inspected Condition	11,564.00	0.85	9,829.00	Kip-FT
2029 Predicted Condition	10,478.00	0.85	8,906.00	Kip-FT

Table F.2 - Permanent Load Calculation

Type	Variable	Value	Units
Dead Load	DC	3,570.00	Kip-FT
Wearing Surface	DW	0.00	Kip-FT
Permanent Load	P	0.00	Kip-FT

Table F.3 - Live Load Factors

Type	Value	Reason	Type
γLL	1.75	Inventory	Code
γLL	1.35	Operating	Code
γLL	1.30	WIM	Lmax
γLL	0.79	WIM*	Unrestricted Lmax

Table F.4 - Live Load Calculation (2018 Condition)

Truck Type	Weight	Classic	FEM	Exp	Unit
HS-20 Truck	36 Tons	2,931	716	N/A	Kip-FT
2018 Truck	15 Tons	600	319	314	Kip-FT
2016 Truck	15 Tons	500	269	251	Kip-FT
Max WIM Truck	43 Tons	1,616	900	N/A	Kip-FT

Table F.5 - Live Load Calculation (1939 Condition)

Truck Type	Weight	Classic	FEM	Exp
HS-20 Truck	36 Tons	2,931	669	N/A
Max WIM Truck	43 Tons	1,616	845	N/A

Table F.6 - Live Load Calculation (2029 Condition)

Truck Type	Weight	Classic	FEM	Exp	Unit
HS-20 Truck	36 Tons	2,931	719	N/A	Kip-FT
Max WIM Truck	43 Tons	1,616	904	N/A	Kip-FT

Table F.7 - LRFR Rating Factor Results (1939 Condition)

Truck Type	Classical				FEM			
	INV	OP	WIM	WIM*	INV	OP	WIM	WIM*
HS-20 Truck	1.12	1.45	1.51	2.48	4.90	6.35	6.60	10.86
2018 Truck	5.46	7.08	7.35	12.10	N/A	N/A	N/A	N/A
2016 Truck	6.55	8.50	8.82	14.52	N/A	N/A	N/A	N/A
Max WIM Truck	2.03	2.63	2.73	4.49	3.88	5.03	5.22	8.59

Table F.8 - LRFR Rating Factor Results (2029 Condition)

Truck Type	Classical				FEM			
	INV	OP	WIM	WIM*	INV	OP	WIM	WIM*
HS-20 Truck	0.87	1.12	1.17	1.92	3.53	4.58	4.75	7.82
2018 Truck	4.23	5.49	5.70	9.37	N/A	N/A	N/A	N/A
2016 Truck	5.08	6.58	6.84	11.25	N/A	N/A	N/A	N/A
Max WIM Truck	1.57	2.04	2.12	3.48	2.81	3.64	3.78	6.22

Table F.9 - LRFR Rating Factor Results (2018 Condition)

Truck Type	Classical				FEM				Experimental			
	INV	OP	WIM	WIM*	INV	OP	WIM	WIM*	INV	OP	WIM	WIM*
HS-20 Truck	1.05	1.36	1.41	1.92	4.28	5.55	5.76	7.85				
2018 Truck	5.11	6.63	6.88	9.37	9.63	12.48	12.96	17.66	9.77	12.67	13.16	21.65
2016 Truck	6.13	7.95	8.26	11.25	11.38	14.75	15.32	20.88	12.21	15.82	16.43	27.04
Max WIM Truck	1.90	2.46	2.55	3.48	3.41	4.41	4.58	6.25				

F.1.2 – Fascia Girder Load Rating Calculations (LFR Method)

Table F.10 - Fascia Girder LFR Member Capacity

Condition	C	Unit
1939 As-Built Condition	11,998.00	Kip-FT
2018 As-Inspected Condition	11,564.00	Kip-FT
2029 Predicted Condition	10,478.00	Kip-FT

Table F.11 - Fascia Girder Dead Load

Type	Variable	Value	UN
Dead Load	DC	3,570.00	Kip-FT

Table F.12 - LFR Rating Factor Results (2018 Condition)

Truck Type	Classical		FEM		Experimental	
	INV	OP	INV	OP	INV	OP
HS-20 Truck	1.09	1.82	4.45	7.43		
2018 Truck	2.56	4.28	11.84	19.77	10.17	16.97
2016 Truck	2.94	4.90	10.02	16.72	12.70	21.20
Max WIM Truck	1.97	3.30	3.54	5.91		

Table F.13 - LFR Rating Factor Results (1939 Condition)

Truck Type	Classical		FEM	
	INV	OP	INV	OP
HS-20 Truck	1.16	1.93	4.73	7.90
2018 Truck	2.72	4.55	12.58	21.01
2016 Truck	3.12	5.21	10.64	17.77
Max WIM Truck	2.10	3.50	3.77	6.28

Table F.14 - LFR Rating Factor Results (2029 Condition)

Truck Type	Classical		FEM	
	INV	OP	INV	OP
HS-20 Truck	0.92	1.53	3.75	6.27
2018 Truck	2.16	3.61	9.98	16.67
2016 Truck	2.48	4.13	8.44	14.10
Max WIM Truck	1.66	2.78	2.99	4.99

F.2 – Floor Beam Load Rating Calculations

F.2.1 – Floor Beam Load Rating Calculations (LRFR Method)

Table F.15 - Floor Beam LRFR Member Resistance

Member Capacity (Shear)				
Type	Rn	ØcØs	C	Unit
2016/2018 Repaired Condition	451.00	0.85	383.00	Kips
1939 As-Built Condition	269.00	0.85	228.00	Kips
2013 Deteriorated Condition	104.00	0.85	88.00	Kips

Table F.16 - Floor Beam Permanent Load Calculation

Permanent Loads			
Type	Variable	Value	UN
Dead Load	DC	43.20	Kips
Wearing Surface	DW	0.00	Kips
Permanent Load	P	0.00	Kips

Table F.17 - LRFR Live Load Factors

Live Load Safety Factor		
Type	Value	Reason
γLL	1.75	Inventory
γLL	1.35	Operating
γLL	1.30	WIM
γLL	0.79	WIM*

Table F.18 - Calculated Live Load (2018 Condition)

Truck Type	Weight	Classic	FEM	Experimental	Unit
HS-20 Truck	36 Tons	52	19	N/A	Kips
2018 Truck	15 Tons	28	10	8.45	Kips
2016 Truck	15 Tons	25	9	8.12	Kips
Max WIM Truck	43 Tons	73	26	N/A	Kips

Table F.19 - Calculated Live Load (1939 Condition)

Truck Type	Weight	FEM	Unit
HS-20 Truck	36 Tons	26	Kips
2018 Truck	15 Tons	13	Kips
2016 Truck	15 Tons	14	Kips
Max Wim Truck	43 Tons	37	Kips

Table F.20 - Calculated Live Load (2013 Condition)

Truck Type	Weight	FEM	Unit
HS-20 Truck	36 Tons	48	Kips
2018 Truck	15 Tons	15	Kips
2016 Truck	15 Tons	24	Kips
Max Wim Truck	43 Tons	67	Kips

Table F.21 - LRFR Rating Factor Results (2018 Condition)

Truck Type	Classical				FEM				Experimental			
	INV	OP	WIM	WIM*	INV	OP	WIM	WIM*	INV	OP	WIM	WIM*
HS-20 Truck	3.62	4.69	4.87	8.01	9.92	12.86	13.36	21.98				
2018 Truck	6.71	8.70	9.04	14.87	18.41	23.87	24.79	40.79	22.24	28.83	29.93	49.26
2016 Truck	7.52	9.75	10.12	16.66	20.01	25.94	26.94	44.33	23.15	30.01	31.17	51.29
Max WIM Truck	2.58	3.34	3.47	5.70	7.16	9.28	9.63	15.85				

Table F.22 - LRFR Rating Factor Results (1939 Condition)

Truck Type	Classical				FEM			
	INV	OP	WIM	WIM*	INV	OP	WIM	WIM*
HS-20 Truck	1.91	2.48	2.57	4.24	7.16	9.28	9.64	15.86
2018 Truck	3.55	4.60	4.78	7.87	14.54	18.84	19.57	32.20
2016 Truck	3.98	5.16	5.35	8.81	13.48	17.47	18.14	29.85
Max WIM Truck - 1	1.36	1.77	1.83	3.02	5.07	6.58	6.83	11.24

Table F.23 - LRFR Rating Factor Results (2013 Condition)

Truck Type	Classical				FEM			
	INV	OP	WIM	WIM*	INV	OP	WIM	WIM*
HS-20 Truck	0.37	0.48	0.50	0.83	3.88	5.04	5.23	8.60
2018 Truck	0.69	0.90	0.93	1.54	12.75	16.53	17.17	28.25
2016 Truck	0.78	1.01	1.05	1.72	7.76	10.06	10.45	17.20
Max WIM Truck - 1	0.27	0.35	0.36	0.59	2.83	3.66	3.80	6.26

F.2.2 – Floor Beam Load Rating Calculations (LFR Method)

Table F.24 - Capacity Calculation

Condition	C	Unit
2018 As-Inspected Condition	451.00	Kips
1939 As-Built Condition	269.00	Kips
2013 Priority Repair Condition	104.00	Kips

Table F.25 - Dead Load Calculation

Type	Value	Unit
Dead Load	43.20	Kips

Table F.26 - LFR Rating Factor Results (2018 Condition)

Truck Type	Classical		FEM		Experimental	
	INV	OP	INV	OP	INV	OP
HS-20 Truck	3.50	5.84	9.60	16.03		
2018 Truck	6.50	10.85	17.82	29.75	21.52	35.92
2016 Truck	7.28	12.15	19.37	32.33	22.41	37.41
Max WIM Truck	2.49	4.16	6.93	11.56		

Table F.27 - LFR Rating Factor Results (1939 Condition)

Truck Type	Classical		FEM	
	INV	OP	INV	OP
HS-20 Truck	1.89	3.15	3.73	6.23
2018 Truck	3.50	5.85	7.58	12.66
2016 Truck	3.92	6.55	7.03	11.74
Max WIM Truck	1.34	2.24	2.65	4.42

Table F.28 - LFR Rating Factor Results (2013 Condition)

Truck Type	Classical		FEM	
	INV	OP	INV	OP
HS-20 Truck	0.42	0.71	2.03	3.38
2018 Truck	0.79	1.31	6.65	11.11
2016 Truck	0.88	1.47	4.05	6.76
Max WIM Truck	0.30	0.50	1.47	2.46